MATHEMATICAL MODELLING AND DESIGN OF SNAP-ACTION DIAPHRAGMS

BY

MOHSIN K. MIRZA

A THESIS SUBMITTED FOR
THE DEGREE OF DOCTOR OF PHILOSOPHY
IN SYSTEMS ENGINEERING

THE CITY UNIVERSITY
DEPARTMENT OF SYSTEMS SCIENCE
LONDON

OCTOBER 1983

To

[redacted]

INDEX

CHAPTER 4

VALIDATION OF THE MODEL

CHAPTER 5

MODEL REFINEMENTS

CHAPTER 6

PARAMETRIC REPRESENTATION AND SENSITIVITY ANALYSIS

ABSTRACT

Mathematical models have been developed and applied to the analysis and design of snap-action diaphragms that can be considered axi-symmetric. An efficient finite element formulation based on axi-symmetric thin shell theory and employing two noded line elements has been produced for studying these unstable devices. The finite element model was validated by comparison with experimental results on a number of diaphragms, for both pressure loadings and point loadings.

A systematic study of two types of snap-action diaphragms (conical and spherical) has been conducted using the finite element model. Non-dimensional design curves have been produced for conical diaphragms and from these a design methodology has been developed. This methodology does not require the use of a computer but it is based on the computer generated design curves.

AKNOWLEDGEMENT

I would like to express my gratitude and appriciation to my supervisors, Dr. Faruq Abdullah and Professor Ludwik Finkelstein, for their encouragement and guidance at every stage of the project.

I wish also to express my thanks to K.D.G. Instruments ltd., Negretti ans Zambra (Aviation) ltd. and Smith Instruments ltd. who each contributed in the provision of diaphragms and associated data.

I would also like to thank all my friends and colleagues for their help.

Finally, I wish to express my thanks to The Science and Engineering Research Council, who provided the financial support for this research project.

CHAPTER 1

INTRODUCTION

1.1 INTRODUCTION

Elastic elements find wide application as sensors in pressure and force measuring instruments. Examples are Bourdon tubes, corrugated diaphragms, and capsules in pressure transducers, and load-cell billets and other elastic structures for force transducers. In the past the design of such elements has been approached mainly from a practical empirical view point using when available simple "strength of materials" type theory. Modern pressure and force sensing industrial instruments are designed to have errors of less than 1%. This has led to methods based on simple theory being inadequate. The result is that design and development has become a costly and time consuming process. In recent years, computer based mathematical models have been developed for some common elastic elements (Turley, 1977; Leong,1981; Abdullah et.al, 1983). These have been used successfully to design instruments in an efficient manner. An example is the design of nesting capsules for pressure sensors. Using conventional methods it takes about one man year of effort to design a new capsule. Capsules are formed by joining two corrugated diaphragms together. The mathematical techniques (computer based) pioneered at The Measurement and Instrumentation Centre, The City University allow designs to be carried out in a fraction of the time taken formerly. The entire design and development process has been streamlined including generation of the paper-tapes containing information on diaphragm profiles. The paper-tapes are then fed into a numerically controlled lathe to produce forming tools for the diaphragms. The security of the design is assured because the tool, if damaged or worn, can be replaced easily.

This thesis is concerned with the development and application of mathematical modelling techniques to "snap-action" diaphragms used in pressure and force sensors. Snap-action diaphragms differ from ordinary diaphragms in that they lose stability and buckle through when the applied load reaches a critical value. On

reduction of the load the diaphragms snap back at a lower load value. At snap-through and snap-back large displacements are involved. The entire load deflection characteristic of a snap-action diaphragm includes a region of negative stiffness which produces the positive action associated with the diaphragm (hence the name snap-action). These devices are used in instruments as pressure, force or temperature operated switches. When used in combination with "back-off" springs, almost zero rate systems with excellent overload capacities can be produced. The mathematical modelling of snap-action diaphragms is more complex than ordinary diaphragms. This is because the load-deflection characteristic is not single valued, and large displacements are involved. Present industrial design of these devices has been developed in a wholly empirical manner since no adequate simple theory has existed. Design is difficult because the snapping behavior is critically dependent on the form and dimensions of the diaphragm.

Although the application of ordinary diaphragms is widespread, the use of the snap-action diaphragm is limited. This is because their design is extremely difficult. It could be argued that if accurate mathematical models and design procedures were available then these devices will find greater applications. For example, they would be ideally suited for gauging the pressure fluctuations that occur in vortex shedding type meters.

The objective of this thesis is to develop such models and a design methodology. The study has been restricted to snap-action diaphragms that can be considered as axi-symmetrical thin elastic shells. In particular, two types of snap-action diaphragms - conical and spherical - have been studied in detail. Numerical models based on the Finite Element method are developed. The finite element technique is now widely used in many branches of engineering. This technique and the finite difference method is commonly used for the analysis and design of sensors and actuators (see Review paper by Abdullah and Finkelstein, 1982).

1.2 THESIS ORGANISATION

The thesis is organised in the following sequence:

Chapter 2 is concerned with a general introduction to different types of axi-symmetric diaphragms and their application. A brief discussion of existing mathematical models and strategy for present study is presented.

Chapter 3 is concerned with the non-linear finite element formulation using the Total Lagrangian approach for the analysis of axi-symmetric shells.

Chapter 4 is concerned with the validation of the finite element model, with published theoretical results and experimental work conducted by the author. A method for accelerating the convergence rate of the model is also suggested.

Chapter 5 is concerned with implementation of the Updated Lagrangian formulation. Accuracy of the results was found to deteriorate at large displacements when the Total Lagrangian formulation was used. Also, a curved non-linear line element is introduced so that diaphragms of complex profiles can be analysed efficiently.

Chapter 6 is concerned with the classification and parametric representation of different axi-symmetrical diaphragms . Results of sensitivity analysis are also presented. Sensitivity analysis determines which parameters have significant effect on diaphragm performance.

Chapter 7 is concerned with a systematic procedure for designing diaphragms ie. determination of the parameters for a given design specification. Based on this procedure, a feasibility study to design a variable range pressure switch has been carried out.

Chapter 8 is concerned with the conclusions and achievements of the project. Recommendations are made for future work to supplement the present study.

CHAPTER 2

SNAP-ACTION DIAPHRAGMS, APPLICATIONS, AND MATHEMATICAL MODELLING

2.1 INTRODUCTION

The background and the objectives of the present study were outlined in the previous chapter. In this chapter, a description of the behaviour of snap-action diaphragms and their applications are presented. A brief discussion of the previous research in the field, leading to the present study, is also included.

2.2 SNAP-ACTION DIAPHRAGMS

In ordinary diaphragms (flat or corrugated), as the displacements increase, the median in-plane tensile stress in the diaphragm also increases. As a result, the resistance of the diaphragm to applied load increases, hence increasing the stiffness of the diaphragm, so the stiffness of the diaphragm increases. If during the mounting of the diaphragm, initial tensile stresses are introduced, the stiffness of the diaphragm is increased considerably. Conversely, if in-plane compressive stresses are introduced in a diaphragm, there is an accompanied reduction in the stiffness and the characteristic becomes regressive. If the compressive forces are large enough there is eventual loss of stability, and sudden change in diaphragm profile takes place (Andreeva, 1966). This behaviour is not restricted to diaphragms only, and can be observed in beams and arches etc. (Surana, 1982, Nayak, 1971, Wood, et.al., 1977, Sabir, 1972).

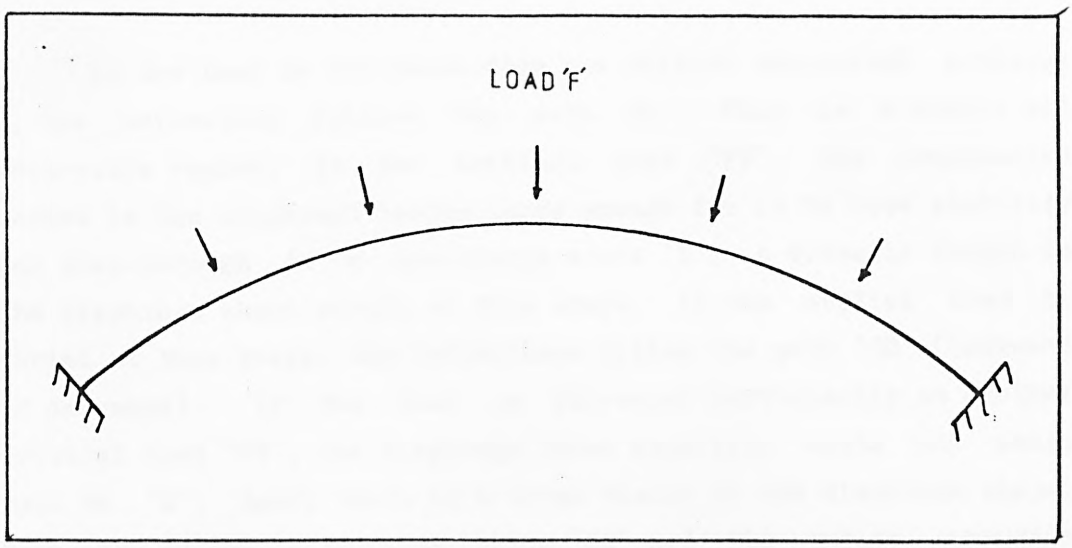

Figure 2.1: Convex Diaphragm

When a convex diaphragm is subjected to force or pressure (from the convex side), compressive stresses in the diaphragm median plane are produced (figure 2.1). If the convexity is large enough, the diaphragm will lose stability and buckle through. Typical load-deflection characteristics of such a diaphragm are shown in figure 2.2.

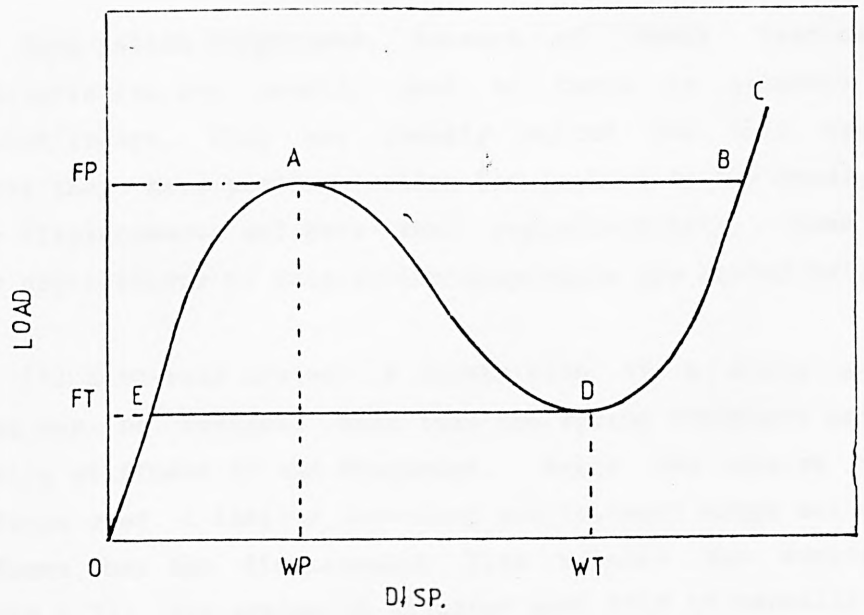

Figure 2.2: Load Deflection Curve

As the load is increased from the initial unstrained position O, the deflection follows the path OA. This is a stable and reversible region. At the critical load 'FP', the compressive forces in the diaphragm become large enough for it to lose stability and snap-through to a new stable state 'B'. A dramatic change in the diaphragm shape occurs at this stage. If the applied load is varied at this stage, the deflections follow the path 'CD' (increase or decrease). If the load is decreased sufficiently at another critical load 'FT', the diaphragm loses stability again and snaps back to 'E'. Again there is a large change in the diaphragm shape. From here on the deflections follow 'OA' and the entire operation can be repeated.

In the two stable regions, OA and CD of the characteristic curve, the variations in the displacements are smooth. The unstable region, given by 'AD', is never observed experimentally. However, its determination becomes important for certain applications as explained in the next section.

Even though large displacements are involved during loading and unloading of snap-action diaphragms, the stresses remain small and no plastic deformation takes place.

2.3 APPLICATIONS

Snap-action diaphragms, because of their load-deflection characteristics are usually used as force or pressure operated switches/relays. They are ideally suited for this application because they have positive action (as implied by the name), produce large displacements and have good reproducibility. Some of the other applications of snap-action diaphragms are listed below.

(i) Zero-rate system: A combination of a diahpragm and a spring can be designed such that the spring stiffness matches the negative stiffness of the diaphragm. Hence the system has zero stiffness over a desired operating displacement range and very high stiffness when the displacement lies outside the desired range (figure 2.3). The system is adjusted such that it normally operates in the 'OD' section of the displacement range in which the stiffness is zero. Such a combination is used on hydraulic circuits and

provides protection to other hardware (valves, etc) that follow. The advantage of this combination is that it does not offer any resistance to load in the normal operating range.

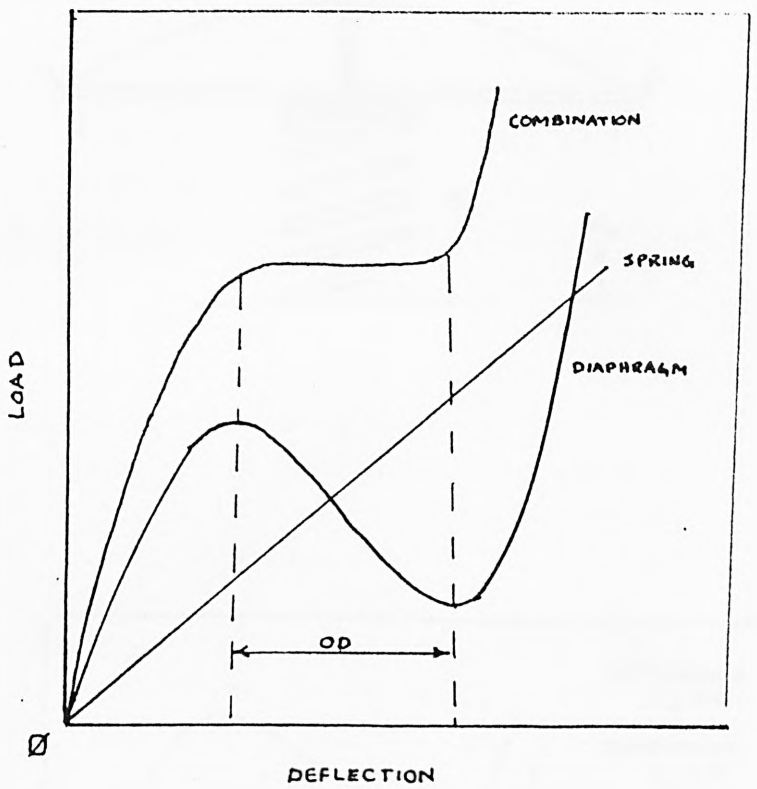

Figure 2.3: Zero Rate System

(ii) Variable Load Switch: A snap-action with a suitable back-off spring can be used as a variable load switch. The spring is chosen such that it has a lower stiffness than the negative stiffness of the diaphragm so that the combination has suitable hysteresis. The load at which the diaphragm triggers can be altered by arranging Xo (figure 2.4).

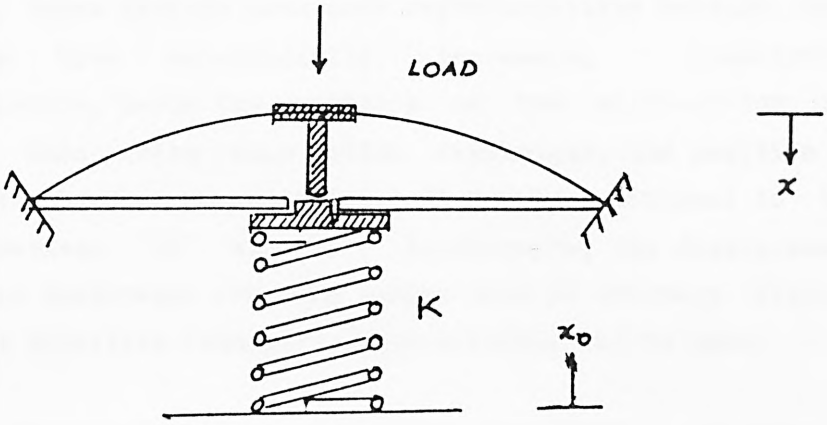
LOAD
x
K
x_0

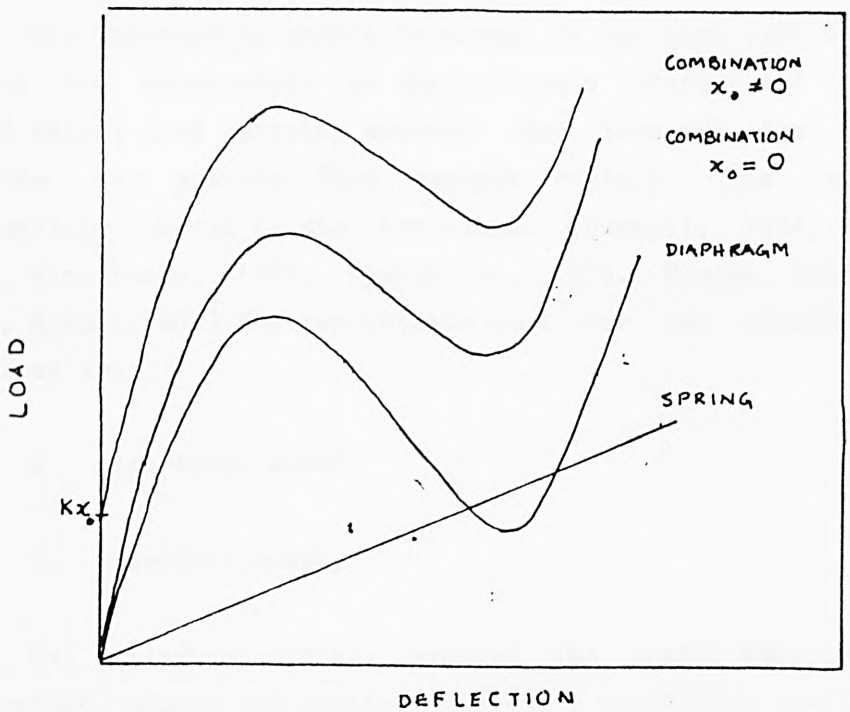
COMBINATION
$x_0 \neq 0$
COMBINATION
$x_0 = 0$
DIAPHRAGM
SPRING
LOAD
Kx_0
DEFLECTION

Figure 2.4

The system may be used to trigger a micro switch at a given load 'F'. Several commercially available variable pressure switches operate on this principle, using an ordinary diaphragm as a load sensing element instead of a snap-action diaphragm (figure 2.4). Generally, these devices have poor reproducability because ordinary diaphragms have monotomically increasing load-deflection characteristics, hence the position of the micro-switch becomes critical. When using snap-action diaphragms, the position of the micro switch becomes non-critical. It can be positioned to trigger anywhere between 'WP' and 'WT'. Furthermore, the displacements in snap-action diaphragms are much larger than in ordinary diaphragms, hence less sensitive (cheaper) micro-switches can be used.

The types of loading used in snap-action diaphragms are uniform pressure and centrally acting point force. Temperature loading can also produce snapping behaviour in the diaphragms, but generally this occurs when bi-metallic devices are used.

2.4 REVIEW OF THE PAST WORK

The interest in shells developed in the late 1950's. This is due to the advancement in the Aerospace Industry and the need for light weight load carrying members. New theories for shells and methods for solving them emerged rapidly. The subject is extensively covered in the literature. (Donnell, 1934, Marguerre, 1938, Timoshenko, 1951, Novozhilov, 1953, Flugge, 1962, Sanders, 1963, Kraus, 1967) The two methods used for the analysis of the problems are:

a. Analytical models

b. Numerical models

(a) Analytical models express the shell behaviour (load deflection, stress and strain, etc) for a particular shell structure in terms of a set of algebraic equations. These equations are derived by introducing simplifications in the physical model of the theory at the expense of losing generality. Such a model, for convex-snap-action diaphragms has been developed by Andreeva (Andreeva, 1966). The model is for diaphragms of very simple

profile and subjected to pressure load. The adequacy of Andreeva's model will be discussed later.

(b) Numerical models. Until the middle of the 1960's the analysis of the buckling of shells in general was restricted to approximate determination of buckling load. The studies were limited to simple shell profiles. Most of the numerical models, up till then, failed to converge prior to the arrival at maximum on the load-deflection curve.

Thereafter, more elaborate finite difference models for studying the instability of shells were developed. Mescall developed a finite difference model based on Reissner's shell theory for axi-symmetrical caps. His study was limited to shells subjected to concentrated loads and was valid for small deflections only.

A succession of research papers on the subject emerged in the 1970's. Notable contributors were - Murray et.al., 1969, Yang, 1972, Sabir et.al., 1972, Bergan et.al, 1973, Gallagher, 1972, Dhatt et.al., 1976, and Wood et.al., 1977. The list mentioned here is by no means exhaustive. Further references and details can be obtained from the forementioned literature.

Implementation and formulation of a very simple, yet accurate and efficient element for the analysis of axi-symmetrical shells is presented in Chapter 3. Apart from the usual complexities involved in non-linear shell analysis, tracing of the load-deflection characteristic for the snap-action diaphragm is further complicated due to the fact that, for a given load the deflection is not unique (figure 2.2).

An important part in the development of the model is the programming techniques used. In this respect, a finite element library system 'FELIB' (SERC, 1980) is used to aid in the efficient development of the program.

Unlike corrugated diaphragms and capsules (Turley, 1977), no systematic study has been carried out to facilitate the analysis and design of snap-action diaphragms. The aim of the present study is to rectify this situation.

CHAPTER 3

FINITE ELEMENT ANALYSIS OF INSTABILITY IN AXI-SYMMETRIC THIN SHELLS

3.1 INTRODUCTION

The objectives of the present study were discussed in the previous chapters. To achieve these aims, an accurate and efficient mathematical model is essential. A non-linear finite element formulation for the analysis of axi-symmetric thin shells is presented in this chapter. A simple and efficient two noded line element (developed by Zienkiewicz and Bauer et.al., 1977) is used for for the analysis. The elements have been shown to yield excellent results for several linear examples. The total Lagrangian finite element formulation presented in this chapter is general and can be applied to the analysis of any axi-symmetrical thin shell problem. Only geometric non-linearities are considered because plastic deformation does not take place in snap-action diaphragms.

3.2 INTRODUCTION TO THE FINITE ELEMENT METHOD

Exact closed form solutions to complex continuum problems cannot be obtained. This may be due to irregular features (geometrical, loading and boundary, etc) in the problem. Analytical solutions to such problems may be obtained by ignoring these irregularities, but this usually leads to serious errors in the results. Alternatively, these complexities may be retained, and an approximate solution may be obtained by numerical methods.

In continuum problems of any dimension, the field variable (pressure, temperature, displacement, etc) possesses infinite degrees of freedom because it is a function of each generic point in the body. Hence the problem is of an infinite number of unknowns. In numerical methods, the number of unknowns is reduced to a manageable size by dividing the domain of interest into small segments and assigning finite degrees of freedom to the segment nodal points. Two popular numerical methods for solving continuum problems are:

Chapter 3

1. Finite difference method

2. Finite element method

3.2.1 FINITE DIFFERENCE METHOD

In the finite difference method (Fenner, 1978) the domain of interest is divided into small segments using a uniform grid. The differential equation describing the behaviour of the variable is expressed in terms of a difference equation using a Taylor series expansion. Solution is obtained after imposing boundary conditions. The method yields very good results (Hafiz, 1981, Turley, 1977, Rahman, 1979). The disadvantages of this method are:

(i) Lacks Flexiblilty: Complex geometrical shapes cannot be handled easily, for example, curved boundaries may need reformulation of the difference equations.

(ii) Computationally Uneconomical: In the finite difference method, a uniform grid is often used. If rapid changes in the variable occur in one section, the entire grid has to be refined. Furthermore, if the geometry is irregular a very fine grid may have to be used throughout the domain of interest just in order to model the irregular region accurately.

3.2.2 FINITE ELEMENT METHOD

The finite element method is an extension of the Ritz method for solving continuum problems. In the Ritz method, an interpolation function with adjustable parameters is chosen. The interpolation function approximates the solution in the domain of interest and must satisfy the boundary conditions. The adjustable parameters can be determined by using the variational method (extremization of a functional with respect to the adjustable parameters. For elasticity problems, the functional is identified as the potential energy of the system). The accuracy of the solution depends on the suitability of the interpolation function. The method can only be applied to simple geometries because a single trial function approximates the variable over the entire geometry (Huebner, 1975).

Chapter 3

In the finite element method, complex geometries are approximated by assembling small segments of simple shapes (called elements). Variables (potential, displacement, etc) are specified at the nodes of the elements. A suitable interpolation function is used to approximate the behaviour of the variable within the element. The interpolation function must retain continuity of the variable across the element boundaries. The unknown variables are determined at the nodal points from the equilibrium equation for the system.

The different stages of finite element modeling are:

(1) Discretization of the domain - The geometry is divided into small segments (elements). The elements may be straight or curved depending on the problem. The number of elements necessary depends on the problem. Generally the accuracy of the results improves as the number is increased.

(2) Choice of interpolation function - Usually polynomials are used for interpolating the variables because their mathematical manipulation is simple. The degree of the polynomial used depends upon the order of partial differential equations of the continuum. The following criteria must be observed in choosing an interpolation function to ensure convergence:

(a) Compatability - Up to one less than the highest partial derivative of the variable in the partial differential equation must be continuous across the element boundaries. Violation of this produces finite strains at the element interfaces.

(b) Completeness - All uniform state of the variable and its partial derivatives appearing in the partial differential equation should have representation in the functional when in the limit, the element size shrinks to zero.

Elements which comply with the above conditions are called conforming elements. However, non-conforming elements have been shown to produce excellent results.

(3) Establishment of Element Properties - Element properties

can be determined by several methods. In elasticity problems, generally, the variational method is used. The method is based on determining the stationarity of the functional $\Pi(a)$ with respect to the nodal variables $\underline{a}$.

$$\text{i.e.} \quad \frac{\partial \Pi}{\partial \underline{a}} = 0$$

With interpolation functions giving piecewise representation of the variable, function $\Pi(a)$ can be defined as the sum of the individual functions defined for all the elements of the assemblage:

$$\Pi(\underline{a}) = \sum_{e=1}^{n} \Pi^{e}(\underline{a}^{e})$$

where e - element number

n - total number of elements

Hence, instead of using the functional defined over the entire domain, the functional for individual elements can be used.

$$\frac{\partial \Pi(a)}{\partial \underline{a}} = \sum_{e=1}^{n} \frac{\partial \Pi^{e}(\underline{a}^{e})}{\partial \underline{a}^{e}}$$

(4) Assembly of System Equations- Individual element equations at step (3) are combined to form system equations, which are representative of the entire domain.

$$\underline{K}(\underline{a}).\ \underline{a} - \underline{F} = 0$$

where $\underline{K}(a)$ - system stiffness matrix

$\underline{a}$ - displacement vector for the system

$\underline{F}$ - loading vector for the system

The combination of the individual element stiffness to form a global or system stiffness matrix is based upon the fact that common nodes have identical field variables.

(5) Solution of System Equation - A set of simultaneous

equations are obtained at step (4). These equations are solved by employing one of several standard methods to determine the variables at the element nodes. Boundary conditions are often imposed at this stage, before solving the equation (Rahman, 1979). Alternatively, the boundary conditions (also known as restraints) may be imposed when assembling the system equations (SERC, 1980).

(6) Additional Calculations - Additional computations may be carried out at this stage ie. determination of stresses and strains from the nodal displacements.

Large computations are involved when using the Finite Element method, hence it is carried out in three different stages. This partitioning of the computation gives an added flexibility because each stage may be developed, altered or extended independently. The three different stages are:

(i) The Pre-Processor - Division of the geometry using small segments (elements) is carried out by a computer program called "Pre-processor". It may be very complex, containing different types of elements and their interfacing. Pre-processors need to be interactive and must have adequate graphics facilities so that suitable representation of the geometry can be achieved in minimum time.

(ii) The Analysis - This is the main program which formulates and solves the system equations to determine the variables at the nodes of the elements.

(iii) The Post-Processor - It is a computer program, generally interactive which gives visual display of the results obtained from the analysis.

The finite element method has gained immense popularity in the recent years and is extensively covered in published literature (Fenner, 1979, Nath, 1974, Huebner, 1975, Zienkiewicz, 1977).

3.3 FINITE ELEMENT ANALYSIS OF AXI-SYMMERTRIC SHELLS WITH GEOMETRIC NON-LINEARITY

The general theory of thin shells can be considerably simplified by taking axial symmetry of the structure into account. The shell theory used here is for axi-symmetric shell structures under axi-symmetric loading, so that one dimensional (line) elements can be used. The subject is reviewed comprehensively by Gallagher (1975).

Only geometric non-linearities are taken into account ie. the stresses are assumed to be much less than the yield stress of the diaphragm material. This is a valid assumption for the analysis of snap-action diaphragms because as the diaphragm snaps through, the dominant in-plane stresses change from compression to tension. The magnitude of the stresses remains small.

3.3.1 NON-LINEAR STRAIN DISPLACEMENT RELATIONS

The non-linear strain displacement relations for the middle surface of the shells of revolution (figure 3.1) are given by Novozhilov (1953), and Kraus (1967). The displacements of the middle surface are uniquely defined by the tangential component 'u' and normal component 'w'. Orthogonal curvilinear coordinates are used throughout to allow analysis of shells of arbitrary shape and not shallow shells only (Batoz et.al., 1976).

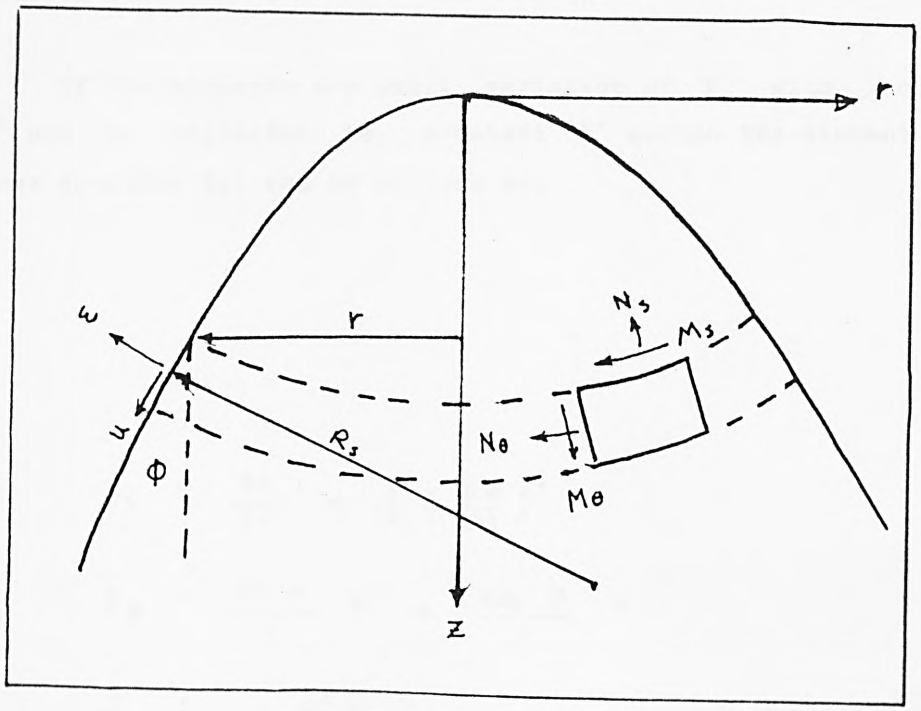

Figure 3.1: Arbitrary shell of revolution

$$\varepsilon_s = \frac{\partial u}{\partial s} - w \cdot \frac{\partial \phi}{\partial s} + \frac{1}{2}\left[\left(\frac{\partial w}{\partial s}\right) + u\frac{\partial \phi}{\partial s}\right]^2$$

$$\varepsilon_\theta = \frac{\sin\phi}{r}\,u + \frac{\cos\phi}{r}\,w \qquad (3.1)$$

$$\chi_s = -\frac{\partial \phi}{\partial s}\cdot\frac{\partial u}{\partial s} - u\frac{\partial^2 \phi}{\partial s^2} - \frac{\partial^2 w}{\partial s^2}$$

$$\chi_\theta = -\frac{\partial \phi}{\partial s}\cdot\frac{\sin\phi}{r}\,u - \frac{\sin\phi}{r}\cdot\frac{\partial w}{\partial s} - \frac{1}{2}\,\frac{\cos\phi}{r}\left(\frac{\partial w}{\partial s}\right)^2$$

where
- ε - midsurface strains
- λ - bending strains
- u - tangential displacements
- w - normal displacements
- r - cylindrical coordinate
- s - meridinal length along shell element
- Φ - slope of the undeformed shell
- θ - circumferential direction

If the elements are small, variation of 'Φ' with respect to 's' can be neglected ie. constant 'ϕ' across the element length. Hence equation 3.1 can be written as:

$$\varepsilon_s = \frac{\partial u}{\partial s} + \frac{1}{2}\left(\frac{\partial w}{\partial s}\right)^2$$

$$\varepsilon_\theta = \frac{\sin\phi}{r}\,u + \frac{\cos\phi}{r}\,w \qquad (3.2)$$

$$\chi_s = -\frac{\partial^2 w}{\partial s^2}$$

$$\chi_\theta = -\frac{\sin\phi}{r}\cdot\frac{\partial w}{\partial s} - \frac{1}{2}\,\frac{\cos\phi}{r}\left(\frac{\partial w}{\partial s}\right)^2$$

The stress strain relations are given by:

$$\begin{bmatrix} N_s \\ N_\theta \\ M_s \\ M_\theta \end{bmatrix} = \frac{E\,t}{1-\nu^2} \begin{bmatrix} 1 & \nu & 0 & 0 \\ \nu & 1 & 0 & 0 \\ 0 & 0 & \frac{t^2}{12} & \frac{\nu t^2}{12} \\ 0 & 0 & \frac{\nu t^2}{12} & \frac{t^2}{12} \end{bmatrix} \begin{bmatrix} \varepsilon_s \\ \varepsilon_\theta \\ \chi_s \\ \chi_\theta \end{bmatrix} \qquad (3.3)$$

OR $\quad \underline{\sigma} = \underline{D}\ \underline{\varepsilon}$

where N - Stress resultants
M - Stress couples
E - Youngs Modulus of the material
t - Thickness of the shell
ν - Poisson ratio
σ - Stress vector
ε - Strain vector
D - Stress Strain matrix

It should be noted that D is a symmetric matrix. This fact is utilized when choosing a solution method for the system equation.

3.4 FINITE ELEMENT FORMULATION

For axi-symmetric shells, line elements (straight or curved) may be used (figure 3.2).

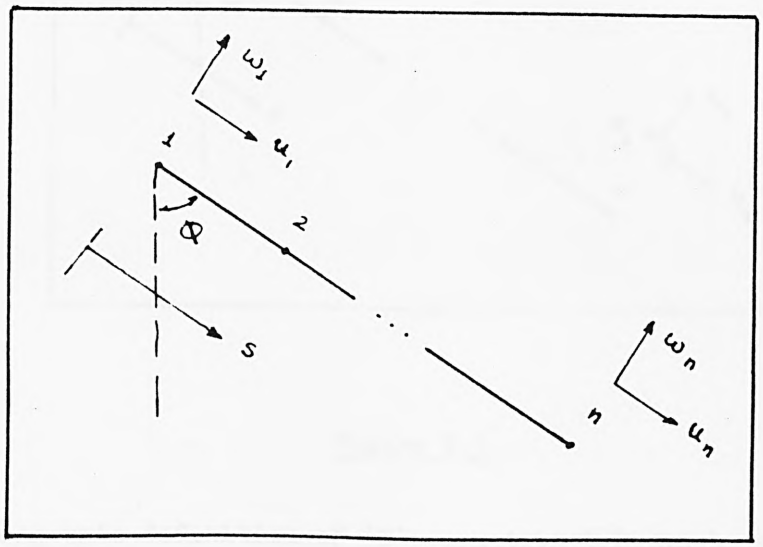

Figure 3.2: n-noded straight element

The displacements inside the element can be determined from the nodal displacements and the interpolation functions:

$$\hat{\underline{u}} = \underline{N}\ \underline{a} \qquad (3.4)$$

To assure convergence, compatibility and completeness requirements must be fulfilled (section 3.2). Because second derivatives of 'w' are present in equation 3.2, not only the variables (u,w) but the slope ($\partial w/\partial s$) must also be continuous across adjacent elements. The variables (u,w) will be continuous because they are common for the adjoining elements. Continuity of slope ($\partial w/\partial s$) can be imposed at the expense of introducing an extra variable 'β' at the nodes (figure 3.3), where 'β' is defined as:

$$\beta = \partial w/\partial s \qquad (3.5)$$

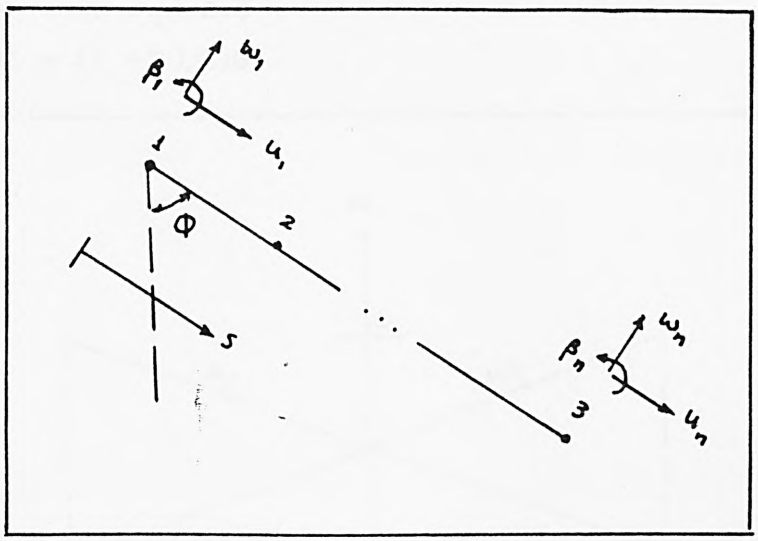

Figure 3.3

Using this definition of 'β', equation 3.2 can be rewritten in matrix form as follows (the linear and non-linear section of the strain displacement relations have been segregated).

$$\begin{bmatrix} \varepsilon_s \\ \varepsilon_\theta \\ \chi_s \\ \chi_\theta \end{bmatrix} = \begin{bmatrix} \frac{\partial}{\partial s} & 0 & 0 \\ \frac{\sin\phi}{r} & \frac{\cos\phi}{r} & 0 \\ 0 & 0 & -\frac{\partial}{\partial s} \\ 0 & 0 & -\frac{\sin\phi}{r}\frac{\partial}{\partial s} \end{bmatrix} \begin{bmatrix} u \\ w \\ \beta \end{bmatrix} + \frac{1}{2} \begin{bmatrix} 0 & 0 & \beta \\ 0 & 0 & 0 \\ 0 & 0 & 0 \\ 0 & 0 & -\frac{\cos\phi}{r} \end{bmatrix} \begin{bmatrix} u \\ w \\ \beta \end{bmatrix} \qquad (3.6)$$

Only first determinates of the variables are present in equation 3.6. A two noded linear element can be used which will fulfill the convergence requirements. The linear interpolation functions, in terms of local coordinates 'η', are:

$$N = (1 - \eta)/2.0$$
$$N = (1 + \eta)/2.0$$

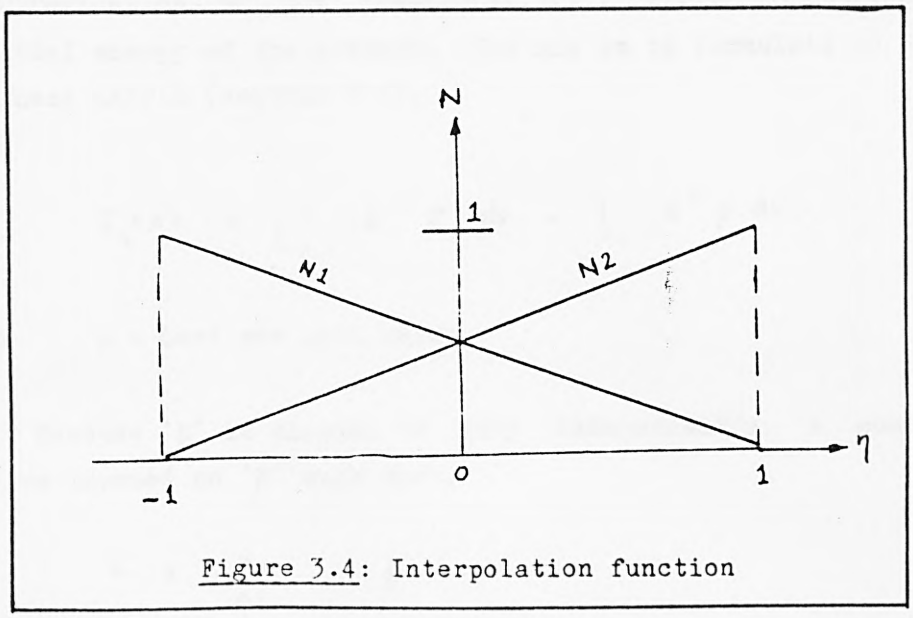

Figure 3.4: Interpolation function

The concept of local coordinates simplifies mathematical manipulations when determining element properties (next section).

The displacements $\underline{a}$ inside the element can be expressed in terms of nodal variables and the interpolation function (equation 3.4)

$$\begin{bmatrix} u \\ w \\ \beta \end{bmatrix} = \left[\begin{array}{ccc:ccc} N_1 & 0 & 0 & N_2 & 0 & 0 \\ 0 & N_1 & 0 & 0 & N_2 & 0 \\ 0 & 0 & N_1 & 0 & 0 & N_2 \end{array}\right] \begin{bmatrix} u_1 \\ w_1 \\ \beta_1 \\ u_2 \\ w_2 \\ \beta_2 \end{bmatrix} \qquad (3.7)$$

3.5 ELEMENT PROPERTIES

The element properties for solid mechanics can be determined by extremization of the functional Π_1, where Π_1 is the total potential energy of the element. The aim is to formulate an element stiffness matrix (section 3.2).

$$\pi_1(a) = \frac{1}{2}\int_v \varepsilon^T \sigma \, dv - \int_v a^T p \, dv \qquad (3.8)$$

where p - Load per unit volume

Because 'β' is allowed to vary independently, a constraint must be imposed on 'β' such that,

$$\gamma = \frac{\partial w}{\partial s} - \beta = 0$$

This can be achieved by using a penalty function.

$$\pi_2 = \frac{1}{2} \alpha \int_v \gamma^T \gamma \, dv$$

γ can be recognised as the shear strain, hence the penalty number α is the shear rigidity.

$$\alpha = \frac{5}{12} \frac{E t}{(1+\nu)}$$

$\underline{\varepsilon}$ and $\underline{\sigma}$, given by equations 3.6 and 3.3 respectively, can be modified to include γ and α.

$$\varepsilon = \begin{bmatrix} \varepsilon_s \\ \varepsilon_\theta \\ \chi_s \\ \chi_\theta \\ \gamma \end{bmatrix} = \begin{bmatrix} \frac{\partial}{\partial s} & 0 & 0 \\ \frac{\sin\phi}{r} & \frac{\cos\phi}{r} & 0 \\ 0 & 0 & \frac{-\partial}{\partial s} \\ 0 & 0 & \frac{-\sin\phi}{r}\cdot\frac{\partial}{\partial s} \\ 0 & \frac{\partial}{\partial s} & -1 \end{bmatrix} \begin{bmatrix} u \\ w \\ \beta \end{bmatrix} + \frac{1}{2} \begin{bmatrix} 0 & 0 & \beta \\ 0 & 0 & 0 \\ 0 & 0 & 0 \\ 0 & 0 & -\beta\frac{\cos\phi}{r} \\ 0 & 0 & 0 \end{bmatrix} \begin{bmatrix} u \\ w \\ \beta \end{bmatrix}$$

OR

$$\varepsilon = B_0\, a + \frac{1}{2} B_L\, a = B\, a$$

where B_0 - linear strain displacement matrix
B_L - non-linear strain displacement matrix

The above strain displacement relations need to be expressed in terms of the nodal variables. This can be achieved by using equation 3.7.

$$B_0 = \begin{bmatrix} \frac{\partial N_i}{\partial s} & 0 & 0 \\ \frac{N_i \sin\phi}{r} & \frac{N_i \cos\phi}{r} & 0 \\ 0 & 0 & \frac{-\partial N_i}{\partial s} \\ 0 & 0 & \frac{-\sin\phi}{r}\frac{\partial N_i}{\partial s} \\ 0 & \frac{\partial N_i}{\partial s} & -N_i \end{bmatrix}$$

$$B_L = \begin{bmatrix} 0 & 0 & N_i\beta \\ 0 & 0 & 0 \\ 0 & 0 & 0 \\ 0 & 0 & -\beta N_i \cos\phi / r \\ 0 & 0 & 0 \end{bmatrix}$$

The stress strain matrix, modified to include the shear stress can be written as:

$$\underline{D} = \frac{Et}{1-\nu^2} \begin{bmatrix} 1 & \nu & 0 & 0 & 0 \\ \nu & 1 & 0 & 0 & 0 \\ 0 & 0 & \frac{t^2}{12} & \frac{\nu t^2}{12} & 0 \\ 0 & 0 & \frac{\nu t^2}{12} & \frac{t^2}{12} & 0 \\ 0 & 0 & 0 & 0 & \frac{5}{12}(1+\nu) \end{bmatrix} \qquad (3.9)$$

$$\sigma = \begin{bmatrix} N_s & N_\theta & M_s & M_\theta & Q \end{bmatrix}^T$$

where Q - Shear resultant

D - Stress-strain matrix

The functional $\Pi_1(a)$ (equation 3.8) can be modified to include the constraints on 'β' by using the new expressions of $\underline{\varepsilon}$ and $\underline{\sigma}$.

$$\pi^*(a) = \int_v (\underline{B}\ \underline{a})^T D B\ \underline{a}\ dv - \int \underline{a}^T f\ dv \qquad (3.10)$$

The equilibruim equations are obtained by determining the variation of $\Pi^*(a)$ with respect to $\underline{a}$, and solving for $\delta\Pi^* = 0$.

$$\delta \pi^{*}(a) = \int_{v} \bar{B}^{T} D \bar{B} \, dv \, a - \int p \, dv = 0 \qquad (3.11)$$

WHERE :

$$\bar{B} = B_0 + B_L$$

AND :

$$B = B_0 + \frac{1}{2} B_L$$

$$d(Ba) = \frac{1}{2}\left(dB_L \, a + B_L \, da\right) = B_L \, da$$

$$\therefore \; dB_L \, a = B_L \, da$$

(B_L IS A FUNCTION OF β ONLY)

Equation 3.11 can be written in a more usual manner ie. using stiffness matrix K (a) and replacing $\int_v p \, dv$ with equivalent nodal forces 'F'.

$$K^{e}(a).a^{e} - F^{e} = 0 \qquad (3.12)$$

$K^{e}(a)$ is a function of displacement a.

The displacements have been specified in local coordinates ie. tangential and normal to the normal element orientation. Before combining element properties to form a systems equation, $K^{e}(a)$ and a^{e} have to be transformed into global coordinates (r,z), figure 3.5.

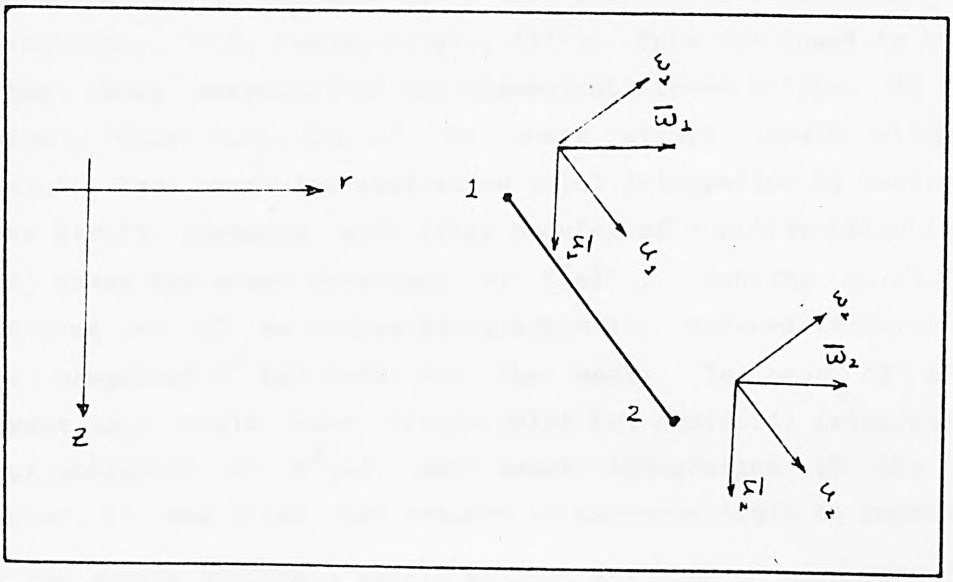

Figure 3.5: Global axes

The transformation can be carried out by using direction cosine matrix such that:

$$\begin{bmatrix} u_i \\ w_i \\ \beta_i \end{bmatrix} = \begin{bmatrix} \cos\phi & \sin\phi & 0 \\ -\sin\phi & \cos\phi & 0 \\ 0 & 0 & 1 \end{bmatrix} \begin{bmatrix} \bar{u}_i \\ \bar{w}_i \\ \bar{\beta}_i \end{bmatrix}$$

OR

$$\underline{a}_i = \underline{\lambda}\ \underline{\bar{a}}_i$$

where $\underline{\lambda}$ - direction cosine matrix

$\underline{a}_i$ - displacement vector for node i in local coordinates

$\underline{\bar{a}}_i$ - displacement vector for node i in global coordinates

It can also be shown that the element stiffness matrix in global coordinates is given by:

$$\underline{\bar{K}}^e = \underline{\lambda}^T \underline{K}^e \underline{\lambda}$$

When exact numerical intergration of equation 3.11 is carried out, there is a tendency for $\underline{K}^e \to \infty$ leading to a solution $\underline{a}^e \to 0$ (Zienkiewicz, 1978, Pawsey et.al., 1971). This was found to be due to the shear component of the element stiffness matrix. In a line element, linear variation of the shear strain occurs along the element. When exact two-quadrature point integration is used, large shear strain combined with large modules of rigidity (Zienkiewicz, 1978) makes the shear component of $\underline{K}^e(a)$. Doherty et.al.(1969) suggested use of selective integration ie. reduced integration of shear component K^e and exact for the rest. In case of a line element this would mean single point (at controid) integration of shear component of $K^e(a)$ and exact integration of the rest. However, it was found that reduced integration could be carried out for the entire stiffness matrix without any loss of accuracy. This simplifies computer programming and reduces the computation time and the results were found to be better than those obtained by more complex formulations (Zienkiewicz and Bauer et.al., 1977)

Assembly of systems equations is carried out by combining individual element equations and using the fact that the adjacent elements have common nodes hence common variables. Further details can be obtained from any text on the finite element method or from the FE library documentation (SERC, 1980).

3.6 SOLUTION OF NON-LINEAR EQUATIONS

The system equations, obtained after assembly of the individual element equations, are of the same format as the element equations (equation 3.12).

$$\underline{K}(\underline{a})\,\underline{a} - \underline{F} = 0$$

where $\underline{K}(a)$ - system stiffness matrix (non-linear)
$\underline{a}$ - nodal displacement vector
$\underline{F}$ - equivalent load vector

The above equation cannot be solved directly because $K(\underline{a})$ is a function of displacement, hence iterative methods have to be used. There are several iterative methods available for solving non-linear equations (Chrisfield, 1980). The Newton-Raphson method was chosen for the purpose because of its proven reliability. Generally the loading vector is taken as an independent variable when solving the above equation iteratively. However, because the relationship between the applied load and the displacement is not unique (section 3.4), the so called dominant displacement method is used (Batoz et.al., 1976). In the dominant displacement method, a single element of the vector '$\underline{a}$' is increased by a fixed amount and the other elements of '$\underline{a}$' are determined so that equilibrium between applied load displacement is maintained.

The system equation for each iteration can be written as:

$$\underline{K}^{i}(\underline{a})\,\underline{a}^{i} - \lambda^{i}\underline{F} = \underline{R}^{i} \qquad (3.13)$$

where λ - Scalar variable to be determined
R - The residual vector
i - Iteration number
F - Known load distribution

The solution seeks to minimize the residual vector at each consecutive iteration 'i'. λ^{i} determines the actual load vector necessary for equilibrium.

$$\underline{R}^{i+1} \simeq \underline{R}^{i} + \delta\underline{R}^{i} = 0 \qquad (3.14)$$

$$\delta\underline{R}^{i} = \frac{\partial \underline{R}^{i}}{\partial \underline{a}^{i}}\,\delta\underline{a}^{i} + \frac{\partial \underline{R}^{i}}{\partial \lambda^{i}}\,\delta\lambda^{i} \qquad (3.15)$$

From equation 3.13:

$$\frac{\partial \underline{R}^i}{\partial \lambda^i} = -\underline{F}$$

$$\delta \underline{R}^i = \underline{K}_T^i \, \delta \underline{a}^i - \delta \lambda^i \, \underline{F}$$

WHERE :

$$\underline{K}_T^i = \frac{\partial \underline{R}^i}{\partial a^i}$$

K_T is known as tangential stiffness matrix, its derivation is given in appendix A.

Hence,

$$\underline{R}^{i+1} = \underline{R}^i + \underline{K}_T^i \, \delta \underline{a}^i - \delta \lambda^i \, \underline{F} = 0 \qquad (3.16)$$

$\delta \underline{a}^i$ can be defined as a sum of 2 vectors such that:

$$\delta \underline{a}^i = \delta \underline{b}^i + \delta \lambda^i \, \delta \underline{c}^i \qquad (3.17)$$

From equations 3.16 and 3.17:

$$\underbrace{\underline{R}^i + \underline{K}_T^i \, \delta \underline{b}^i}_{1} + \delta \lambda^i \underbrace{(\underline{K}_T^i \, . \, \delta \underline{c}^i - f)}_{2} = 0$$

The above equation can be satisfied if 1 and 2 are zero. This leads to two sets of simultaneous equations to be solved at each stage.

$$\underline{K}_T^i \cdot \delta \underline{b} = -\underline{R}$$

$$\underline{K}_T^i \cdot \delta \underline{c} = \underline{F} \qquad (3.18)$$

The mth element of the displacement vector a is a known constant.

$$\delta a_m^i = 0$$

From equation 3.17:

$$\delta b_m^i + \delta \lambda^i \, \delta c_m^i = 0$$

$$\delta \lambda^i = -\delta b_m^i / \delta c_m^i \qquad (3.19)$$

HENCE :

$$\lambda^{i+1} = \lambda^i + \delta \lambda^i$$

AND :

$$\underline{a}^{i+1} = a^i + \delta \underline{b}^i + \delta \lambda^i \cdot \delta c^i \qquad (3.20)$$

The procedure is repeated until no further improvements in the results are obtained.

The algorithm is summarized in the following steps:

(i) Displacement vector a is assumed with its mth component (the dominant displacement) specified. For the diaphragms, the vertical displacement of the centre is used as the dominant displacement. λ^o is also assumed. Loading vector $\underline{F}$ is known, (F = equivalent nodal forces for unit applied load, $\lambda \underline{F}$ determines the actual load necessary for equilibrium).

(ii) Calculate $\underline{R}^i$ (details given in appendix A)

(iii) Calculate $\underline{K}_T^i$ (details given in appendix A), hence $\delta \underline{b}^i$ and $\delta \underline{c}^i$ can be calculated from equation 3.18.

(iv) Calculate $\delta\lambda^{i}$, λ^{i+1} and $\underline{a}^{i+1}$.

(v) Repeat steps (ii) to (iv) until convergence is obtained.

The following displacement norm is used as the convergence criteria:

$$n = \left| \frac{(\underline{a}^{i+1})^T(\underline{a}^{i+1}) - (\underline{a}^{i})^T(\underline{a}^{i})}{(\underline{a}^{i})^T.(\underline{a}^{i})} \right| \leq \Delta$$

The value of Δ is determined experimentally. It was found that no significant improvement in the results were obtained when it reached 0.0001. Hence Δ = 0.0001 is used.

3.7 SOLUTION OF SIMULTANEOUS EQUATIONS

Two sets of simultaneous equations (equation 3.18) have to be solved at each iteration. The properties of the tangential stiffness matrix have to be taken into account when choosing a method for solving the simultaneous equations. The primary requirements of the solution mentioned are the computational economy, fast response, low storage, and assured convergence. The accuracy of the results is assured by the iterative solution procedure (section 3.6)

In instability analysis, the tangential stiffness matrix is not always positive definite and may be ill-conditioned (Bergan et al., 1978). Because of these reasons, iterative methods such as the Gauss-Seidal method cannot be used. Cholesky's compact elimination method could not be used for the same reasons. The most suitable and reliable method for solving simultaneous equations was found to be the the Gaussian elimination method. The subroutine used takes the banded nature of tangential stiffness matrix into account (reduces computer storage) and incorporated partial pivoting, row interchange (Fox, 1964) so that the program will not crash when a diagonal element becomes zero.

3.8 PRE-PROCESSOR

Pre-Precessor is a computer program, used to discretize the diaphragm profile, impose boundary conditions (restraints) and determine equivalent nodal forces due to distributed applied load. The program has to be interactive and must have adequate graphics capabilities. This is necessary so that suitable modifications can be made to obtain satisfactory discretization. The salient features of the pre-processor developed are listed below:

(i) Filtering for smoothing diaphragm profile: Experimental data acquisition for diaphragm profile is prone to errors. Recursive filtering techniques were used to obtain a smooth diaphragm profile. This was achieved by replacing i^{th} ordinate with

$$z_i = \frac{z_{i-1} + n_i z_i + z_{i+1}}{n_i + 2.\phi}$$

where n_i - determines the bandwith of the filter

(ii) Cubic spline interpolation - This was used to introduce extra elements in different regions for diaphragm profile data obtained experimentally. The advantange of cubic spline interpolation is that it retains continuity of the slope (Hayes, 1970, NAG, 1980).

(iii) Discretization of diaphragm profile for design parameters - For sensitivity analysis and diaphragm designing, the diaphragm profiles were described with geometric parameters (sections 6.3 and 6.4). Coordinate geometry was used to discretize such diaphragm profiles.

(iv) Equivalent Nodal Forces - For distributed applied load, equivalent nodal forces have to be determined. This can be done by virtual work method (Zienkiewicz, 1977). Equivalent nodal forces f for an element are given by:

$$\underline{f}^{e} = \int_{A} \underline{N}^{T} b \, dA$$

where $\underline{N}$ - shape functions.

b - load per unit area.

$dA = 2.r.ds$

$$ds = \sqrt{\left(\frac{\partial r}{\partial \eta}\right)^2 + \left(\frac{\partial z}{\partial \eta}\right)^2} \cdot d\eta$$

η - local coordinate system

Hence the equivalent nodal forces are dependent on the diaphragm profile.

3.9 CONCLUSION

A Finite Element formulation for the analyis of axi-symmetric thin shells is presented in this chapter. Only the geometric non-linearities have been taken into account. The formulation is general and can be used for the analyis of any axi-symmetric shell problem, provided a suitable pre-processor is available.

A simple two noded line element is used for the analysis. A similar element, for linear analysis of shells, was developed by Zienkiewicz et.al. and applied to a number of problems. The element was shown to yeild excellent results for the examples studied.

The computer program was developed on a Prime 550 (a multi-user mini-computer), using routines from a finite element library, 'FELIB' (SERC, 1980). The library has been developed by SERC at the Rutherford and Appleton laboratory. The aim is to take

account of the modular nature of finite element programming by building up programs in fully transportable Fortran using a library of subroutines specific to finite element manipulations. The library and its use has been documented to a very high standard.

CHAPTER 4

VALIDATION OF THE MODEL

4.1 INTRODUCTION

The finite element formulation for the analysis of axi-symmetric diaphragms was presented in the previous chapter. The model is based on the Total Lagrangian (T.L.) formulation, whereby all the incremental solutions are determined with reference to the initial diaphragm profile. The model cannot be used with any confidence until its accuracy and limitations have been tested thoroughly. Validation of the model has been carried out by comparing the results from the model with those published in literature (analytic and numeric). As there are very few examples published on axi-symmetric diaphragms, validation has been supplemented with extensive experimental work.

The stress distribution in a spherical cap is also studied and compared with the distribution in a flat diaphragm. The study gives insight into the behaviour of snap-action diaphragms.

The convergence of the Total Lagrangian formulation is also studied, and suggestions are made so as to accelerate the convergence rate.

4.2 MODEL VALIDATION

4.2.1 ANALYTIC RESULTS

Extensive work has been carried out by Andreeva (1966) on elastic elements for instruments. She has presented an analytic model for snap-action diaphragms. The model was developed by combining the membrane and the bending theory for shells of revolution. The model is inaccurate because it assumes that the shape of the elastic surface does not alter with deformation. Hence, it can only be applied when the displacements are small. The pressure-centre deflection characteristic of a spherical diaphragm is given by equation 4.1. A similar equation derived by Andreeva

for flat diaphragms compares favourably with the finite difference model developed by Turley (1977).

$$\frac{P}{E}\left(\frac{R}{T}\right)^4 = a\left(\frac{W}{T}\right) - b\left(\frac{W}{T}\right)^2 + c\left(\frac{W}{T}\right)^3 \qquad (4.1)$$

where P - Applied pressure on the convex side
E - Youngs Modulus for the diaphragm material
R - Radius of the diaphragm
T - Thickness of the diaphragm
W - Deflection of the diaphragm centre

For the spherical diaphragms:

$$a = 5.86 + 4.88 \times \left(\frac{H}{T}\right)$$
$$b = 7.72 \times \left(\frac{H}{T}\right)$$
$$c = 2.76$$

where H - Height of the diaphragm centre.

Results obtained from using equation 4.1 and the finite element model are shown in figure 4.1.

It can be seen from figure 4.1 that the analytic model is inadequate, and cannot be used to study the behaviour of snap action diaphragms.

The finite element results were obtained using 10 elements to approximate the profile. For H/T = 3, 16 equal increments were needed to trace the load-deflection curve. On a Prime 550, it took 3 CPU minutes for the computation.

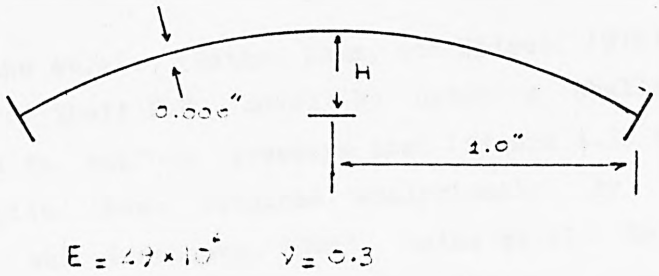

$E = 4.7 \times 10^6$ $\nu = 0.3$

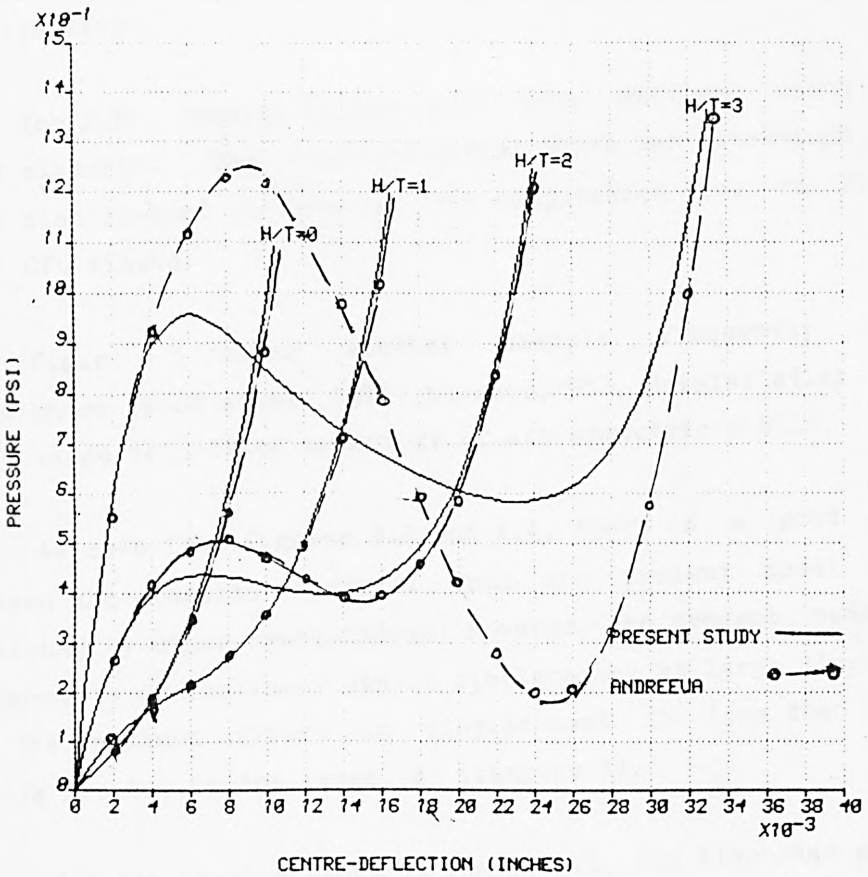

Figure 4.1: Results from the Analytic and the F.E. model

4.2.2 NUMERICAL MODELS

Bathe et.al. (Bathe, Ramm, and Wilson, 1975) demonstrated the accuracy of their F.E. model by using a shallow spherical cap subjected to uniform pressure load (figure 4.2) and compared their results with those obtained analytically by Korishin et.al. (Korishin and Isanbaeva, 1968). Bathe et.al. developed their F.E. model using total Lagrangian formulation, with an eight noded parabolic element. Obviously, this type of element is computationally uneconomical when used for diaphragms of complex profiles. This is because of the large number of degrees of freedom per element, hence the large number of equations to be solved at each iteration.

The F.E. results (figure 4.2) were obtained using 10 two noded elements. The load deflection curve was determined using 10 equal displacement increments. The computation time on Prime 550 was 1 CPU minute.

Figure 4.3 shows another example frequently used by researchers (Wood et.al.,1977, Suraner,1982, Haisler et.al,1972), to study large deflection behaviour of axi-symmetric shells.

As seen from figures 3.2 and 4.4, there is a good agreement between the results obtained from the present model and those published by other researchers. However, the present model has a tendency to overestimate centre displacement at large displacements. But the maximum errors in displacement are less than 5%. These errors are due to the large 'B' (chapter 3).

For the results shown in figure 4.3, the diaphragm profile was approximated with 12 two noded line elements. 18 displacement increments were needed to trace the load deflection for R1/RO = 0.42. The computation time on Prime 550 was 5.4 CPU minutes. Each iteration takes approximately 1.6 CPU seconds to formulate and solve 68 simultaneous equations. In certain instances, a large number of iterations (>10) were required for convergence.

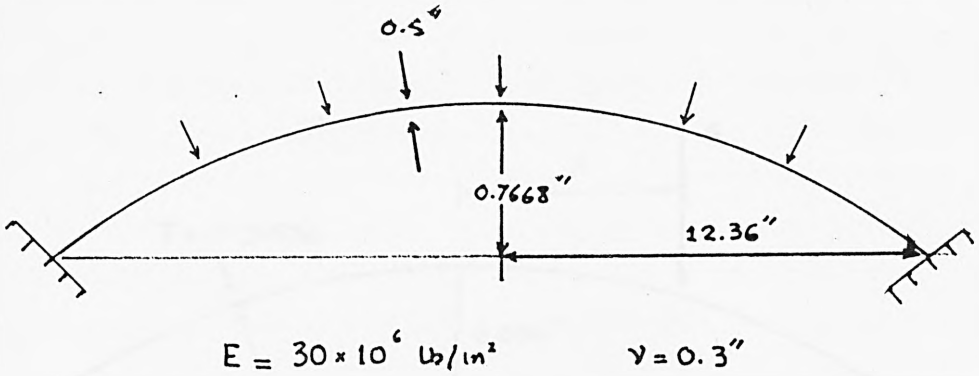
0.5"
0.7668"
12.36"
E = 30 x 10^6 lb/in^2
ν = 0.3"

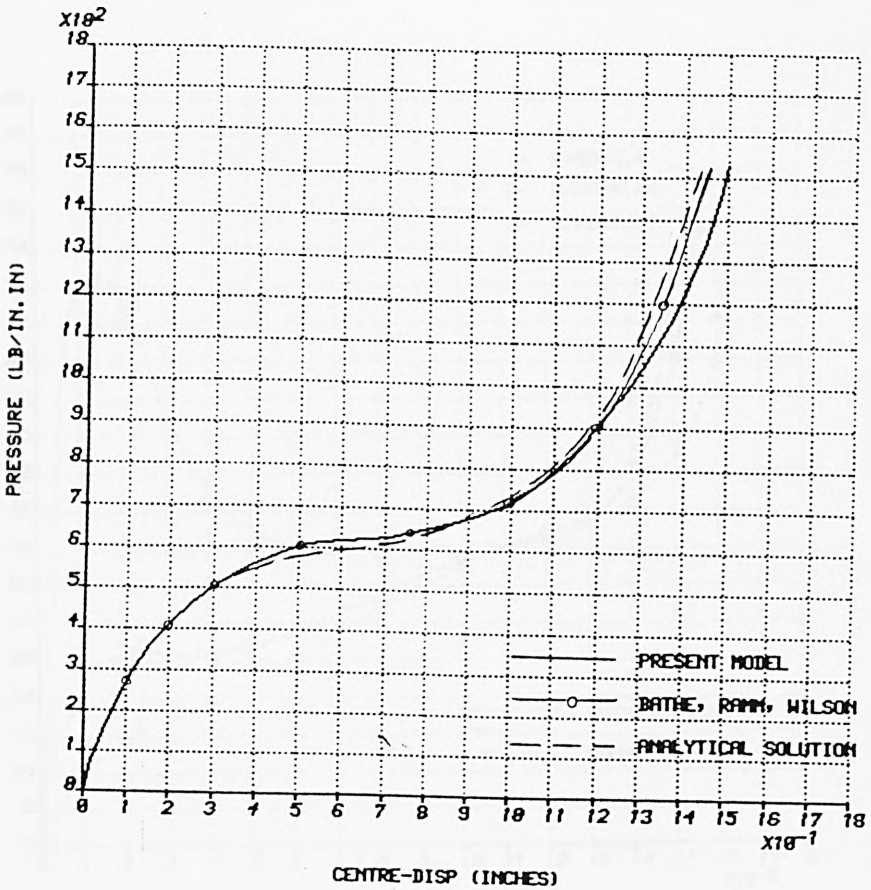
X10^2
PRESSURE (LB/IN.IN)
CENTRE-DISP (INCHES)
X10^-1
PRESENT MODEL
BATHE, RAMM, WILSON
ANALYTICAL SOLUTION

Figure 4.2

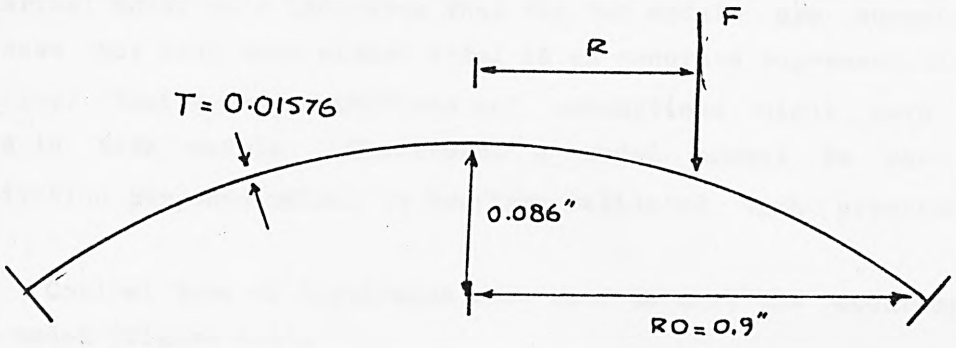
F
R
T = 0.01576
0.086"
RO = 0.9"

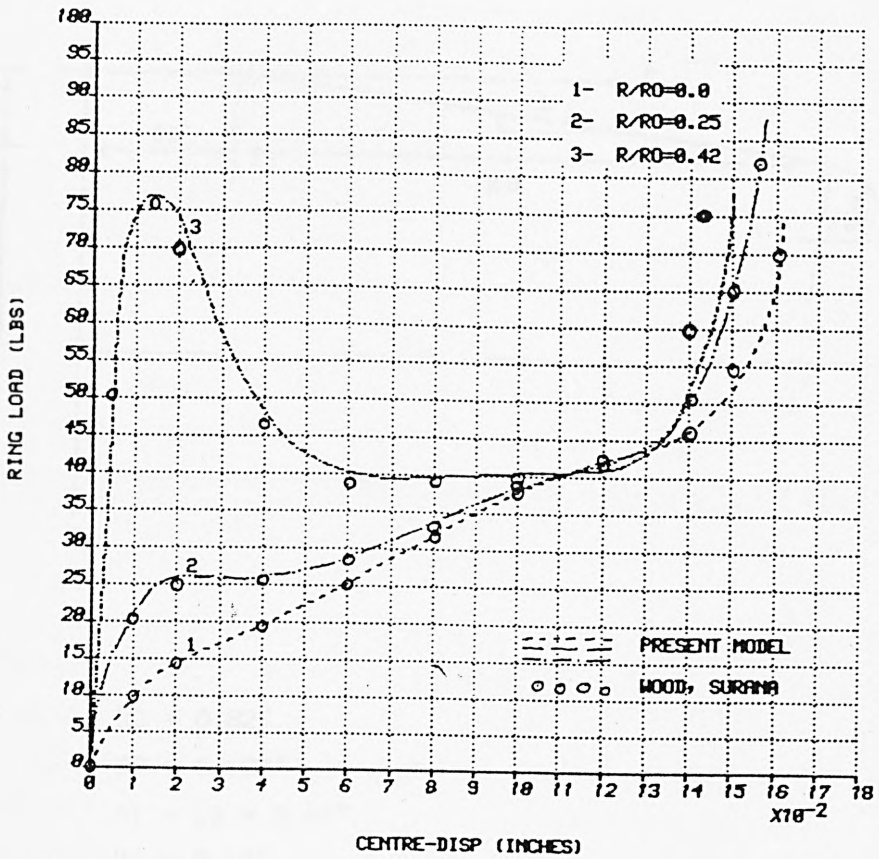
1- R/RO=0.0
2- R/RO=0.25
3- R/RO=0.42
PRESENT MODEL
WOOD, SURANA
RING LOAD (LBS)
CENTRE-DISP (INCHES)
X10^-2

Figure 4.3

4.2.3 EXPERIMENTAL RESULTS

Experimental work is essential in determining the accuracy of a numerical model. Comparison of one numerical model with another numerical model only indicates that the two models are compatible. It does not mean that either model is an accurate representation of reality. Similar approximations and assumptions might have been made in both models. Therefore, a model cannot be used for prediction purposes unless it has been validated with experiments.

Conical type of diaphragms were used to test the accuracy of the model (figure 4.4).

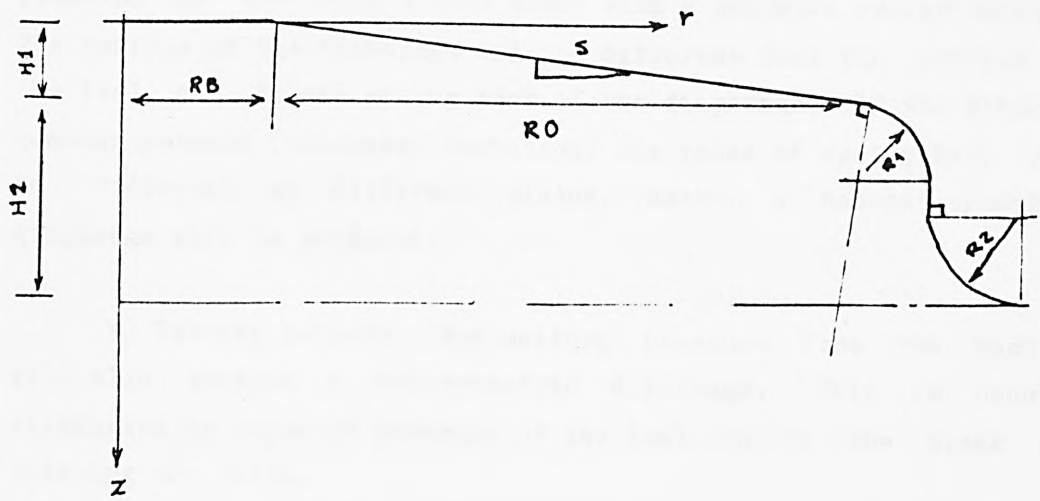

where RO = 0.82"
RB = 0.187"
R1 = R2 = 0.07"
H2 = 0.15"
E = 29.0E6 lb/in^2
ν = 0.3

Figure 4.4

The diaphragms were designed by the author and produced by K.D.G. Instruments Ltd. Different diaphragm characteristics (load-centre deflection) were obtained by varying diaphragm thickness 'T' and height 'H1'. This type of diaphragm was chosen so as to facilitate the determination of the diaphragm profile. Only the slope 'S' needs to be determined so as to evaluate 'H1'. The other parameters are fixed (figure 4.4). The diaphragm slope was determined using a universal measuring machine which can accurately measure 0.0001" displacements. Only the diaphragms with a high degree of axi-symmetry were chosen for validation. This is determined by measuring 'z' (for a constant r) across several diameters. If 'z' varies by more than 5%, the diaphragm is rejected. The non-axi-symmetry (formed by an axi-symmetric tool) arises due to:

a) Non-homogeneous material: Diaphragms are formed by pressing the tool onto a flat blank with a suitable rubber backing. The profile of the diaphragm will be different from the profile of the tool due to the spring back of the diaphragm. If the blank is non-homogeneous (thickness variation) the rates of spring back will be different at different places, hence, a non-axi-symmetric diaphragm will be produced.

b) Forming Defects: Non-uniform pressure from the backing will also produce a non-symmetric diaphragm. This is usually eliminated by repeated pressure of the tool on to the blank and rotating the blank.

c) Mishandling: Mishandling the diaphragm before it has been hardened by heat treatment also destroys the diaphragm symmetry.

Only diaphragms free from surface defects were chosen for model validation. Surface defects in diaphragms occur due to the presence of dirt particles on the tool or the blank when a diaphragm is being formed. The presence of dirt particles produces indentations on the surface of the diaphragm. The effect of surface defects is to localise stresses and strains producing non-axi-symmetric bifurcation.

The discretized profile of an 0.08" thick diaphragm is shown in figure 4.5.

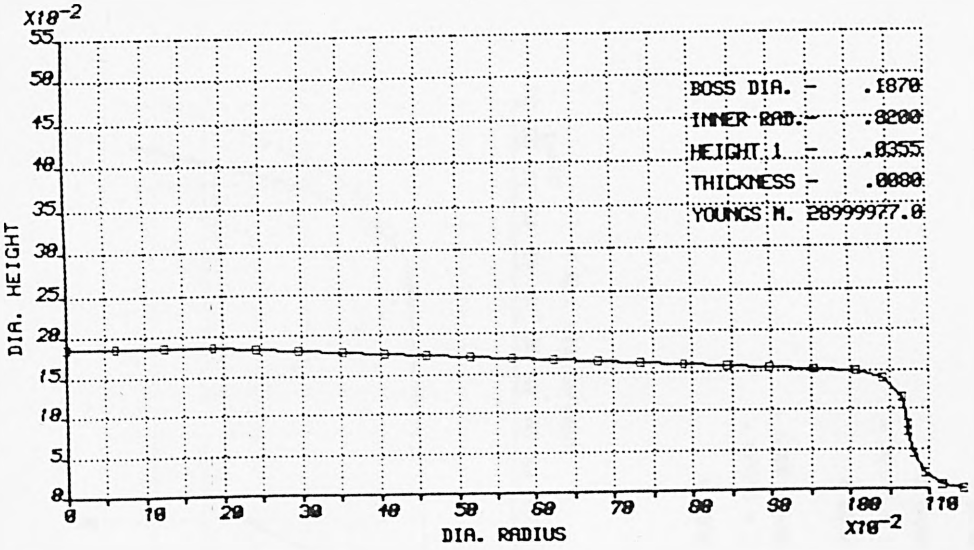

Figure 4.5: F.E. representation of the dia. profile

The results of the experimental tests for pressure load and point load, and their corresponding computer simulations are shown in figures 4.6 and 4.7 respectively. The same diaphragms were used for pressure and centrally applied load experiments. If a diaphragm becomes unstable (snap) for point load applied at the centre, it must snap for pressure load as well. However, the reverse case is not necessarily true.

The load-deflection characteristic of a diaphragm could not be determined experimentally in the unstable region (negative stiffness). This is because as the load is varied in the region of the peak load carrying capacity, the diaphragm either snaps through to the next stable position (load increased), or follows the initial load-deflection curve (load decreased). Similar behaviour is exhibited at the minimum point of the load deflection curve. Also, the determination of maximum and minimum points of load-deflection curve were found to be difficult because of the nearly zero diaphragm stiffness.

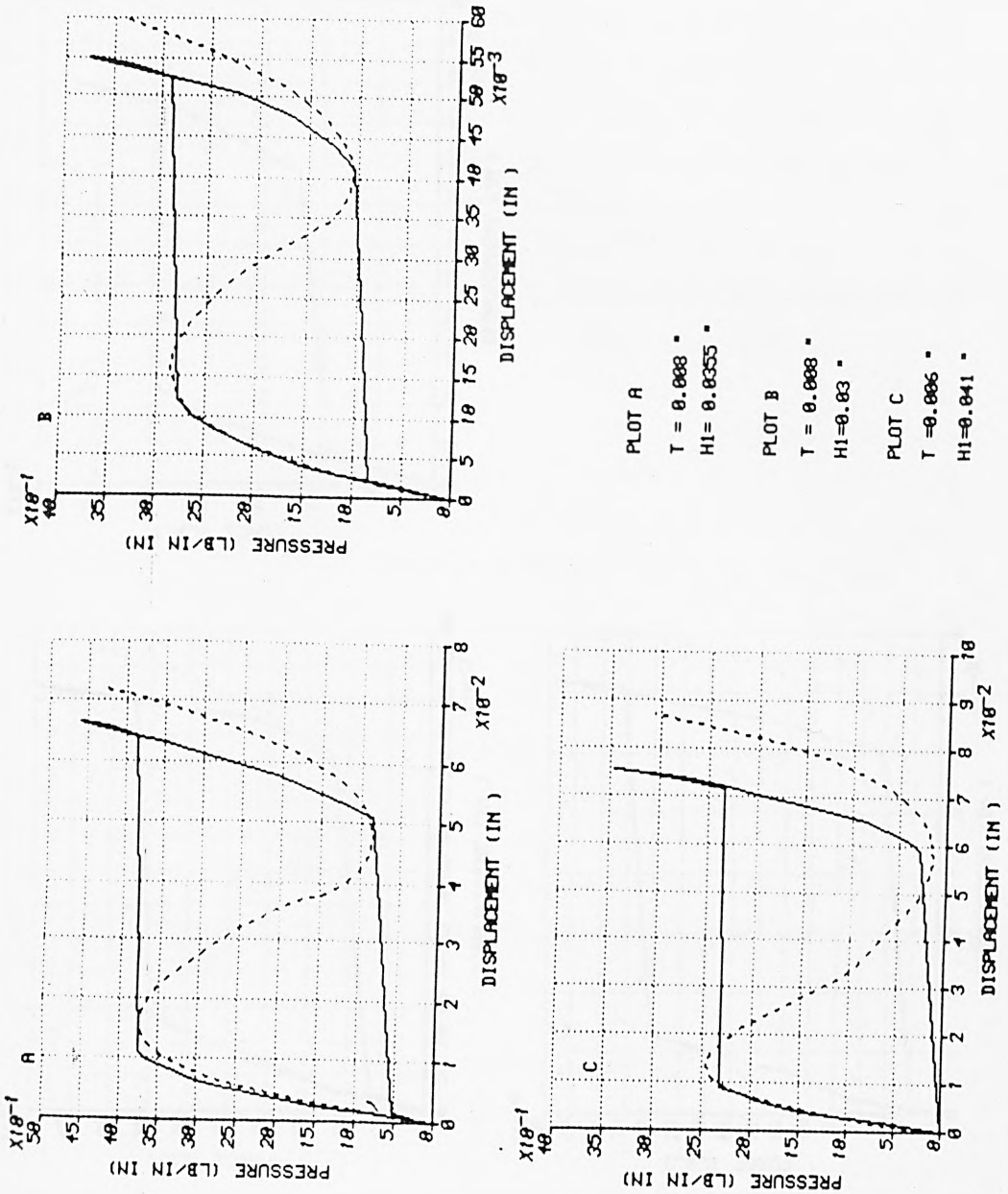

Figure 4.6: Results for pressure loading

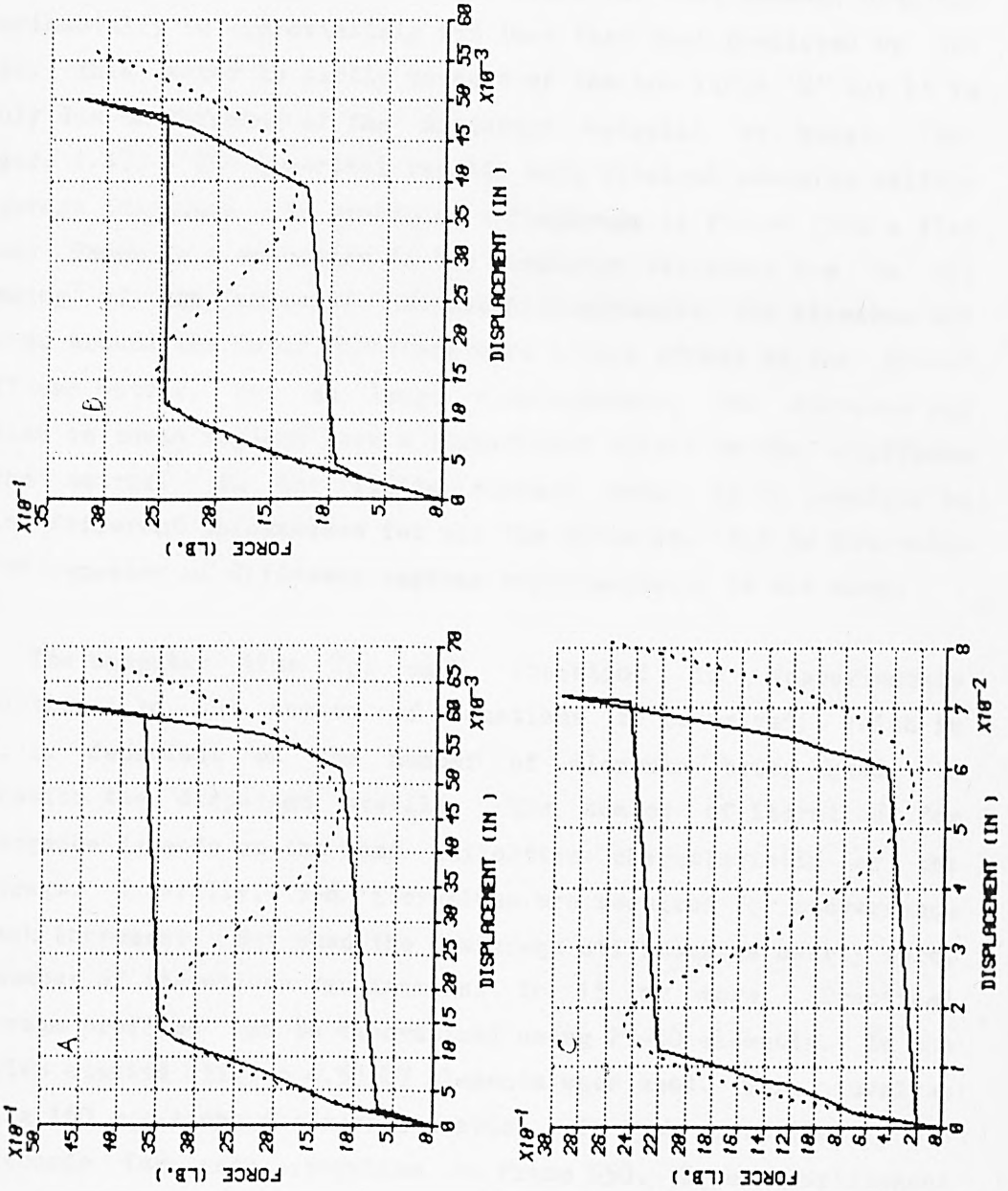

Figure 4.7: Results for point loading

There is a good agreement between experimental and numerical results for all the diaphragms and under pressure as well as point loading. There are errors (at large displacements) between the predicted centre-displacement and that obtained experimentally. The maximum error for 0.006" diaphragms where the displacement obtained experimentally is approximately 15% less than that predicted by the model. This error is partly because of the too large 'B' but it is mainly due to thinning of the diaphragm material at height 'H2' (figure 4.4). The numerical results were obtained assuming uniform diaphragm thickness. In practice, a diaphragm is formed from a flat blank. There is a reduction in the diaphragm thickness due to the 'drawing' of the material. At low displacements, the stresses and strains around the outer curvature have little effect on the global stiffness matrix, but at large displacements, the stresses and strains in these regions have a significant effect on the stiffness of the matrix. In the finite element model, it is possible to define different thicknesses for all the elements. But to determine the thicknesses of different regions experimentally is not easy.

The computer time for each iteration is approximately proportional to the number of equations to be solved; which in turn, is dependent on the number of elements being used to discretize the diaphragm profile. The number of iterations for convergence depends on the load deflection characteristic of the diaphragm. Generally, 5-6 iterations are required for convergence at each increment. But when the diaphragm stiffness is nearly zero, the number of iterations can increase to 15 or more. Practical diaphragm profiles can be discretized using 25-30 elements. In the examples studied (figure 4.5) 27 elements were used. This involves solving 160 equations for each iteration. It took approximately 3.5 CPU seconds for each iteration on Prime 550. Equal displacement increments ($\delta a_m = 0.5xT$) were used in tracing the load deflection curve. The F.E. program determines and stores the peak 'FP' of the characteristic curve. The program then continues and when the load exceeds 'FP', the program (having traced the entire curve) stops.

The number of elements to discretize the diaphragm profiles were determined experimentally. Generally, as the number of elements is increased, the accuracy of the results improves. When further increment of the elements has negligible effect on the

results, the discrete representation of the diaphragm can be assumed satisfactory.

4.3 STRESSES IN DIAPHRAGMS

The load deflection curves for a flat and a convex diaphragm are shown in figures 4.8 and 4.9 respectively. The stresses in the diaphragms corresponding to different equilibrium positions (marked in figures 4.8 and 4.9), are shown in figures 4.10 and 4.11.

Comparison of the stresses in ordinary diaphragms with that of a convex diaphragm is of interest because it gives an insight into the behavior of a snap-action diaphragm.

In both cases, the in-plane stresses (σ_s and σ_θ) are dominant as compared with the bending stresses (M_s and M_θ). In flat diaphragms the sign of stresses does not change as the load increases. However, for equal consecutive increments of the centre-displacement, the in-plane stresses increase at a faster rate, illustrating non-linear stress displacement relationship.

From figure 4.11 it can be seen that hysteresis in convex diaphragms is due to the stress changing from compression to tension, and vice versa. The reduction in the diaphragms stiffness is due to compressive stresses in it. Even though the displacements involved in a snap-action diaphragm are large, the magnitude of stress remains small compared with the yield stress of the material. This is important because it justifies the omission of material non-linearities in the formulation.

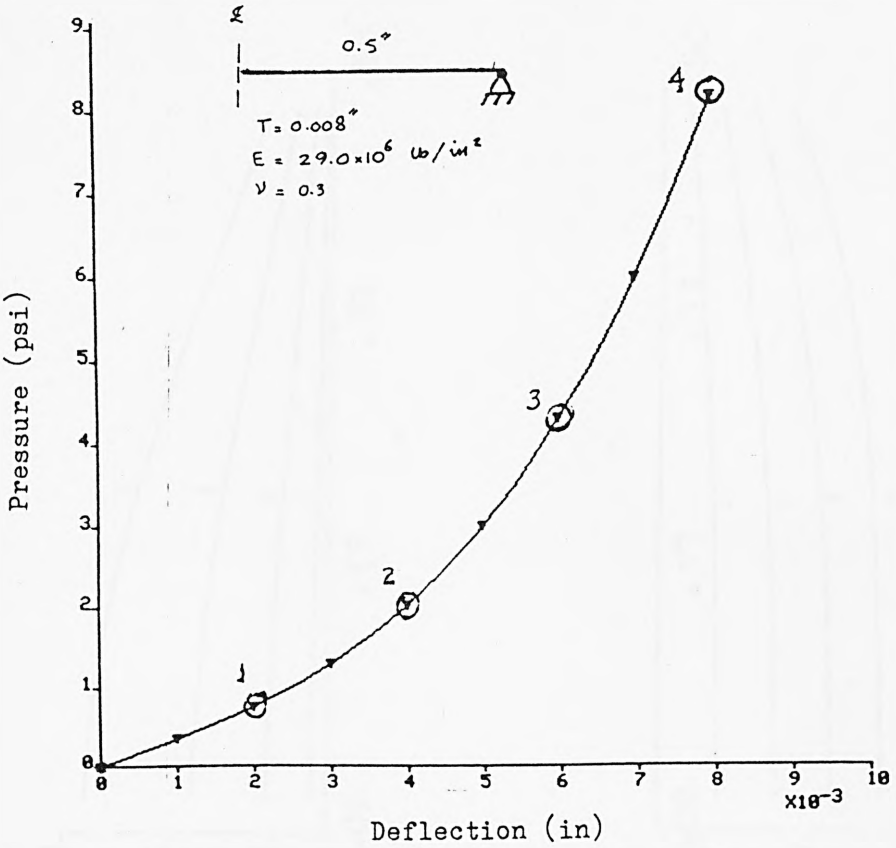

Figure 4.8: Flat diaphragm

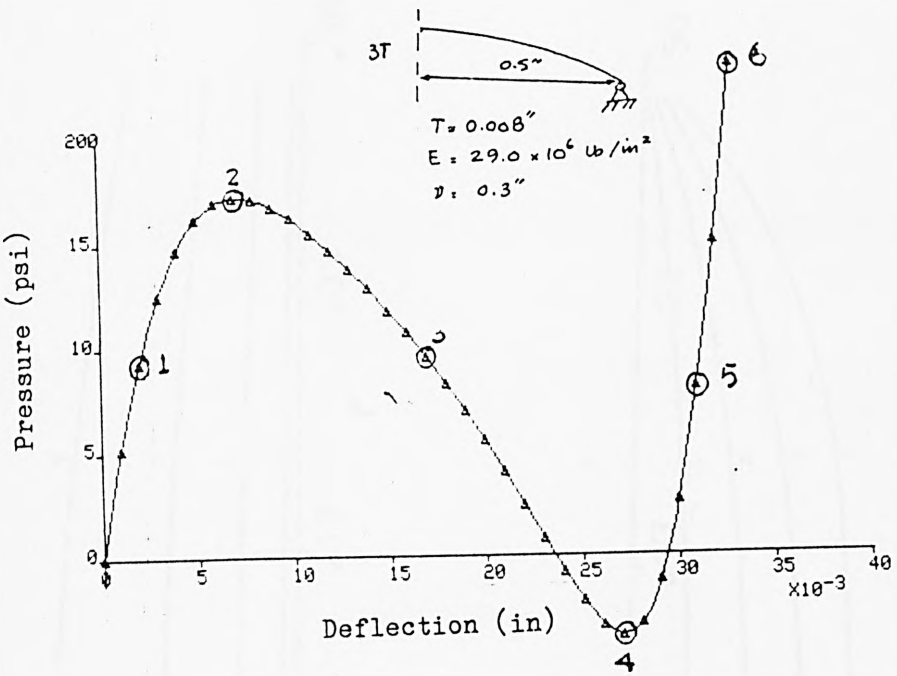

Figure 4.9: Spherical diaphragm

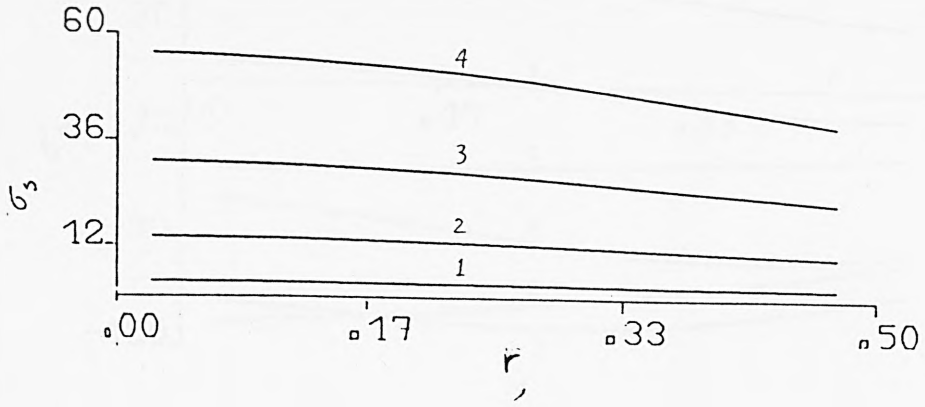
60
36
12
σ_s
4
3
2
1
.00
.17
.33
.50
r

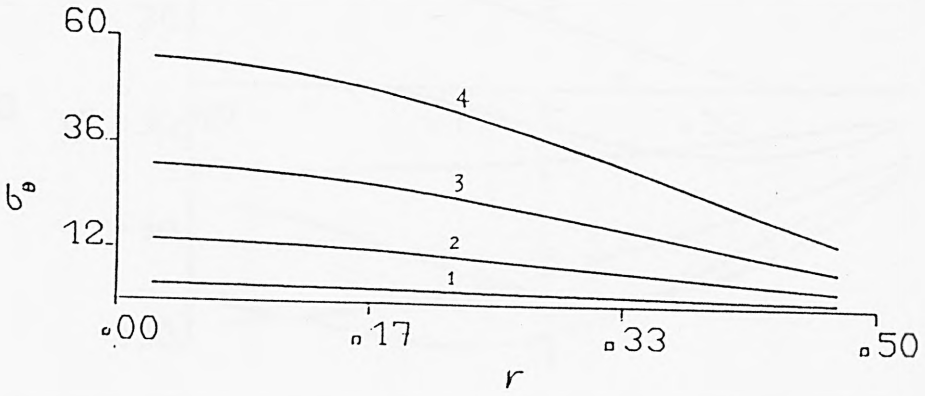
60
36
12
σ_B
4
3
2
1
.00
.17
.33
.50
r

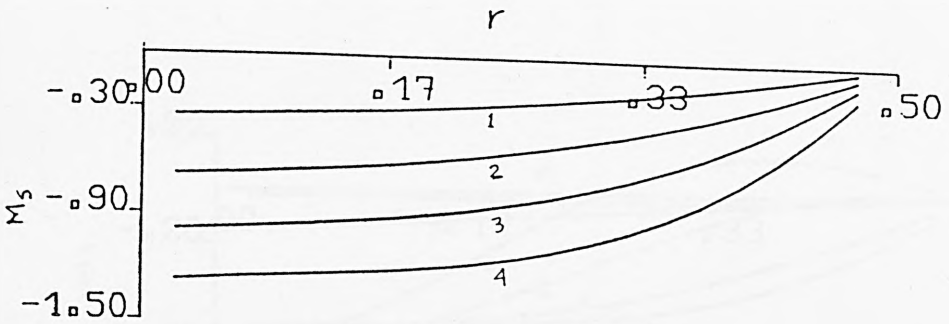
r
-.30
-.90
-1.50
M_s
.00
.17
.33
.50
1
2
3
4

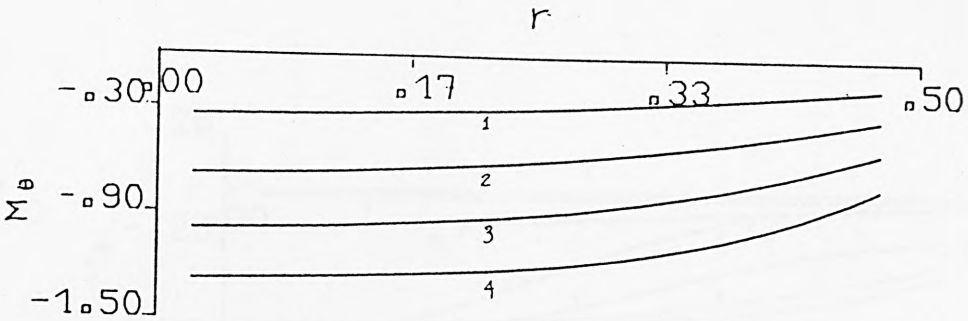
r
-.30
-.90
-1.50
M_B
.00
.17
.33
.50
1
2
3
4

Figure 4.10

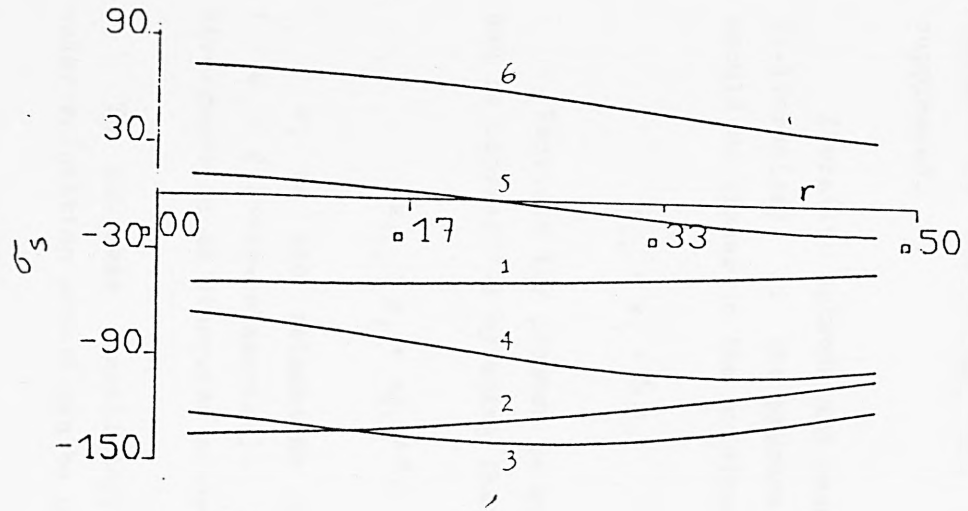
90
30
-30
-90
-150
σ_s
.00
.17
.33
.50
r
1
2
3
4
5
6

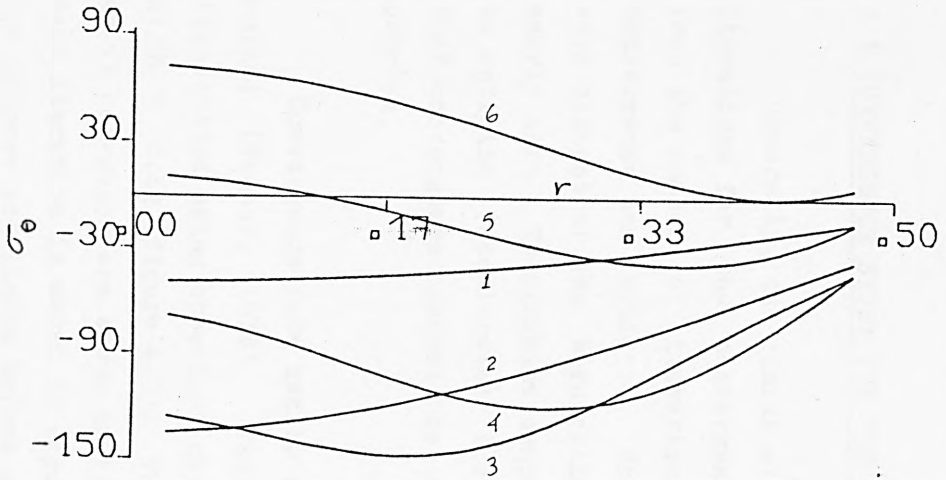
90
30
-30
-90
-150
σ_θ
.00
.17
.33
.50
r
1
2
3
4
5
6

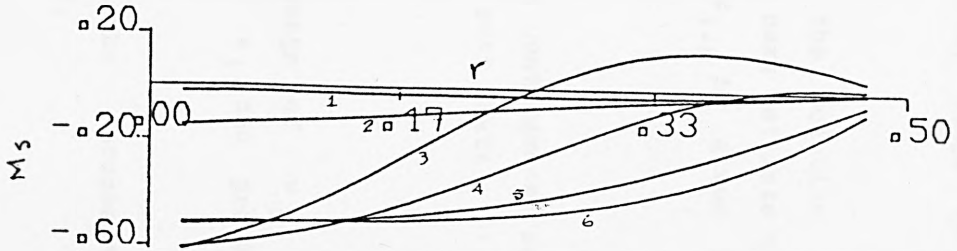
.20
-.20
-.60
M_s
.00
.17
.33
.50
r
1
2
3
4
5
6

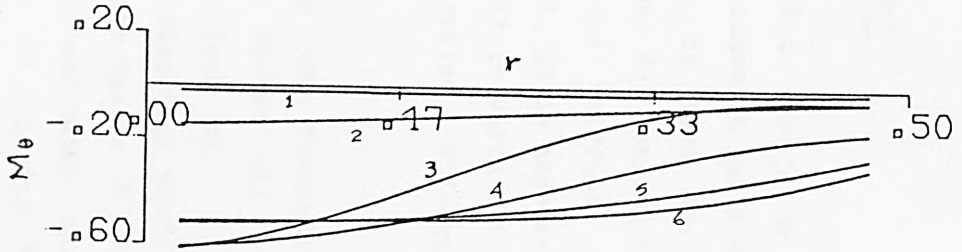
.20
-.20
-.60
M_θ
.00
.17
.33
.50
r
1
2
3
4
5
6

Figure 4.11

4.4 CONVERGENCE STUDY FOR THE TOTAL LAGRANGIAN MODEL

Generally, the finite element model was found to take 5 or 6 iterations for the convergence, but for certain cases it was found that the number of iterations increased to 15 or more before convergence was achieved. The number of iterations for convergence were highest at the bifurcation points, where the stiffness is nearly zero. To minimize computation time and cost, it is necessary to optimize (accelerate) the convergence rate. It is worth noting that convergence cannot be imposed on an otherwise divergent process.

Convergence rate can be accelerated by using the relaxation method (Fenner, 1978). Implementation of the method will be illustrated using spherical cap subjected to ring load at R1/RO = 0.42 (figure 4.3). The variations in the diaphragm profile as it converges are shown in figure 4.12. The update factor 'λ' for each iteration is shown in figure 4.13. Figure 4.13 indicates that the process oscillates before eventual convergence. To minimize the number of iterations, the oscillatory behaviour needs to be suppressed.

Iterative methods are based on estimating the solution x_i (i-iteration). If the process is convergent the next estimate x_{i+1} should be closer to the solution than x_i, where x_{i+1} is given by:

$$x_{i+1} = x_i + \delta x_i$$

Provided the process is convergent, then the convergence rate can be accelerated by using the relaxation method such that:

$$x_{i+1} = x_i + \omega_i \delta x_i$$

w_i is the relaxation factor. Normal range of w_i is $1 < w_i < 2$ (over-relaxation). Larger values of w_i can produce divergence in an otherwise convergent process.

To suppress oscillatory behavior of the processes, under-relaxation method can be used ($0 < w_i < 1$).

Unfortunately it is not simple to predict the optimal value of w. Usually empirical methods are used to estimate w_i (Rahman, 1979).

In the case of a spherical cap, the first estimate of λ from the assumed diaphragm profile 1 (figure 4.12) produces the oscillatory behavior ($\lambda_1 = 378$ and $\lambda_2 = -900$). By using the under-relaxation method ($0 < w_i < 1$) the oscillatory behavior can be suppressed. By experimentation, it was found that $w_1 = 0.5$ would produce the desired effect. The relaxation factor w_i is applied for the first iteration only, such that:

$$\lambda_1 = \lambda_0 + 0.5 \times \delta\lambda_0$$

The effectiveness of the method is evident from figures 4.14 and 4.15. The number of iterations have been reduced from 15 iterations to 5. The accuracy of results is unaffected because it is modified only for one iteration. The method was checked for several other cases and similar results were obtained. However, more work needs to be done to automate the proceedure.

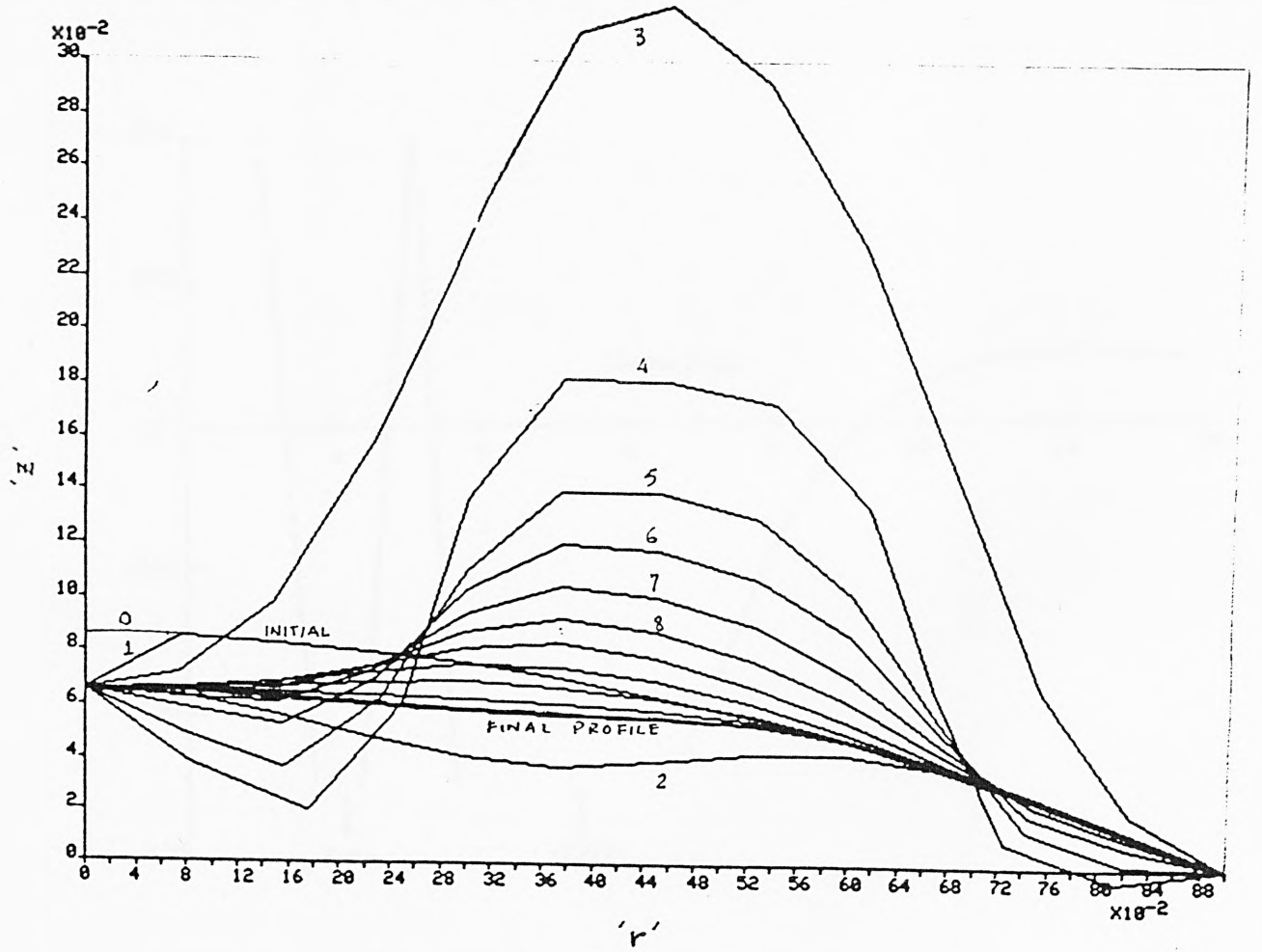
X10-2
30
28
26
24
22
20
18
16
14
12
10
8
6
4
2
0
'z'
0
1
INITIAL
2
3
4
5
6
7
8
FINAL PROFILE
0 4 8 12 16 20 24 28 32 36 40 44 48 52 56 60 64 68 72 76 80 84 88
X10-2
'r'

Figure 4.12

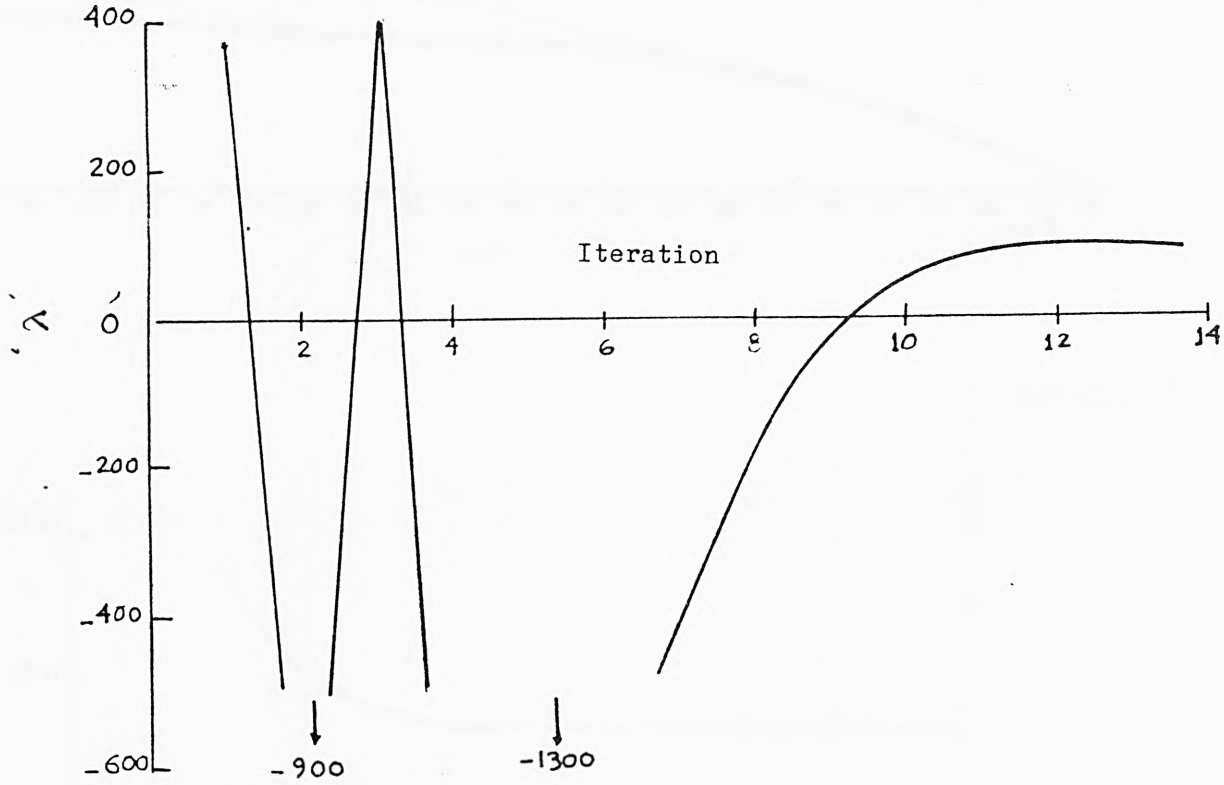

Figure 1.13

Figure 1.14

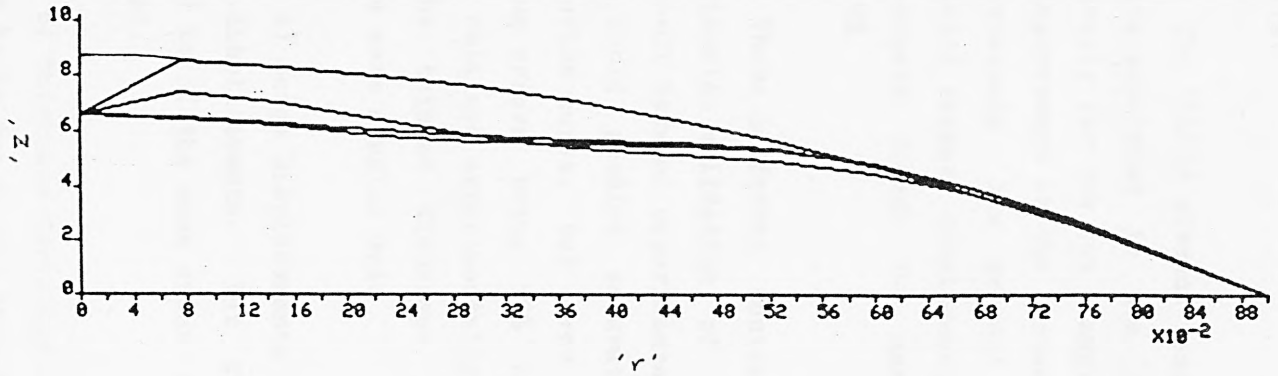

Figure 1.15

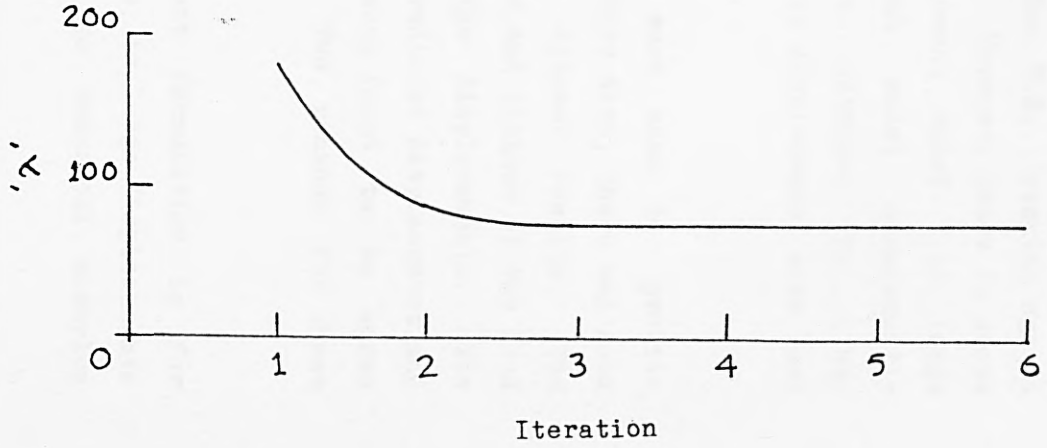

4.9 CONCLUSION

The major part of this Chapter is concerned with the validation of the finite element model.

The analytic model presented by Andreeva was found to be inadequate for the analysis of the snap-action diaphragms. Wide deviations were observed between the finite element and the analytic results.

The finite element results were also compared with numerical results published in the literature. The F.E. results agreed favourably for the two examples considered. However, there is scope for improvement in the present finite element model. At large displacements the present finite element model consistently predicted larger displacements than those obtained by other researchers, though the maximum errors in displacement were less than 5%.

Three different conical diaphragms were used to provide experimental validation of the model. Here also, there was good agreement between experimental and finite element results. The model could predict accurately the maximum and minimum of the load deflection curve, but over estimated large displacements. The maximum errors being 15% between the predicted displacement and those obtained experimentally. The errors were found to be worse for the thinner diaphragm (T = 0.006"). Two reasons for these errors were singled out:

a) Large Displacements - Finite element formulation is for small displacements. But the errors due to large displacements should be of the same order as those in the numerical examples studied.

b) Thickness Variation - The main reason for the errors would appear to be due to the thinning of the diaphragm material. This is supported by the fact that the errors for the thinner diaphragm (T = 0.006") are larger. Because of the percentage change in the thickness, the thinner diaphragm is larger: 'H2' being constant for all the diaphragms (figure 4.4).

Further validation of the model was carried out using two other diaphragms produced by Smith Instruments ltd. Good agreement was found between the experimental and the numerical results.

The study of stress distribution in diaphragms was also carried out. It was found that the in-plane stresses are dominant. For snap-action diaphragms, even though there are large displacements involved, the magnitude of maximum stresses remains small, because the stresses change from compressive to tensile.

In most cases it was found that 5-6 iterations were required for convergence. Occassionally, the number of iterations increased to 20 or more. By using 'under-relaxation' method, the convergence rate could be improved dramatically. For the example illustrated, the number of iterations were reduced from 15 to 6 for convergence. The method has not been automated due to difficulty in determining the optimal factor.

CHAPTER 5

MODEL REFINEMENTS

5.1 INTRODUCTION

Validation of the total Lagrangian finite element model was carried out in the previous chapter. The accuracy of the model was found to deteriorate at large displacements. This is because the formulation requires the shear strain to remain small. This condition is only fulfilled when the displacements are small.

The so called Updated Lagrangian Formulation (U.L.) is introduced in this chapter. In the U.L. formulation, all the incremental solutions are determined with respect to the previous equilibrium state. Therefore, for each incremental solution the displacements remain small.

The convergence properties of the U.L. formulation are also studied in this chapter.

Straight frustrum type elements when used to approximate complex diaphragm profiles (e.g. a corrugated diaphragm) can be very costly in terms of the computer storage and processing time. In such cases, more complex curved elements have an advantage because curved boundaries can be approximated using fewer elements. A finite element formulation using a curved non-linear element is introduced in this chapter.

5.2 LAGRANGE UPDATE METHOD

In chapter 3, a Total Lagrangian Finite Element formulation for the analysis of axi-symmetric diaphragms was presented. Computer implementation of the T.L. formulation is relatively simple because the initial diaphragm profile is used for all the incremental solutions. However, the accuracy of the T.L. formulation deteriorates as the rotation 'B' becomes large. This is because of the Penalty type of constraint imposed, so that ($\beta - \frac{\partial w}{\partial s}$) remains small (chapter 3). The singularity of the

Penalty functional is assured by using reduced integration (integrating at single quadrature point where $(\beta - \frac{\partial w}{\partial s}) \to 0$). To improve the accuracy of the results, 'β' should remain small so that the 'parasitic shear' (Pawsey et.al., 1973) remains small throughout the element and not at the quadrature point only.

To allow for large displacements, the so called Updated Lagrangian formulation (U.L.) can be used (Wood et.al., 1977, Murray et.al., 1969).

Computer implementation of the U.L. formulation is similar to the Eulerian formulation (Zienkiewicz and Nayak, 1971), where the initial position becomes the current equilibrium state prior to some incremental change.

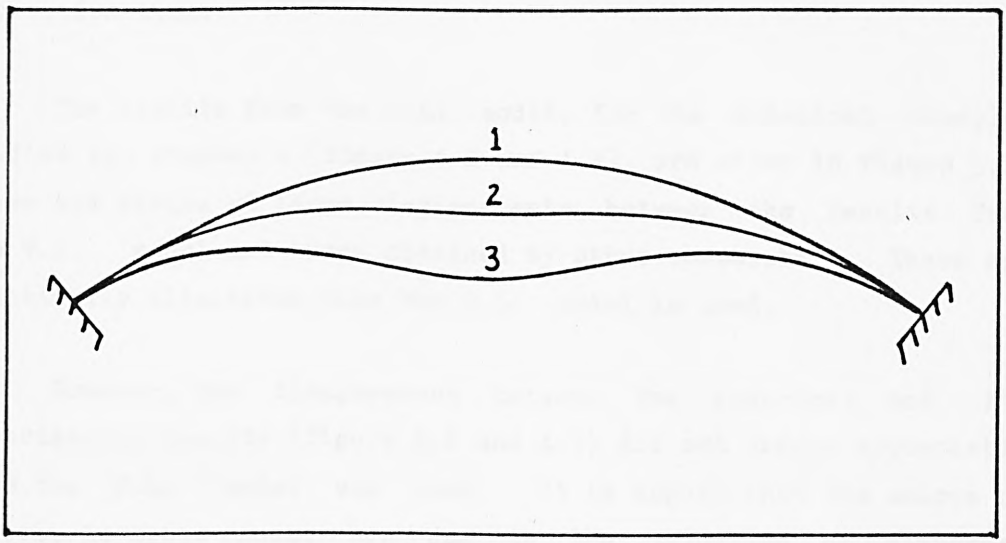

Figure 5.1

To determine the equilibrium position 3 (figure 5.1), the U.L. formulation regards the previous equilibrium state (position 2) as the initial position. Hence, the incremental displacements remain small at any stage. While in the T.L. formulation, state 1 is regarded as the initial position all the time. Conceptually the U.L. formulation is simple but leads to programming complications especially when uniform pressure load is used. The complication arises because:

(a) The diaphragm profile has to be updated prior to new increment.

(b) The updated profile has locked-in stress, hence they have to be included when determining the residual vector:

$$\underline{R} = \int_V \bar{B}^T \sigma \, dV - \lambda \int_V f \, dV$$

(c) The equivalent nodal forces have to be recalculated, at the beginning of each increment, when a uniformly distributed load is applied.

Because of the above mentioned reasons the excecution time for each iteration of the U.L. formulation is relatively longer than the T.L. formulation, but in both cases the solution of the simultaneous equation consumes the major part of the total excecution time.

The results from the U.L. model, for the numerical examples studied in chapter 4 (figure 4.2 and 4.3), are shown in figure 5.2. There are errors at large displacements, between the results from the T.L. model and those obtained by other researchers. These are practically eliminated when the U.L. model is used.

However, the disagreement between the numerical and the experimental results (figure 4.6 and 4.7) did not change appreciably when the U.L. model was used. It is argued that the source of errors, in these cases, are due to the reduction of diaphragm thickness at the outer curvatures and not the large displacements. It is possible to model variable diaphragm thickness at the expense of computation complexity, but because the errors are predictable and not very significant, this was not regarded as necessary.

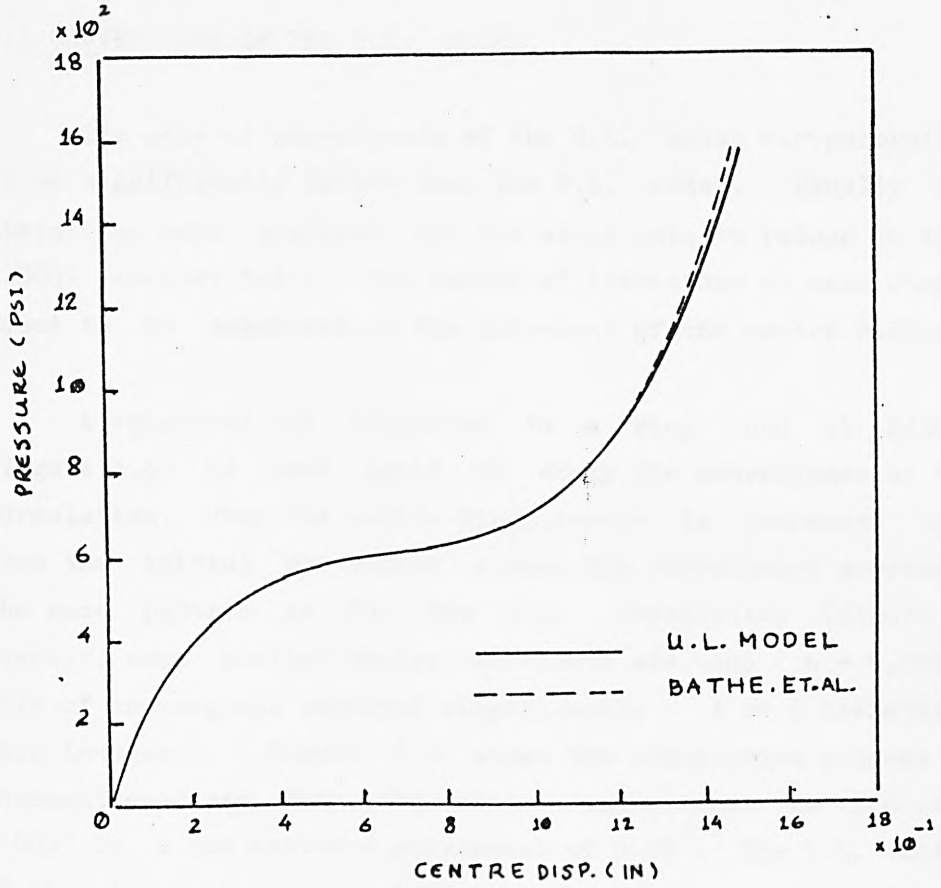

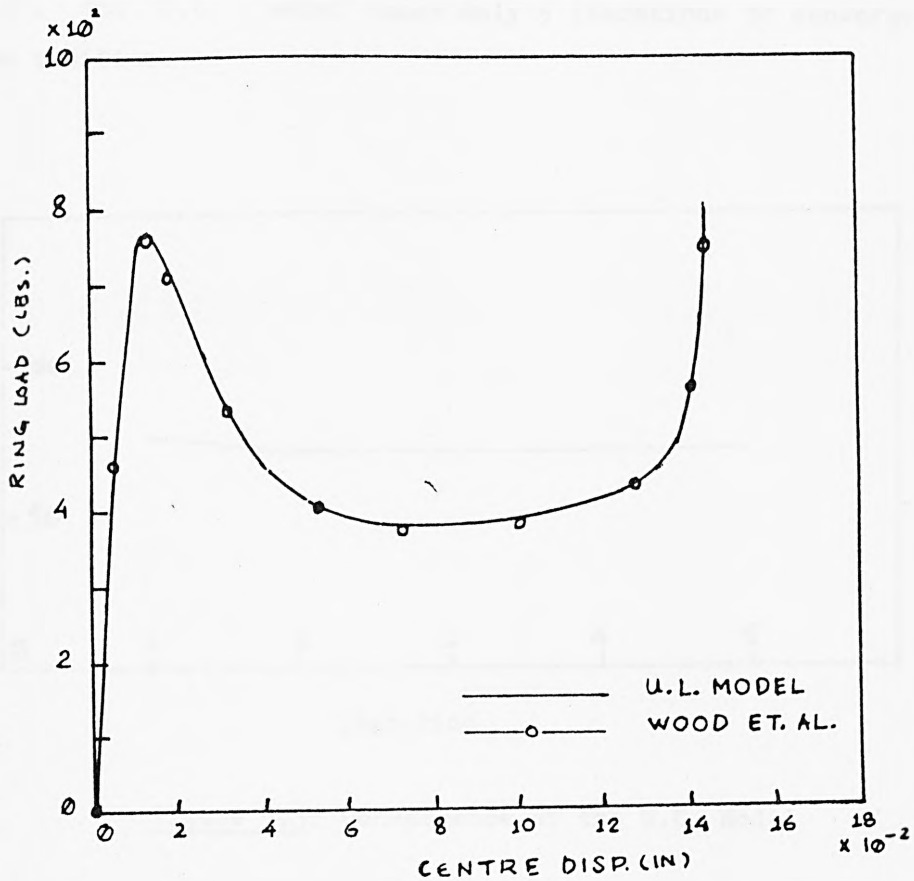

Figure 5.2: Results from U.L. model.

5.3 CONVERGENCE OF THE U.L. MODEL

The rate of convergence of the U.L. model was generally found to be significantly faster than the T.L. model. Usually 4 or 5 iterations were required for the error norm to reduce to less than 0.0001 (chapter 3.6). The number of iterations at each stage were found to be dependent on the increment of the centre-displacement.

A spherical cap subjected to a ring load at R/RO = 0.42 (figure 4.3) is used again to study the convergence of the U.L. formulation. When the centre-displacement is increased by 0.02" from the initial unstrained state, the convergence process showed the same pattern as for the T.L. formulation (figure 4.12). However, when smaller centre-increments are used (a = 0.005"), the rate of convergence improved significantly : 4 or 5 iterations for each increment. Figure 5.3 shows the convergence process for the forementioned cap, when the centre-displacement is increased by 0.005" to a new centre-displacement of 0.02". The T.L. model took 15 iterations to converge (figure 4.13) to a centre-displacement of 0.02". The U.L. model takes only 5 iterations to converge to the same position.

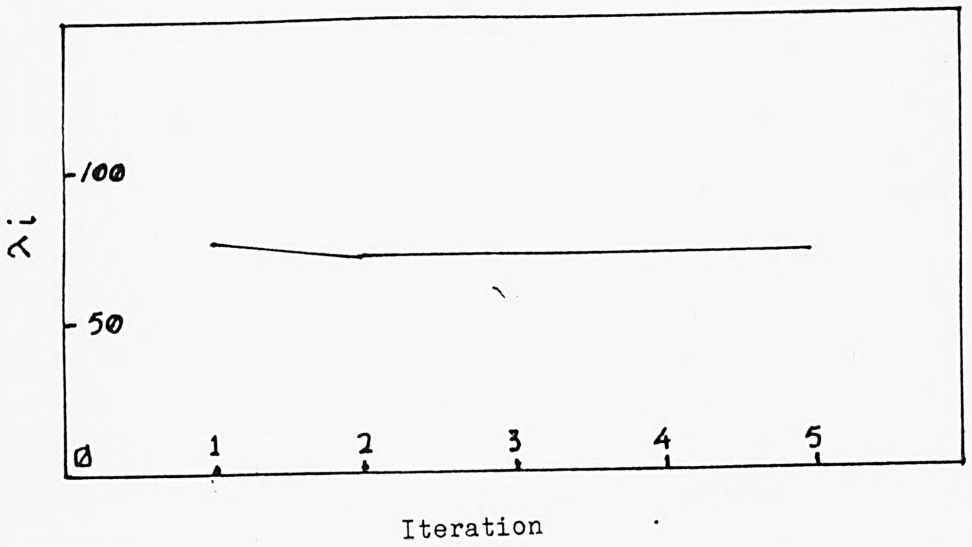

Figure 5.3: Convergence of the U.L. Model

The improvement in the convergence rate is not so dramatic for all the cases. But generally it was found that the U.L. model takes 40% less excution time than the T.L. model in tracing the load-deflection characteristic of a diaphragm.

5.4 ATTEMPTED USE OF A NON-LINEAR AND CURVED ELEMENT

Curved elements have an advantage over straight elements when approximating diaphragms of complex profile, for example, corrugated diaphragms. The obvious reason being that fewer curved elements are required to discretize a curved geometry.

The quadratic interpolation functions (SERC,1982) for a three noded line element (figure 5.4) are given by equation 5.1.

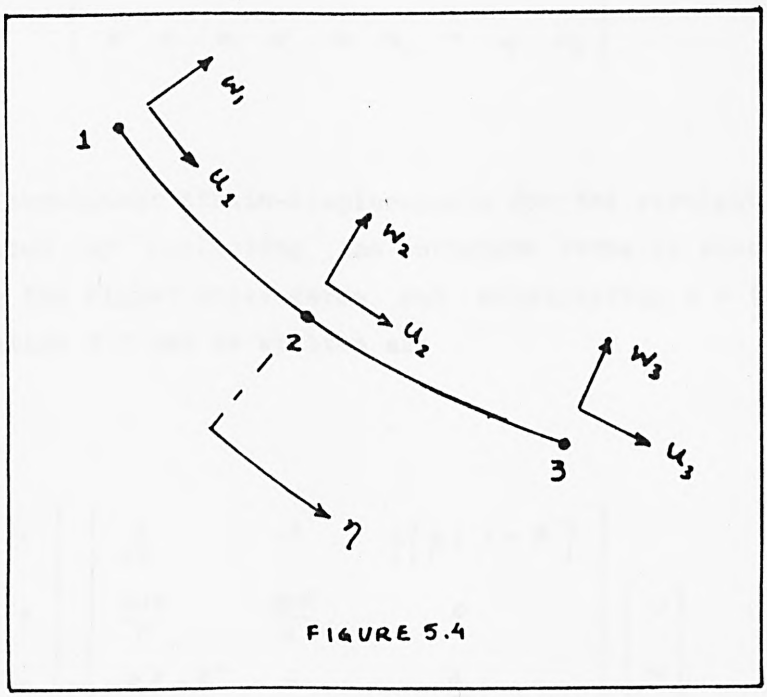

FIGURE 5.4

$$N_1 = \eta(\eta - 1)/2.0$$
$$N_2 = 1 - \eta^2 \qquad (5.1)$$
$$N_3 = \eta(\eta + 1)/2.0$$

The nodal displacements are given by:

$$\underline{a}_{i=1,3} = \begin{bmatrix} u_i & w_i & \beta_i \end{bmatrix}^T$$

Anywhere within the element, the displacements are given by:

$$\hat{u} = \underline{N}\,\underline{a}$$

where

$$\underline{N} = \begin{bmatrix} N_1 & 0 & 0 & N_2 & 0 & 0 & N_3 & 0 & 0 \\ 0 & N_1 & 0 & 0 & N_2 & 0 & 0 & N_3 & 0 \\ 0 & 0 & N_1 & 0 & 0 & N_2 & 0 & 0 & N_3 \end{bmatrix}$$

The non-linear strain-displacements for the straight elements were obtained by neglecting the curvature terms in equation 3.1 . Neglecting the higher order terms and substituting $B = \frac{\partial w}{\partial s}$ (chapter 3.5), equation 3.1 can be written as:

$$\begin{bmatrix} \varepsilon_s \\ \varepsilon_\theta \\ \chi_s \\ \chi_\theta \\ \gamma_{sz} \end{bmatrix} = \begin{bmatrix} \frac{\partial}{\partial s} & -\phi' & \frac{1}{2}\left[\beta + 2u\phi'\right] \\ \frac{\sin\phi}{r} & \frac{\cos\phi}{R} & 0 \\ -\phi'\frac{\partial}{\partial s} - \phi'' & 0 & -\frac{\partial}{\partial s} \\ -\frac{\phi'\sin\phi}{r} & -\frac{\sin\phi}{r}\cdot\frac{\partial}{\partial s} & -\frac{1}{2}\frac{\cos\phi}{r}\cdot\beta \\ 0 & \frac{\partial}{\partial s} & -1 \end{bmatrix} \begin{bmatrix} u \\ w \\ \beta \end{bmatrix} \qquad (5.2)$$

where:

$$\phi' = \frac{\partial \phi}{\partial s}$$

$$\phi'' = \frac{\partial^2 \phi}{\partial s^2}$$

Separating the linear and the non-linear part of the above equation, the strain-displacement relations can be written as:

$$\varepsilon = \varepsilon_0 + \varepsilon_L$$

$$= \underline{B}_0 \underline{a} + \frac{1}{2} \underline{B}_L \underline{a}$$

$$B_0 = \begin{bmatrix} \frac{\partial}{\partial s} & -\phi' & 0 \\ \frac{\sin\phi}{r} & \frac{\cos\phi}{r} & 0 \\ -\phi' \frac{\partial}{\partial s} - \phi'' & 0 & -\frac{\partial}{\partial s} \\ -\frac{\phi'}{r} \cdot \sin\phi & -\frac{\sin\phi}{r} \cdot \frac{\partial}{\partial s} & 0 \\ 0 & \frac{\partial}{\partial s} & -1 \end{bmatrix} \qquad (5.3)$$

$$B_L = \begin{bmatrix} 0 & 0 & \beta + 2u\phi' \\ 0 & 0 & 0 \\ 0 & 0 & 0 \\ 0 & 0 & -\frac{\cos\phi}{r} \cdot \beta \\ 0 & 0 & 0 \end{bmatrix} \qquad (5.4)$$

Ø' and Ø" are given by the following equations (Zienkiewicz, 1977):

$$\phi' = \frac{\partial \phi}{\partial s} = \frac{\partial \phi / \partial \eta}{\partial s / \partial \eta}$$

$$\phi'' = \frac{\partial^2 \phi}{\partial s^2} = \frac{\frac{\partial^2 \phi}{\partial \eta^2} \cdot \frac{\partial s}{\partial \eta} - \frac{\partial \phi}{\partial \eta} \cdot \frac{\partial^2 s}{\partial \eta^2}}{\left(\frac{\partial s}{\partial \eta}\right)^3}$$

$$\frac{\partial^2 \phi}{\partial \eta_2} = \sum_{i=1}^{3} \frac{\partial^2 N_i}{\partial \eta^2} \cdot \phi_i$$

$$\frac{\partial s}{\partial \eta^2} = \sqrt{\left(\frac{\partial R}{\partial \eta}\right)^2 + \left(\frac{\partial z}{\partial \eta}\right)^2}$$

$$\frac{\partial^2 s}{\partial \eta^2} = \frac{\frac{\partial^2 r}{\partial \eta^2} + \frac{\partial^2 z}{\partial \eta^2}}{\sqrt{\left(\frac{\partial r}{\partial \eta}\right)^2 + \left(\frac{\partial z}{\partial \eta}\right)^2}}$$

The rest of the formulation is straight forward and follows the same procedure as for the straight and linear element (chapter 3). Suitable modifications were made in the existing finite element (total Lagrangian) program. Due to the modular nature of the finite element program, the modifications were relatively simple to make. The pre-processor had to be modified accordingly.

The numerical examples used to validate the finite element model (chapters 4 and 5) with linear frustrum element, were used again to check the behavior of non-linear curved elements. For a given centre-displacement, the load predicted by the 'curved element' models were found to be much higher than those predicted by the other models, ie. the stiffness matrix becomes over-stiff.

There are two basic differences between the present model and the other models:

(1) The use of quadratic interpolation function

(2) Inclusion of the curvatures in the strain-displacement matrix

To single out the cause of the error, each addition was checked separately. By setting the curvatures Ø' and Ø'' to zero, the effect of the 3 noded quadratic element can be investigated. The results obtained from the model with these modifications, were similar to those produced by the other models. Hence, it can be assumed the errors are not due to the interpolation functions.

The relationship between Ø' and the radius of the curvature 'Rs' (figure 5.6) is given by:

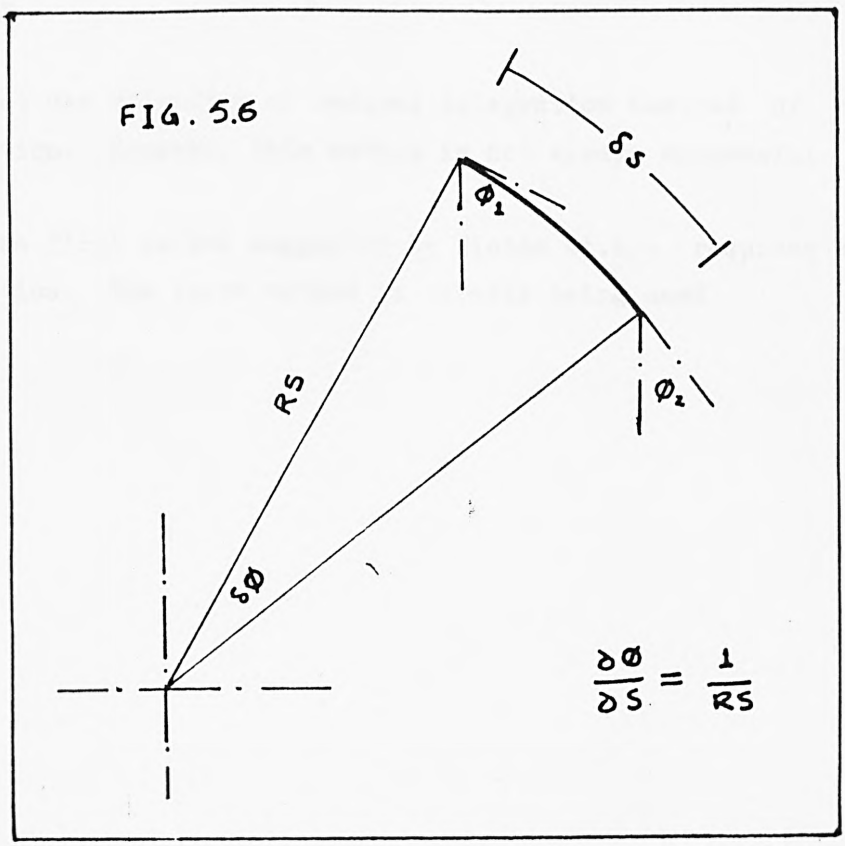

For a spherical cap, used to test the model, the radius of curvature 'Rs' is a known constant, and Ø'' is zero. The program was found to determine Ø' and Ø'' correctly.

A possible explanation for the spurious results could be due to the 'locking' of the elements. Hinton et.al.(1978) encountered the problem when analysing thin plates using conventional displacement-based finite element method. Penalty function terms which occur in the total potential energy functional are regarded as the cause of the over-stiff matrix. In extreme cases, the constraint imposition leads to the deterioration of the stiffness matrix and causes locking.

The techniques suggested by Hinton et.al. for avoiding locking are:

(a) Formulation based on functionals with no penalty terms should be adopted.

(b) Imposing constraints associated with the penalty terms directly at the integration points at the element level prior to assembly.

(c) Use selective or reduced integration instead of complete integration. However, this method is not always successful.

The first method suggested by Hinton et.al. requires complete reformation. The third method is already being used.

5.5 CONCLUSION

The updated Lagrangian formulation removes any restrictions on the large displacements. The disagreements observed between the results obtained from the total Lagrangian formulation and those published in the literature were practically eliminated with the U.L. formulation. However, the errors at large displacements, between the experimental and numerical results could not be improved significantly. The source of errors in these results are not due to the large displacements but because of the thickness variations in the diaphragms. There is a reduction in the diaphragm thickness at the outer curvature when it is press-formed from a flat blank. The numerical results are based on the assumption that the diaphragm thickness remains constant over the entire diaphragm geometry.

Significant improvement in the convergence rate was observed with the U.L. formulation. Using U.L. model, it is estimated that the load-deflection curve of a diaphragm can be determined in half the time taken by the T.L. model.

A curved non-linear element has also been introduced in this chapter. Curved elements are attractive because they can approximate complex diaphragm profiles more economically. Unfortunately, spurious results were obtained when the curved elements were used. The source of the errors is assumed to be due to the locking phenomena in the elements.

CHAPTER 6

PARAMETRIC REPRESENTATION AND SENSITIVITY ANALYSIS

6.1 INTRODUCTION

In the previous chapters it was shown that the Finite Element model can be used to predict accurately the load deflection characteristic of a diaphragm. In this chapter, investigations are carried out to determine the effect of the diaphragm form and the dimensions on its behavior. This investigation is essential so that a methodology for the diaphragm design can be established. The study is carried out in three different stages:

(1) Classification of axi-symmetric diaphragms: There are three types of axi-symmetric diaphragms that could be studied (corrugated, conical, and spherical). For the present study, only conical and spherical types of diaphragms are considered.

(2) Parametric Representation: The diaphragm profile can be described with a set of geometric parameters. This helps to investigate the effect of the diaphragm profile on its performance.

(3) Sensitivity Analysis: The analysis determines which geometric parameters have significant effect on its behaviour. Further investigations can then be carried out to establish a design procedure using these 'important parameters'. Quantitative results from the analysis can be used to impose manufacturing tolerances on the parameters so that the design complies with the specifications.

Results of sensitivity analysis for the two types of diaphragms, subjected to uniformly distributed pressure and concentrated load, are presented in this chapter. Ring type of loading is not considered because generally it is of no practical interest.

6.2 PARAMETRIC REPRESENTATION OF A CONICAL DIAPHRAGM

A diaphragm is termed conical if its major load carrying section can be defined with a straight line (figure 6.1) . The diaphragm may or may not have a centre-boss.

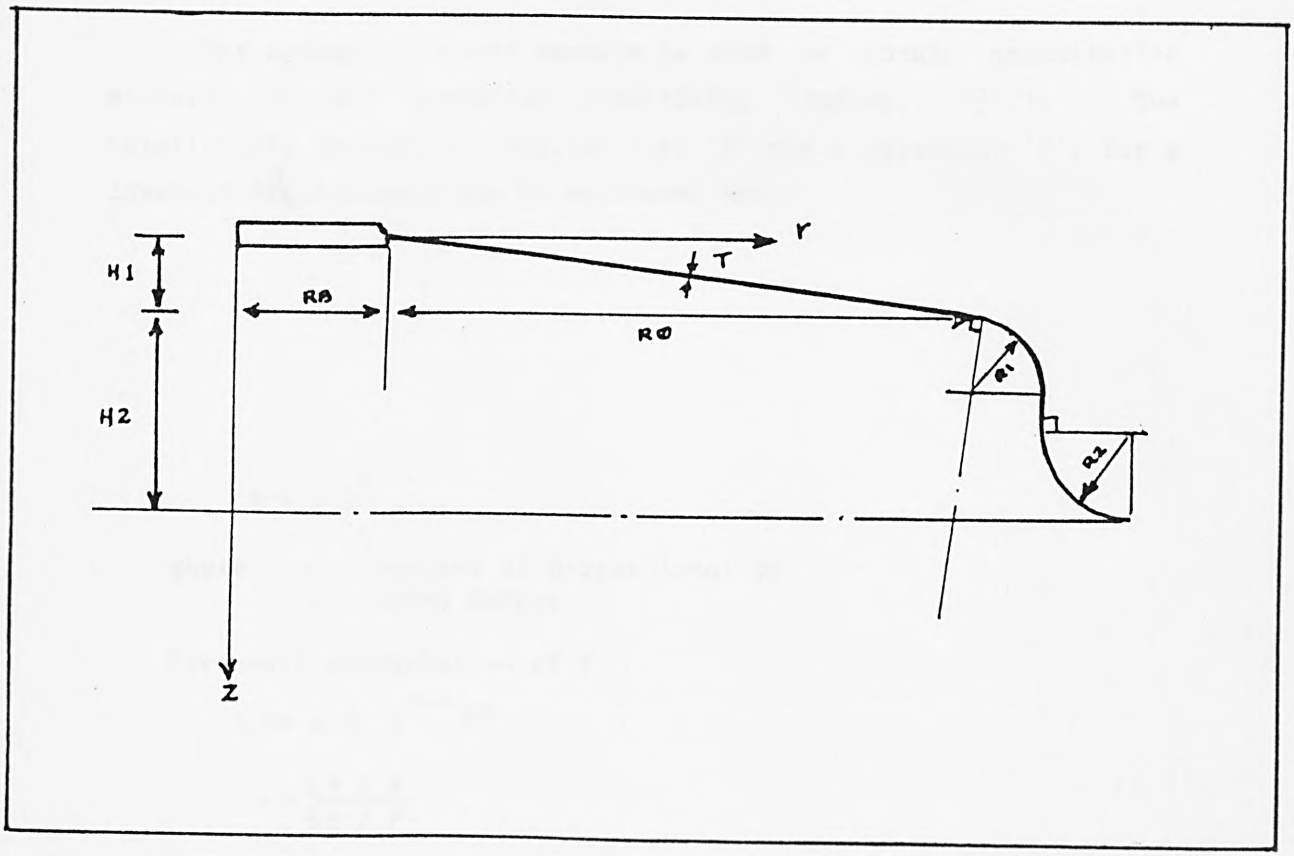

Figure 6.1

A pre-processor has been developed which uses the parameters shown in figure 6.1 to generate and discretize the diaphragm profile. If RB = 0.0, discretized data for a conical diaphragm without a centre-boss is produced.

6.3 SENSITIVITY ANALYSIS FOR A CONICAL DIAPHRAGM

Sensitivity tests were carried out by consecutive perturbation of the parameters describing a conical diaphragm. Each parameter in turn was increased by 10% while keeping others constant. The effect of variation of material properties is investigated by considering Youngs Modulus (E) as an independent parameter.

The concept of index numbers is used to obtain quantitative measure of the parameter sensitivity (Turley, 1977). The relationship between the applied load 'F' and a parameter 'P', for a constant displacement can be expressed as:

$$F = C.P^{n}$$

where C - contant of proportionality
n - index number

For small perturbation of P

$$\delta F = n.C.\ P^{n-1}.\delta P$$

$$n = \frac{\delta F / F}{\delta P / P} \qquad (6.1)$$

n = 0 implies that the parameter 'P' does not have any effect on the load 'F'. Index numbers 'n1' and 'n2' are calculated at the maximum amd the minimum of the load-deflection curve of a diaphragm.

The nominal values of the parameters used for the analysis are:

RB = 0.2 "
RO = 0.7"
R1 = 0.07"
R2 = 0.07" (6.2)
H1 = 0.028"
H2 = 0.14"
T = 0.007"
E = 2.9E6 lbs/sq in.

The profile of the diaphragm generated by the pre-processor for the above parametric values is shown in figure 6.2.

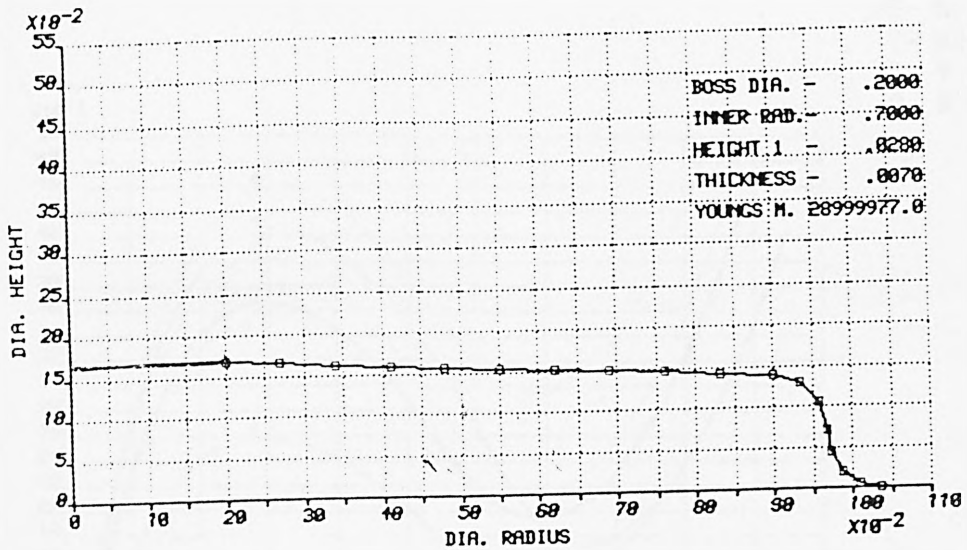

Figure 6.2

The results for the sensitivity tests are shown graphically and in tabular form for the index numbers (figures 6.3, 6.4, and table 6.1 respectively).

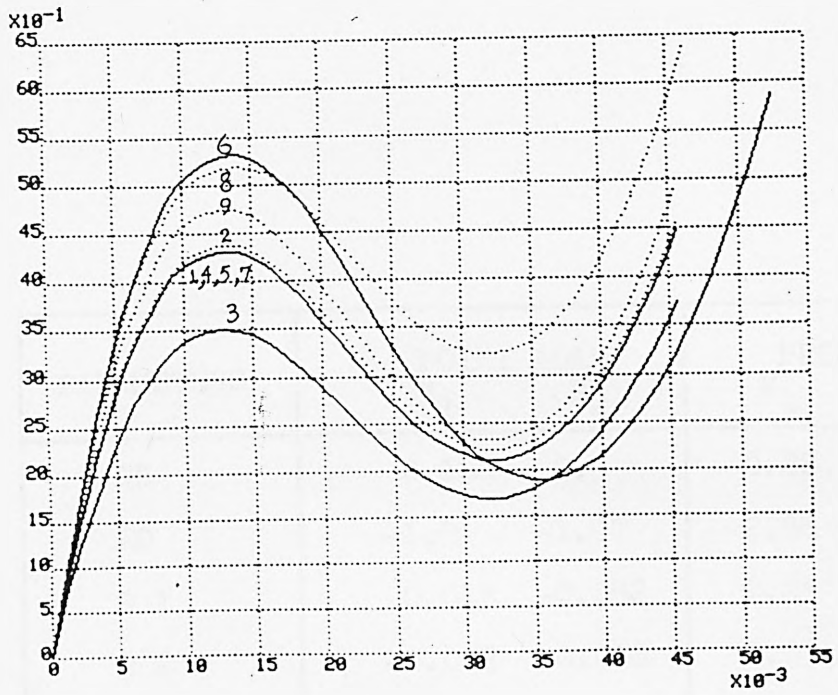

1- Initia.
2- RB
3- RO
4- R1
5- R2
6- H1
7- H2
8- T
9- E

Figure 6.3:Sensitivity for point loading

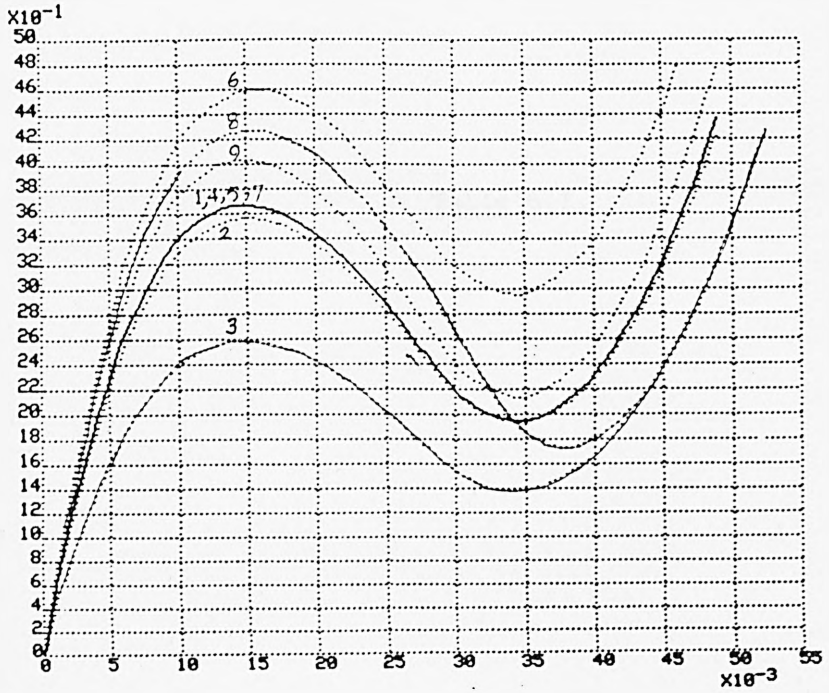

Figure 6.4:Sen s itivity for pressure loading

PARAMETERS	POINT LOAD N_1	N_2	PRESSURE N_1	N_2
RB	0.168	0.5	-0.28	-0.06
RO	-1.9	-1.97	2.96	-2.97
R 1	0.015	-0.082	0.05	-0.01
R 2	-0.002	-0.018	0.03	-0.01
H 1	2.36	-0.011	1.628	1.6
H 2	0.003	-0.02	-0.04	-0.01
T	1.98	5.35	1.95	4.39
E	1.00	1.00	1.0	1.0

Table 6.I

The results of the sensitivity analysis for a conical diaphragm without a centre-boss were very similar to those with a centre-boss.

The important parameters deduced from figures 6.3 and 6.4, and table 6.1 are:

H1, RO, RB, T, E

6.4 PARAMETRIC REPRESENTATION OF A SPHERICAL DIAPHRAGM

A diaphragm is categorized as spherical if its major load bearing part can be generated by using an arc of an appropriate radius. Generally, industrial diaphragms are a hybrid of the conical and spherical types. Study of hybrid diaphragms is not feasible because of the infinite combinations possible.

The profile of a spherical diaphragm can be generated using the parameters shown in figure 6.5.

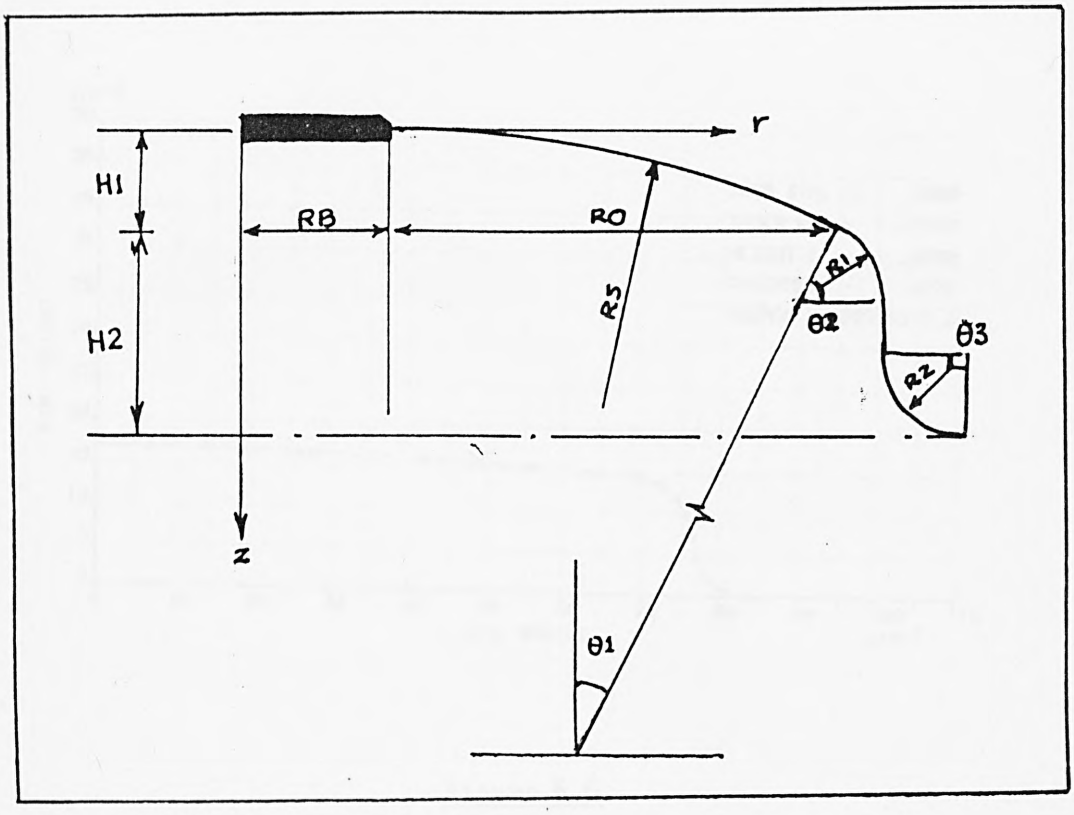

Figure 6.5

where $RS = (R\phi^2 + H1^2) / (2.\phi \times H1)$

$\theta 1 = ATAN\ (R\phi / (R\phi - H1))$

$\theta 2 = \pi/2.\phi - \theta 1$

$\theta 3 = \pi / 2.\phi$

Discretized data for a spherical diaphragm can be generated using the above information. Figure 6.6 shows the profile generation and discretization of such a diaphragm produced by the pre-processor. The parametric values are the same as for a conical diaphragm, and are given by 6.2 .

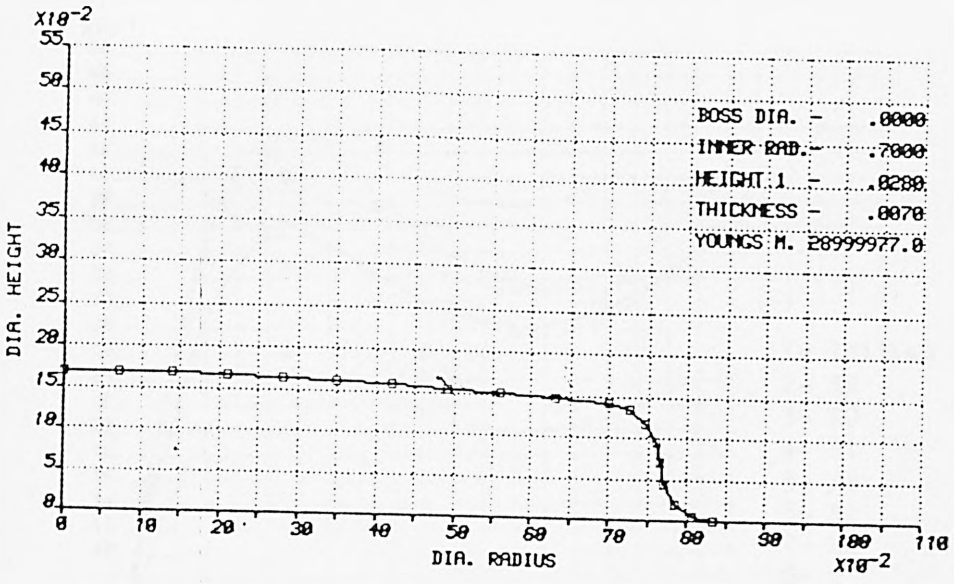

Figure 6.6

6.5 SENSITIVITY ANALYSIS FOR A SPHERICAL DIAPHRAGM

Results of sensitivity tests for a spherical diaphragm subjected to pressure load are presented in this section. A spherical diaphragm does not show bifurcation for a point load applied at the centre. This is because of the small initial slope in the diaphragm profile, even for large 'H1'.

When a point load at the centre is applied, tensile inplane stresses are produced. The instability in diaphragms occur due to the inplane compressive forces. A suitable ring type loading can produce instability in spherical diaphragms but this is of little practical use and therefore ignored for the sensitivity analysis.

Results of sensitivity analysis for a spherical diaphragm with centre-boss and without centre-boss under pressure loading are presented on the following pages. Index numbers 'n1' and 'n2' were determined using equation 6.1, at the peak and trough positions of the load-deflection curve.

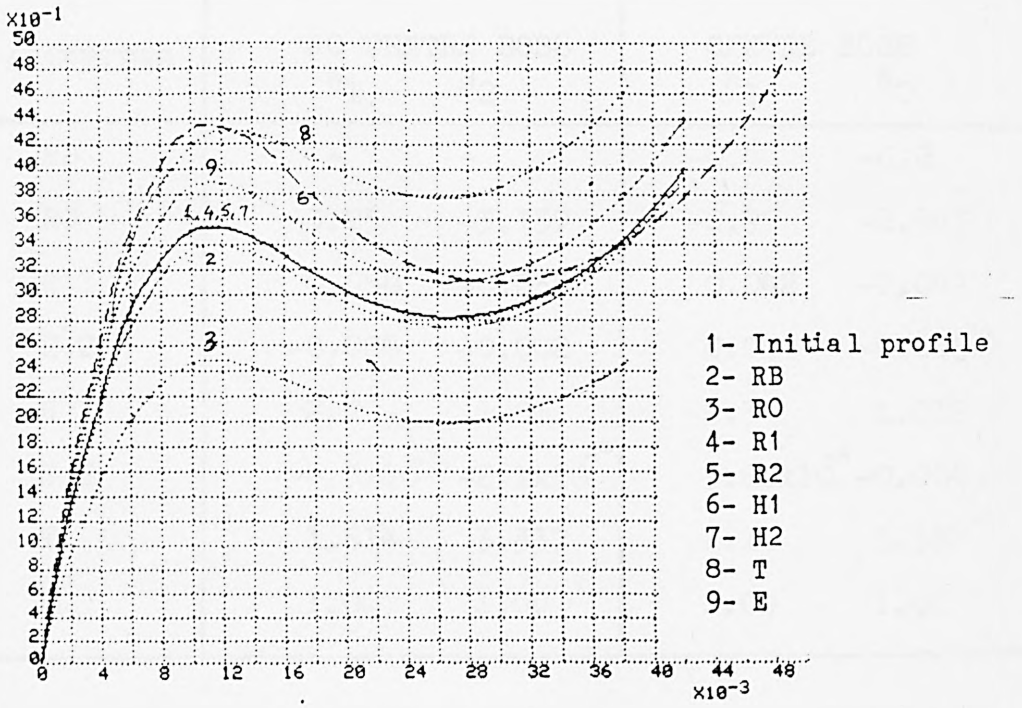

Figure 6.7

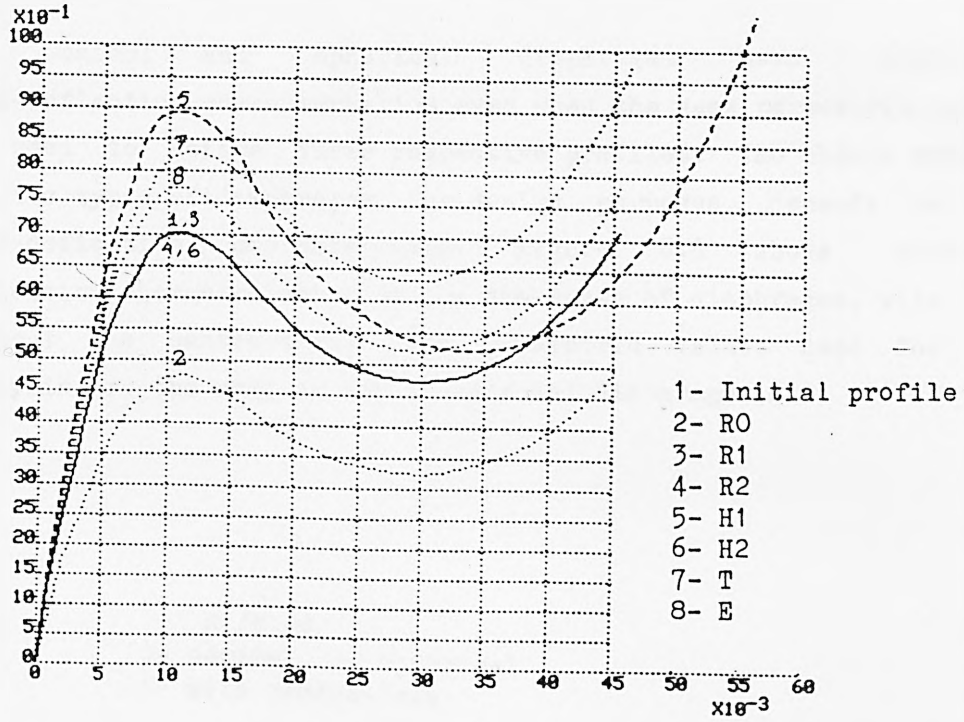

Figure 6.8

PARAMETERS	NO CENTRE BOSS N_1	NO CENTRE BOSS N_2	CENTRE BOSS N_1	CENTRE BOSS N_2
RB	-	-	-0.4	-0.2
RO	-3.25	-3.157	-2.97	-2.945
R 1	0.058	-0.035	0.042	-0.041
R 2	-0.006	-0.002	0.004	-0.005
H 1	2.7	1.01	2.3	1.016
H 2	-4.3×10^{-4}	-2.1×10^{-4}	5.66×10^{-4}	-0.004
T	1.814	3.337	2.18	3.35
E	1.00	1.00	1.00	1.00

Table 6.2

6.6 COMPARATIVE STUDY OF THE TWO TYPES OF DIAPHRAGMS

Conical and spherical diaphragms have different load-deflection characteristics even when the same parametric values are used to define their respective profiles. The choice between the two types of diaphragms, for design purposes, depends on the load-deflection characteristic. Figure 6.9 shows pressure deflection characteristics of the two types of diaphragms, with and without the centre-boss. The parametric values used for the analysis are the same as for the conical diaphragm (6.2) .

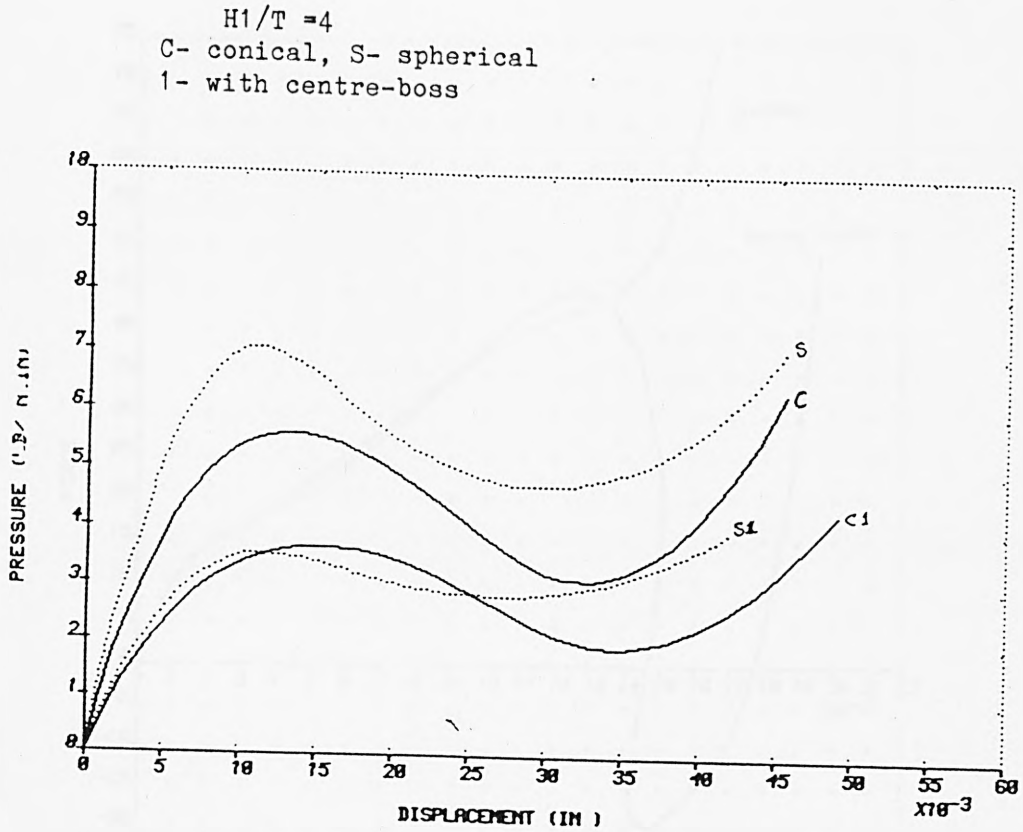

Figure 6.9

6.7 BOUNDARY CONDITIONS

The effects of different boundary conditions on the diaphragm behavior are investigated in this section. A dome shape diaphragm, clamped at the perimeter, does not show any hysteresis when subjected to a point load at the centre (figure 4.3). However, when the diaphragm is allowed to rotate at the perimeter (simple support), the diaphragm shows marked hysteresis (figure 6.10)

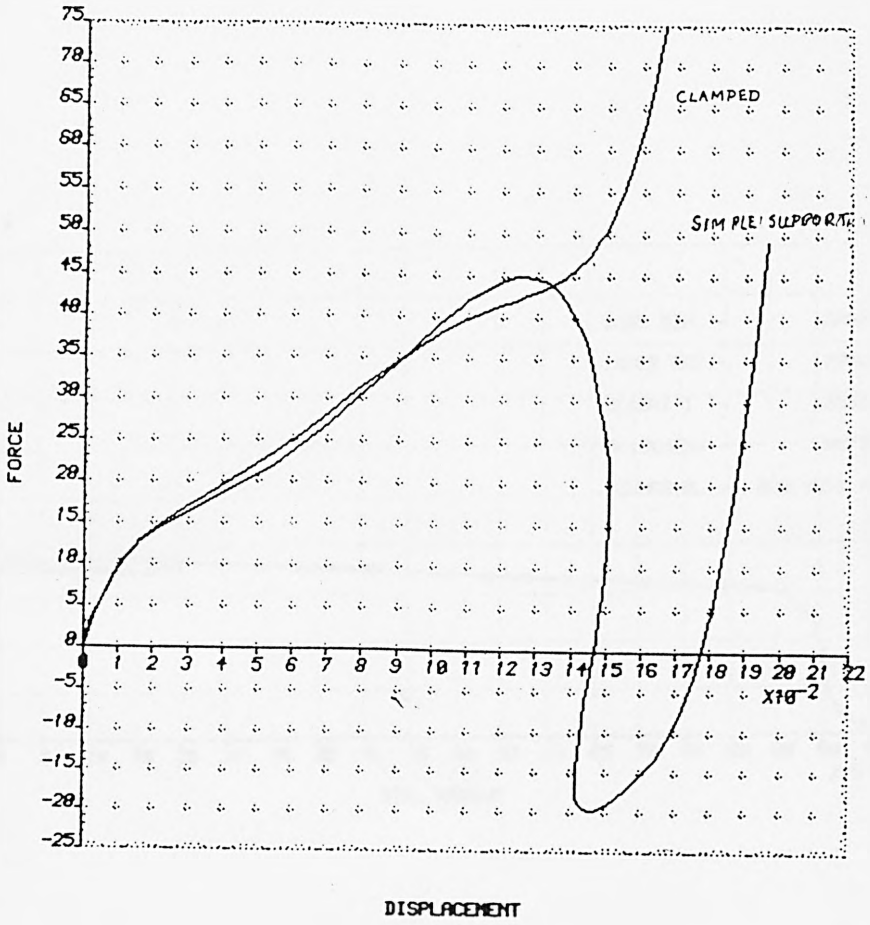

Figure 6.10

Industrial diaphragms have more complex profiles (figures 6.2 and 6.6). Figure 6.11 shows the discretized profile of such a diaphragm. The different boundary conditions for which the diaphragm (figure 6.11) was tested are:

a. Clamped at position 1

b. Simply supported at position 1

c. Clamped at position 2

d. Simply supported at position 2

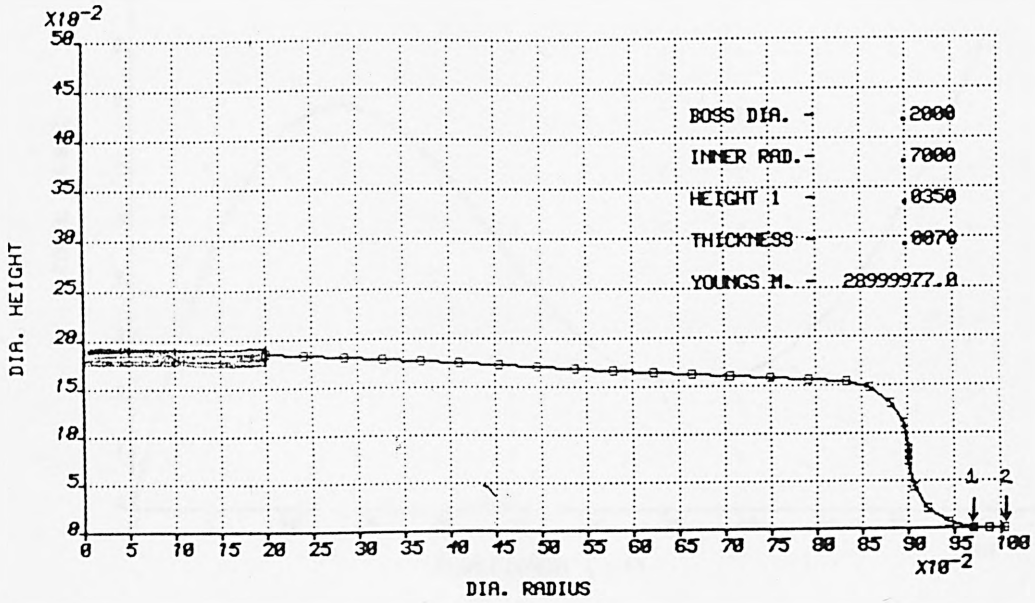

Figure 6.11

Results of the test (figure 6.12) indicate that the different boundary conditions have negligible effect on the load deflection characteristic of such a diaphragm.

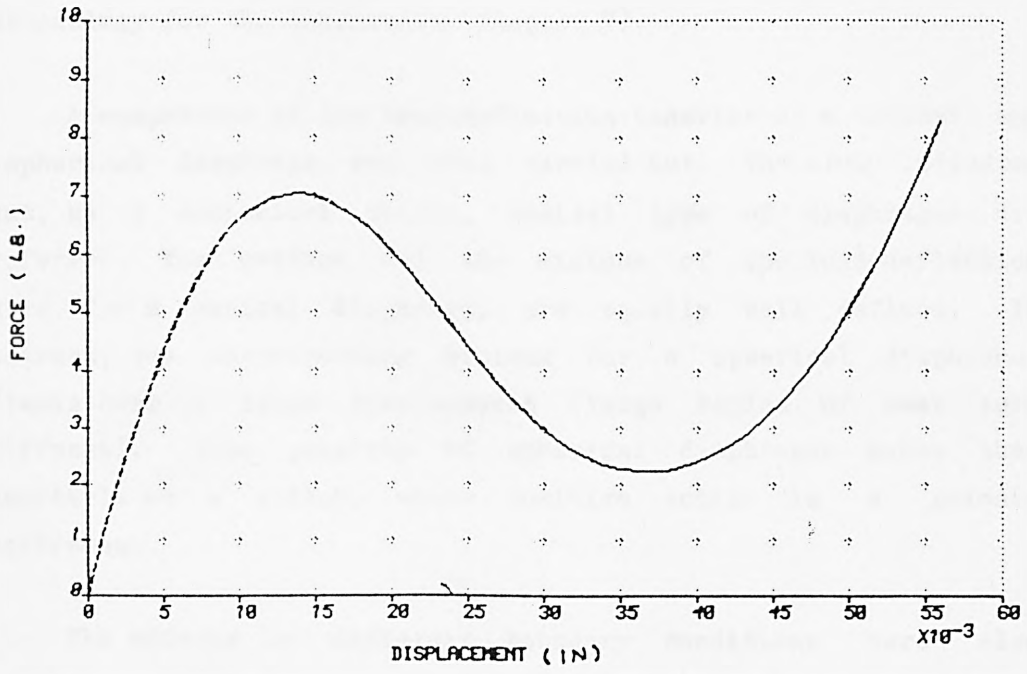

Figure 6.12

6.8 CONCLUSIONS

The variations in a diaphragm behavior, due to geometry changes, were investigated in this chapter. This was achieved by identifying the different types of diaphragms (conical and spherical), and describing their profiles with a set of geometric parameters. The important parameters were then determined using sensitivity analysis. The investigation indicates that the following parameters have significant effect on the performance of the two types of diaphragms:

H1, RO, RB, T, E.

Apart from 'H1', it was found that all the other parameters increase or decrease the maximum and the minimum of the load-deflection curve without altering the displacements at which they occur. These facts are utilized when developing a design methodology for the diaphragms (Chapter 7).

A comparison of the load-deflection behavior of a conical and a spherical diaphragm was also carried out. The study indicates that, as a mechanical switch, conical type of diaphragms are preferred. The maximum and the minimum of the load-deflection curve, for a conical diaphragm, are equally well defined. In contrast, the corresponding minimum for a spherical diaphragm, extends over a large displacement (large region of near zero stiffness). This property of spherical diaphragms makes them unsuitable as a switch, where positive action is a primary requirement.

The effects of different boundary conditions were also investigated in this chapter. The load-deflection characteristic of a simple spherical cap was found to change dramatically when the boundary conditions changed from a clamped support to a simple support. However, the boundary conditions were found to have negligible effect on the behavior of more complex shaped diaphragms.

CHAPTER 7

DESIGN CONSIDERATIONS AND METHODOLOGY

7.1 INTRODUCTION

In the previous chapter, parametric representation of the two types of diaphragm (conical and spherical) was carried out. Using the sensitivity analysis techniques, the geometric parameters which have significant effect on the diaphragm behaviour were determined. In this chapter a design methodology has been presented to determine the critical parameters for given design specifications. Therefore, a new diaphragm can be designed more economically and efficiently.

Conventional methods for designing new instruments are based on the experience and expertise of the designer, aided by simple analytic models of questionable validity (chapter 2). Prototypes of the instrument are manufactured and tested. Modifications in the design are suggested to eliminate the errors between the desired performance and the test results. The process is repeated until a satisfactory design has been obtained. The eventual design is invariably a compromise because the process cannot be repeated indefinitely to eliminate all the errors.

An accurate mathematical model can expedite the design and development of new instruments. The model can be used to replace experimentation and production of hardware. Suitable modifications can be made with the aid of sensitivity results to obtain the desired performance of an instrument. However, this method will still be time consuming and computationally expensive.

A better approach is to use the accurate finite element model to generate a set of results for a range of diaphragms. The results can then be generalized using 'Dimensional Analysis' techniques so that they can be used for any similar diaphragm. Using these design curves, new diaphragm designs can be generated in a fraction of the time needed by other methods.

Such a methodology has been developed and presented in this

chapter, for design of conical diaphragms subjected to concentrated or uniformly distributed load.

7.2 DESIGN SPECIFICATION AND OBJECTIVES

The load-deflection characteristics of a snap-action diaphragm can be identified from its salient feature ie. the maximum load and the corresponding displacement (FP,WP), minimum load and the corresponding displacement (FT,WT), and the negative stiffness (S) for the diaphragm (figure 7.1).

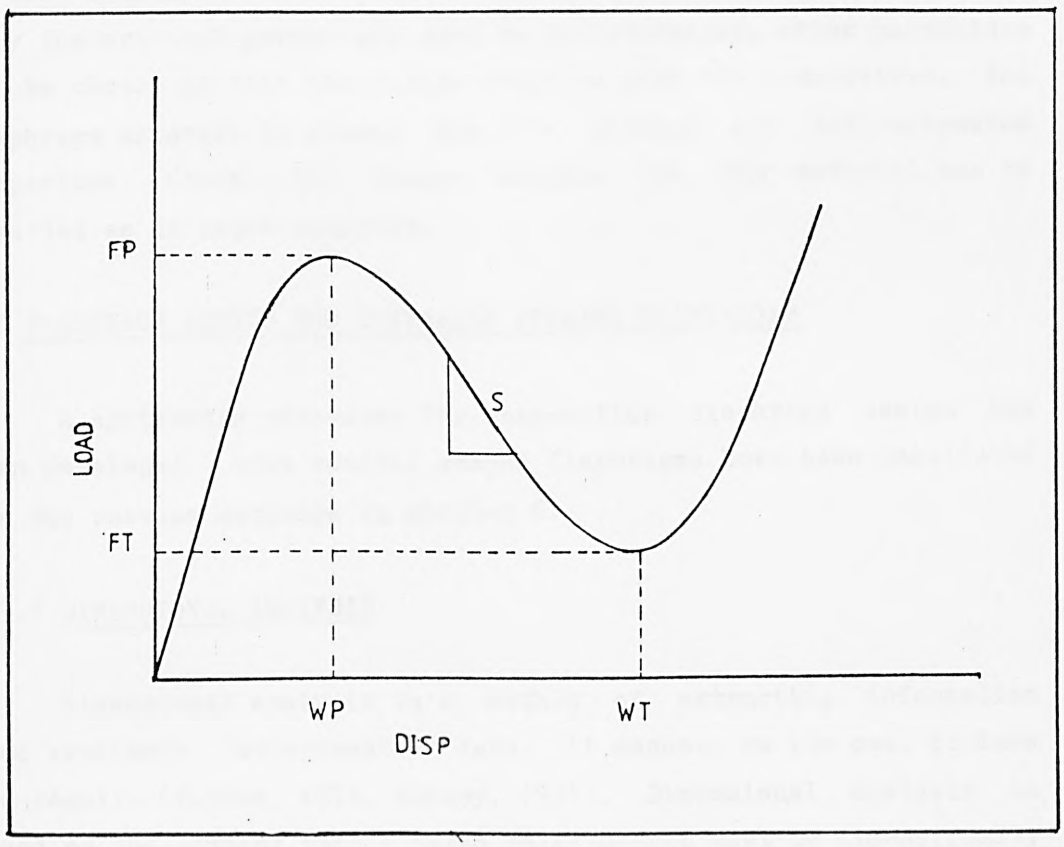

Figure 7.1

Specification of the negative stiffness is necessary if the diaphragm is to be used in conjunction with a 'back-off' spring for overload protection or variable range switch (chapter 2). However, a diaphragm cannot be designed to comply with any arbitrary specifications. Therefore, some of the design specifications will have to be given priority. From the priority specification, the feasibility range for the other specifications can be determined. This fact can be utilized to help the designer choose feasible

design specifications.

Given a design specification, the objctive is to determine a suitable diaphragm profile and materials. The profile suggested should comply with constraints on the size of diaphragm (specified by the designer), and thin-shell theory constraints.

As shown in the previous chapter, a conical diaphragm can be described with a suitable set of parameters. The important parameters (RB, RO, T, H1 and E) were determined using sensitivity analysis. The other parameters were found to have negligible effect on the load-deflection characteristics of a diaphragm. Therefore, only the critical parameters need to be determined, other parameters can be chosen so that the design complies with the constraints. The diaphragm material is chosen for its elastic and anti-corrosion properties. Hence, the Youngs modulus for the material can be regarded as an input constant.

7.3 DIAPHRAGM DESIGN FOR CENTRALLY APPLIED POINT-LOAD

A systematic procedure for snap-action diaphragm design has been developed. Only conical shaped diaphragms have been considered for the reasons metioned in chapter 6.

7.3.1 DIMENSIONAL ANALYSIS

Dimensional Analysis is a method of extracting information from available 'experimental' data. It cannot, on its own, produce new results (Taylor, 1974, Massey, 1971). Dimensional analysis is based on the concept that a valid relationship must be dimensionally balanced. This is achieved by comparing the fundamental units of all the possible parameters describing a system. Useful dimensionless groups can be derived in this way. The dimensionless groups should be meaningful, ie. should convey the relationship between parameters, so that they can be used for extrapolation or interpolation. When the 'relationships' are derived from experimental data, they are generally approximate.

For a snap-action diaphragm, point load (F) applied at the centre can be expressed as a function of critical parameters

(chapter 6) and the centre displacement.

$$F = f_1(RO, RB, T, E, W) \qquad (7.1)$$

Apart from 'H1', the other parameters have a scaling effect on 'F'. The results of sensitivity tests (tables 6.1 and 6.2) indicate that $F \propto E$. Therefore, equation 7.1 can be written as:

$$F = f_2(RO, RB, T, N) \Big|_{H1 \text{ - constant}} \qquad (7.2)$$

To investigate the relationship between 'F' and 'RO' and 'RB', the finite element program can be used. A diaphragm profile is assumed and each parameter is altered gradually (steps of 10%) while keeping the others constant. Figure 7.2 shows a discretized profile of such a diaphragm. The definition of 'RO' is different from the previous chapter 6.1. The values of parameters are given below and in figure 7.2:

R1 = R2 = 0.07"
H2 = 0.15"
γ = 0.3
E = 29.0E6 lbs/sq. in.

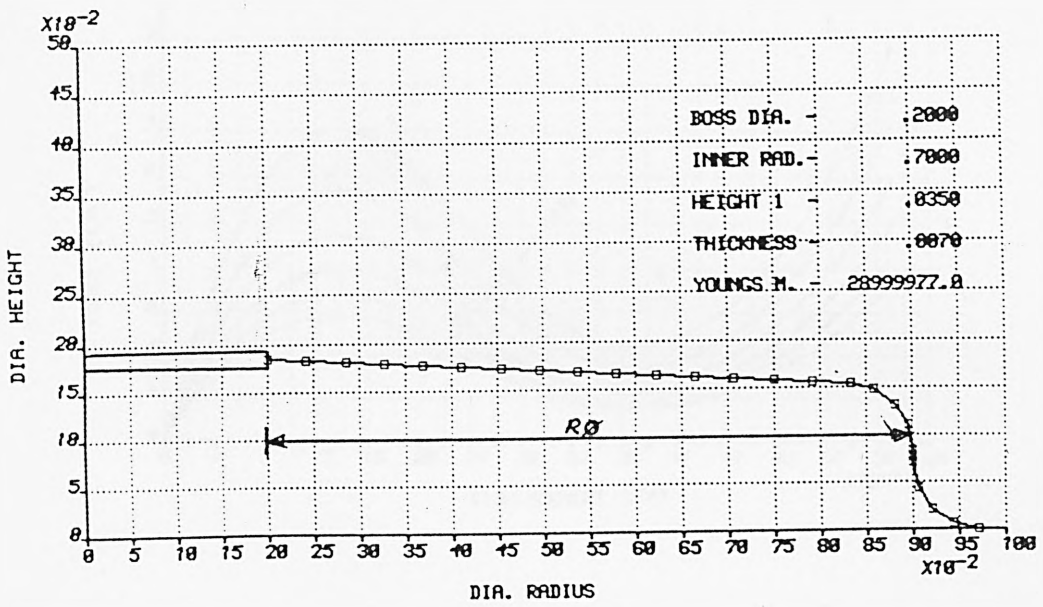

Figure 7.2

Figures 7.3a and 7.3b show the effect of 'RO' and 'RB' on load deflection characteristics of a diaphragm.

By curve fitting or other numerical methods of approximating data (Hayes, 1970), it can be shown that:

$$F \propto 1/RO^2$$

$$F \propto RB$$

provided the other parameters are constant.

The validity of the above approximate relations for entire 'W' can be verified by determining F x RO^2 and F/RB for different 'RO' and 'RB'. Graphically, this is shown in figures 7.4a and 7.4b respectively.

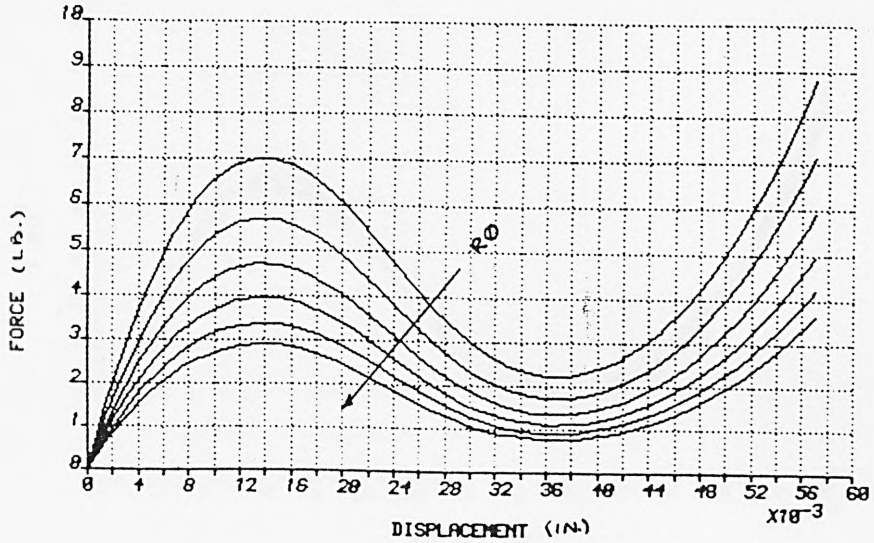

Figure 7.3a

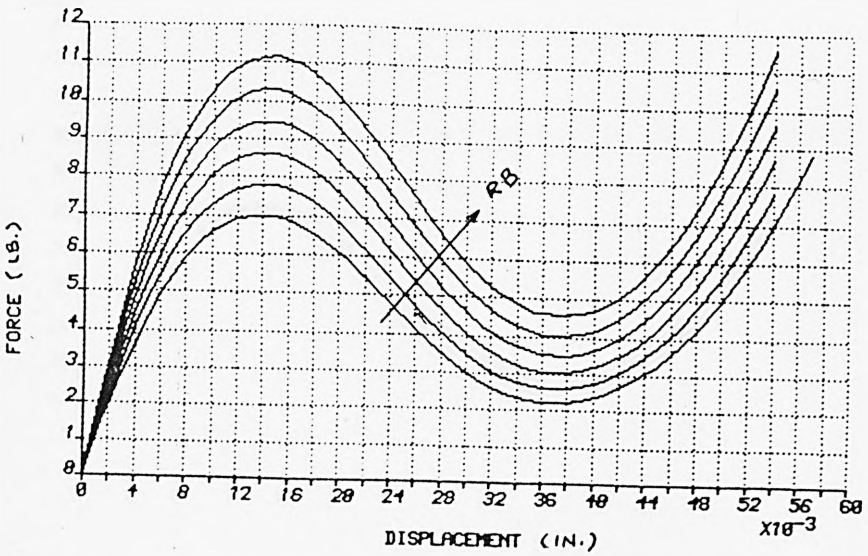

Figure 7.3b

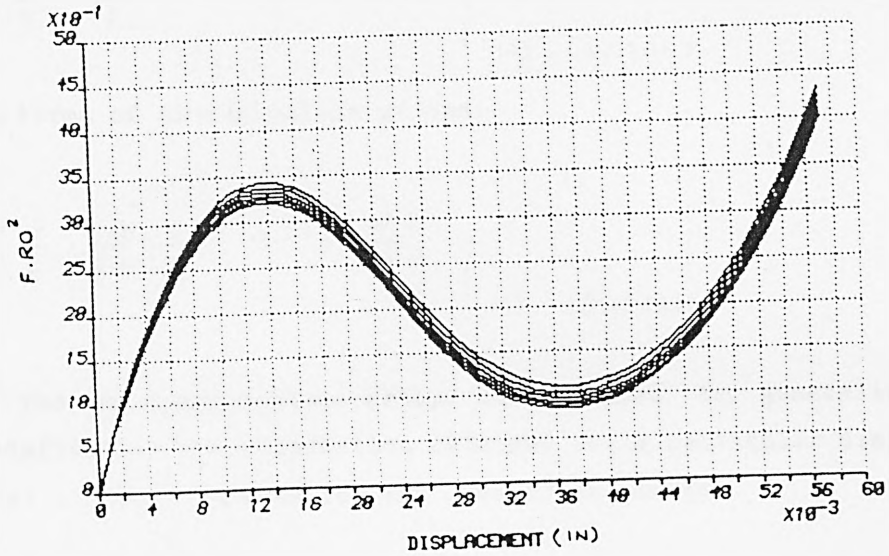

Figure 7.4a

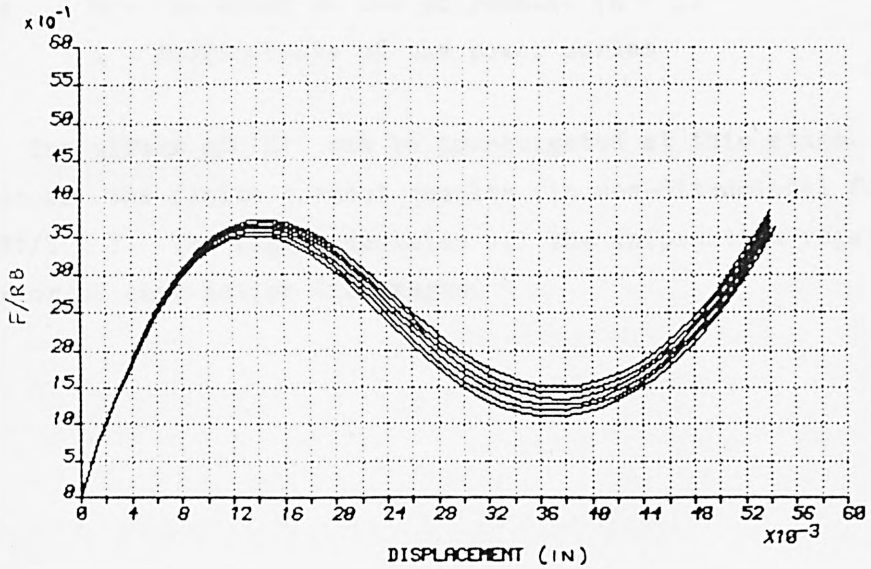

Figure 7.4b

Therefore, equation 7.2 can be expressed as:

$$\frac{F}{E} \cdot \frac{RO^2}{RB} = f_3(w, t) \Big|_{H1 \text{ - CONSTANT}} \qquad (7.3)$$

or in terms of dimensionless groups:

$$\left(\frac{F}{E} \cdot \frac{RO^2}{RB} \cdot \frac{1}{t^3}\right) = f_4\left(\frac{w}{t}\right) \Big|_{H1 \text{ - CONSTANT}} \qquad (7.4)$$

The two dimensionless groups can be used to generalize the load-deflection characteristics obtained for a particular diaphragm, so that it could be used for any similar diaphragm.

Numerical methods of data approximation can be used to determine f_4 . In terms of power series, the characteristic curve of a diaphragm can be expressed as:

$$\frac{F}{E} \cdot \frac{RO}{RB} \cdot \frac{1}{t^3} = \sum_{i=1}^{n} A_i \left(\frac{w}{t}\right)^i \qquad (7.5)$$

where n - The order of the polynomial ($n > 3$)
A - Coefficients of the power series

The effect of 'H1' can be investigated at this stage. Figure 7.5 shows the finite element results (in non-dimensional form), for $3 < H1/T < 7$. The figure contains all the information regarding the behavior of snap-action diaphragms.

The approximate relationships have been obtained for:

$$2.3 < RO/RB < 5.3$$

Projections outside this practical range will need further validation.

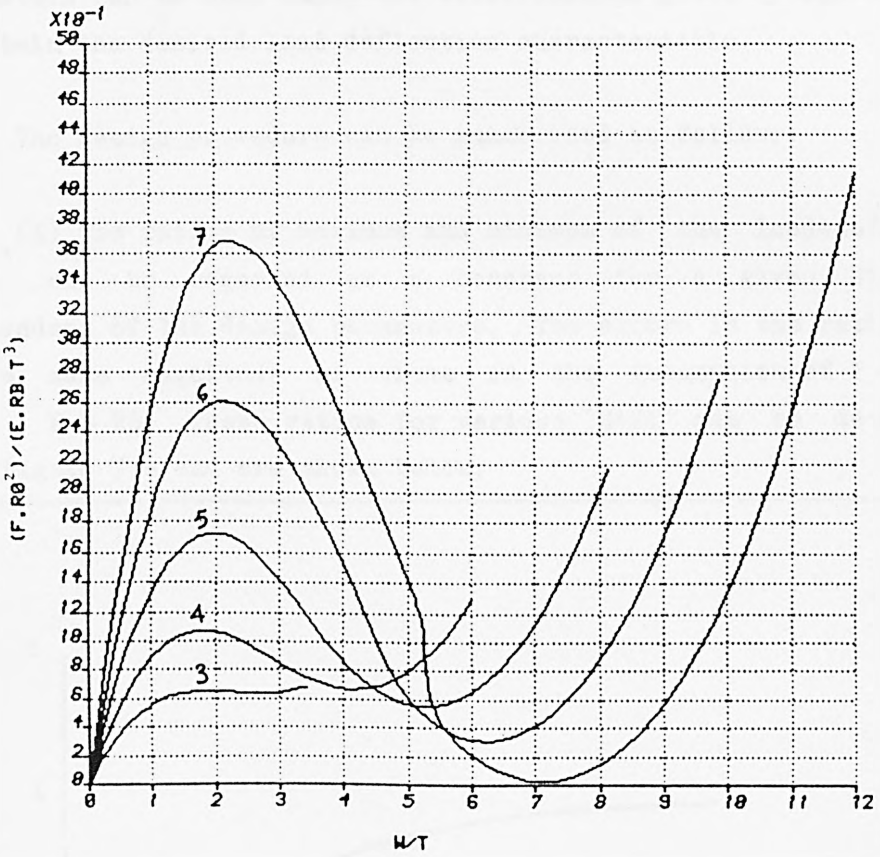

Figure 7.5

H1/T < 3 is not used because the diaphragm remains stable. This was checked for various diaphragm profiles and thicknesses. Also for H1/T > 7, numerical results indicate a sudden stiffening of the diaphragm in the unstable region. This again was confirmed for various diaphragm profiles. Profile plots of the diaphragm for increasing centre-displacement indicate sudden changes in the profile take place when H1 is large (H1/T > 7), hence the sudden stiffening of diaphragms.

7.3.2 DESIGN PROCEDURE

The design procedure described in this section is approximate. The finite element program is used to determine accurate load-deflection for the diaphragm parameters obtained from the approximate procedure. Necessary modification in the design parameters can be made using the relationships given by equation 7.3 to obtain the desired load-deflection characteristic.

The design procedure can be summarized as follows:

(i) The ratios of maximum and minimum of the load-deflection curve can be regarded as a constant for a given H1/T ie. independent of the design parameters. The errors in the ratios are of the same magnitude as those in the assumption of $F \propto 1/RO^2$ and $F \propto RB$. These ratios for various 'H1/T' can be determined from figure 7.6 and are shown below:

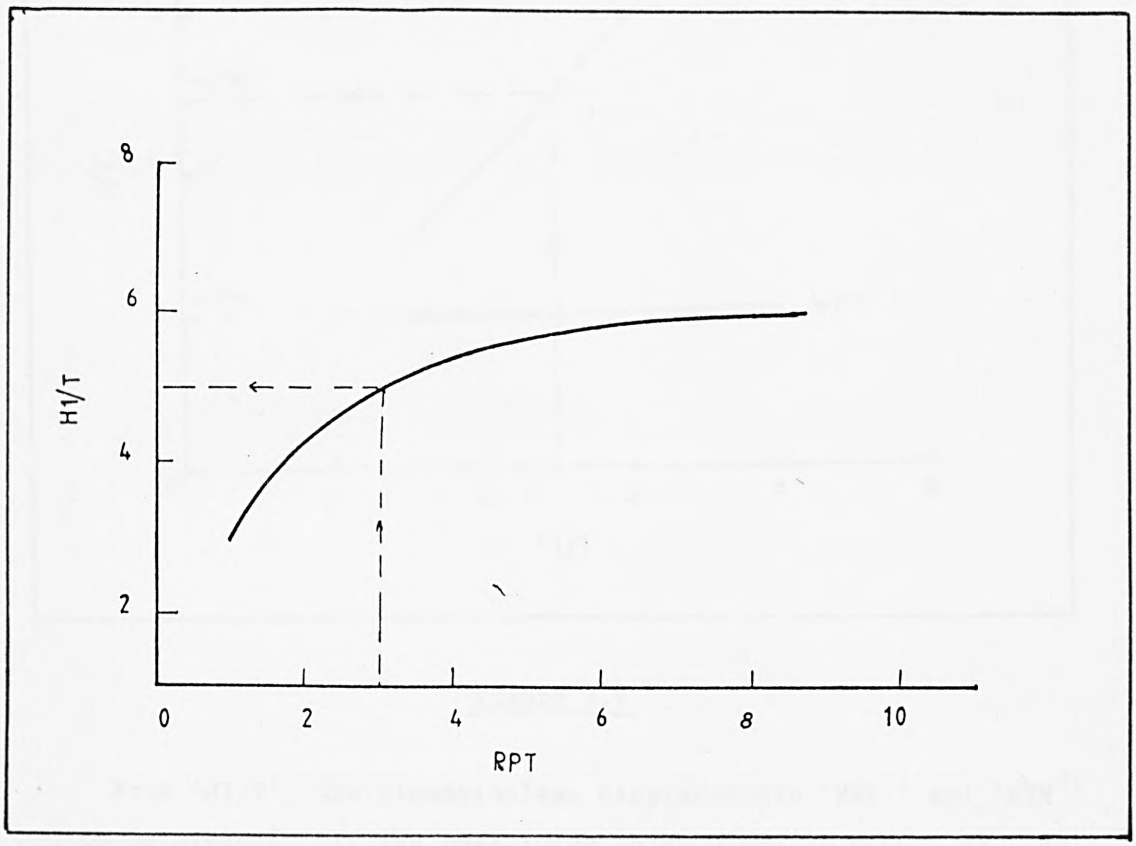

Figure 7.6

The ratio 'RPT' of maximum force 'FP' and minimum force 'FT' for H1/T = 7 is not considered because it approaches infinity (figure 7.5). For a given peak force, the range of possible minimum

force is given by:

$$\frac{FP}{8.7} < FT < \frac{FP}{1.0}$$

This can be used to help the designer choose a suitable 'FT'. Then from 'RPT', 'H1/T' can be determined (figure 7.6).

(ii) For various 'H1/T', the dimensionless displacements 'WPN' and 'WTN' corresponding to maximum and minimum load are shown graphically in figure 7.7.

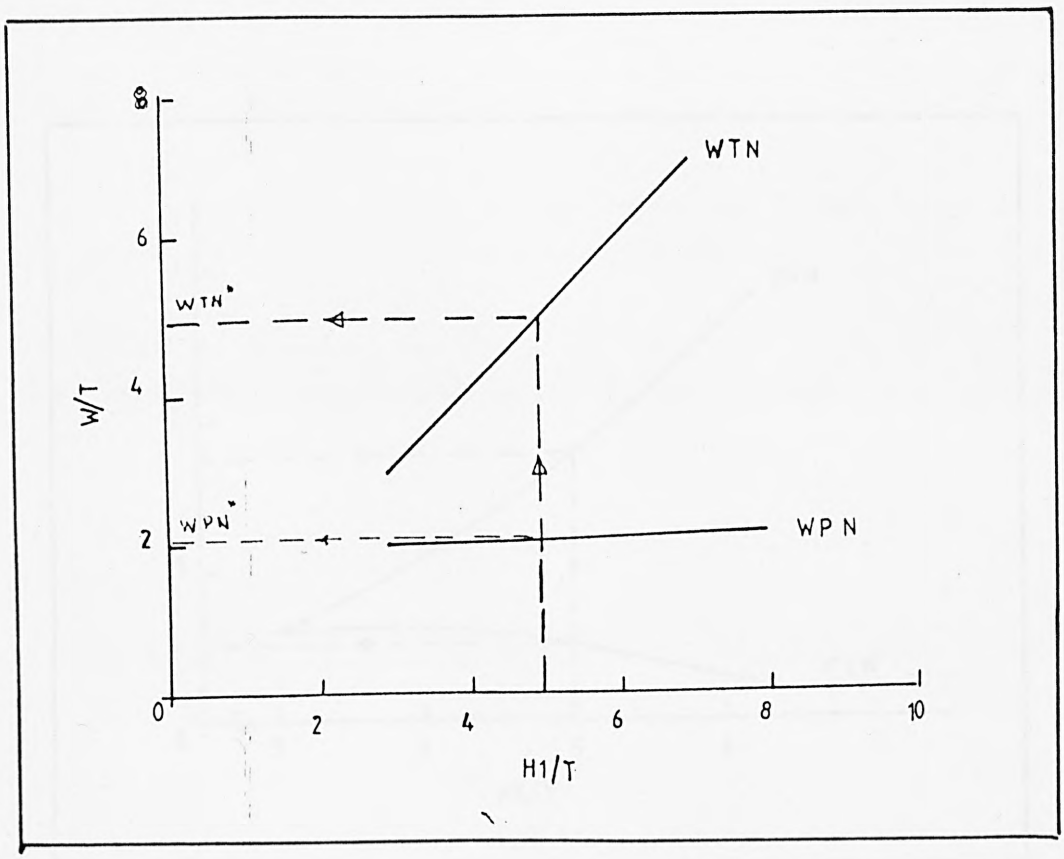

Figure 7.7

From 'H1/T', the dimensionless displacements 'WPN*' and 'WTN*' can be determined. If the peak force is required to occur at 'WP' displacement, the necessary diaphragm thickness is given by:

$$T = WP/WPN^*$$

From 'T', 'H1' can be determined as well. The displacement

corresponding to the minimum load is given by (figure 7.7):

$$WT = WTN^{*} \times T$$

If 'WT' is not suitable, then either displacement corresponding to peak force 'WP' will have to be changed, or the ratio 'RPT' has to be changed.

(iii) 'RO' and 'RB' can be determined iteratively using the relationship between non-dimensional peak load 'FPN' and 'H1/T' (figure 7.8).

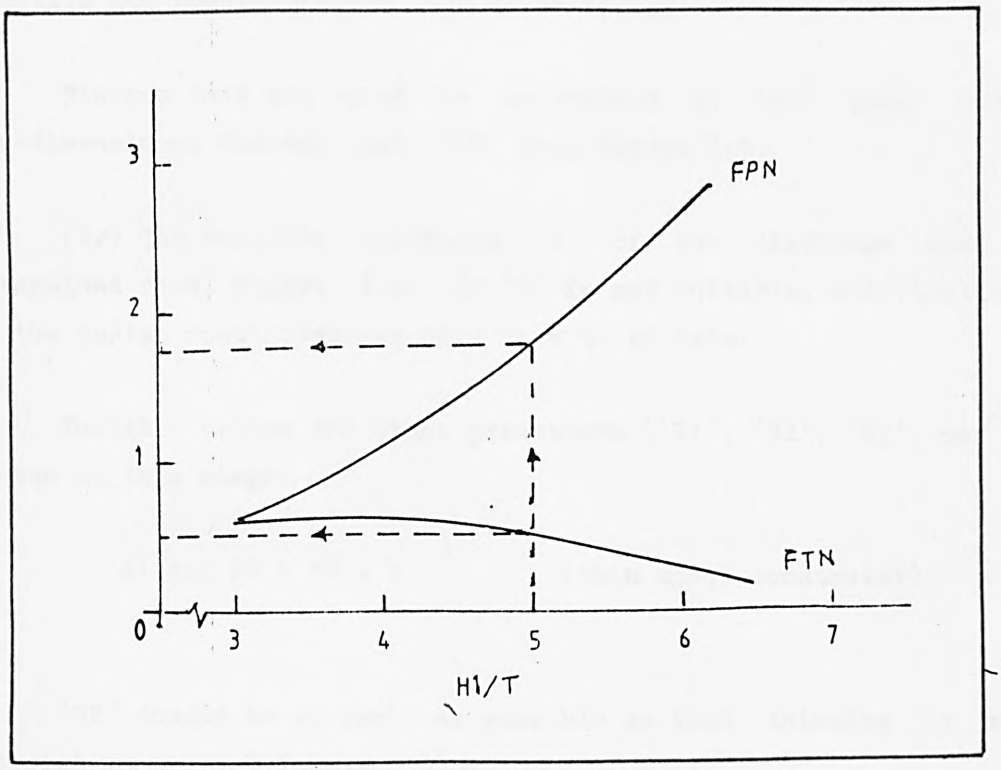

Figure 7.8

The iteration can be initiated by assuming a value for 'RO/RB'.

1. Assume RO/RB

2. $$RB = \frac{FPN}{FP} \cdot \frac{E.T^3}{\frac{RO}{RB}}$$

3. Calculate RB

If 'RO' and 'RB' are not suitable (violate the constraint on maximum diaphragm radius or too small) then 'RO/RB' is increased and step 2 onwards is repeated. If RO/RB > 5.25 then the design is not feasible and specifications have to be changed.

Minimum load can also be determined at this stage using non-dimensional minimum load 'FTN' from figure 7.8.

(iv) The negative stiffness 'S' of the diaphragm can be determined from figure 7.9. If 'S' is not suitable, modifications in the design specifications will have to be made.

Suitable values for other parameters ('R1', 'R2', 'H2') can be chosen at this stage:

R1 and R2 > 10 x T (thin shell constraint)

'H2' should be as small as possible so that thinning in the material is minimal (chapter 5).

The procedure presented above is not unique. The sequence of the calculation may be altered according to different requirements.

Other methods based on constrained optimization techniques can also be adopted to determine the critical geometric parameters. These techniques lack flexibility, and therefore, are not considered suitable for the problem.

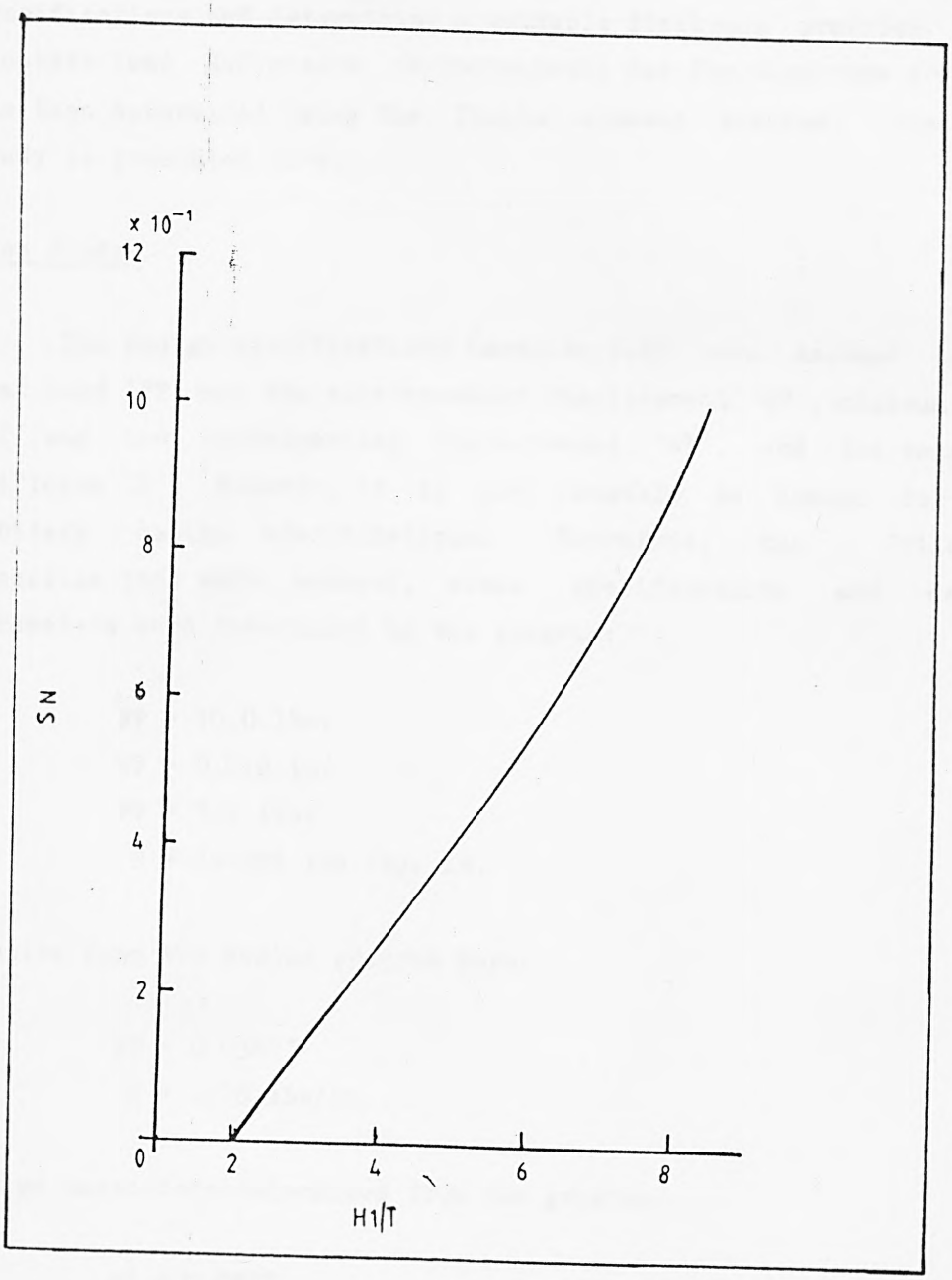

Figure 7.9

7.3.3 VALIDATION OF DESIGN PROCEDURE

The validation of design procedure presented in the previous section was carried out by using several example design specifications and determining a suitable diaphragm profiles. The accurate load deflection characteristic for the diaphragm profiles was then determined using the finite element program. One such study is presented here.

Case Study

The design specifications (section 7.2) were assumed to be peak load 'FP' and the corresponding displacement 'WP', minimum load 'FT' and the corresponding displacement 'WT', and the negative stiffness 'S'. However, it is not feasible to design for any arbitary design specifications. Therefore, the following specifications were assumed, other specifications and design parameters were determined by the program:

FP = 10.0 lbs.
WP = 0.018 in.
FT = 3.5 lbs.
E = 29.0E6 lbs./sq. in.

Results from the design program were:

WT = 0.0387"
S = -320 lbs/in.

Design parameters determined from the program:

H1 = 0.087"
T = 0.008"
RO = 0.0758"
RB = 0.0237"

The other parameters necessary to define the diaphragm profile can be determined from the shell constraints ie. the curvatures must be greater than 10 x thickness:

$$R1 = R2 = 10 \times T = 0.08"$$

'H2' should be small so that reduction in diaphragm thickness remains small:

$$H2 = 2 \times R1 = 0.16"$$

Results from the finite element program, for the above mentioned parameters, are shown in figure 7.10 (curve 1). The errors between the desired 'FP' and 'FT' and those determined using the finite element program, can be eliminated using the fact that:

$$F \propto RB$$
$$F \propto 1/RO^2$$

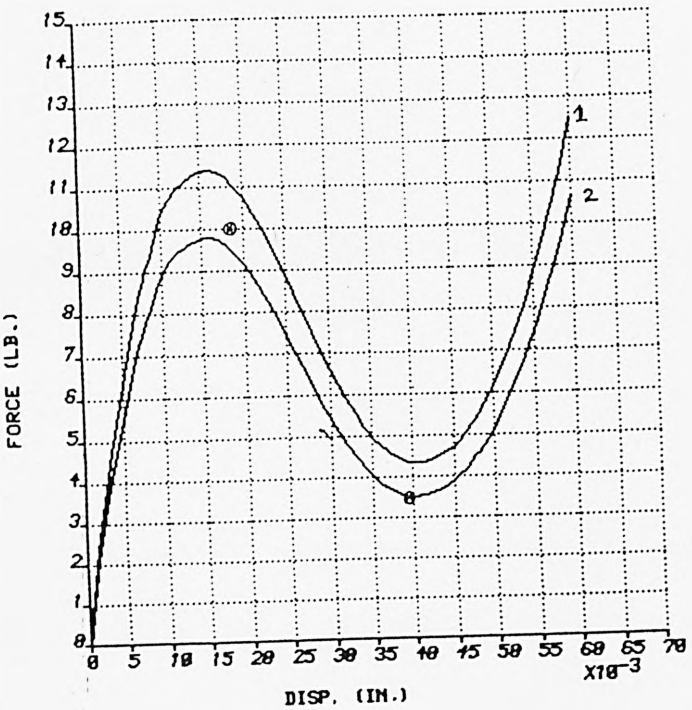

Figure 7.10

To obtain FP = 10, 'RB' can be modified to:

$$RB = 10.0 \times 0.037 = 0.0208"$$

Results from the finite element program for this modification are shown in figure 7.10. The errors between design specifications and the finite element results are less than 2%. However, the negative stiffness predicted by the design program was -320 lbs/in, while that obtained from the finite element model is -400 lbs/in. It is possible to make modifications in the parameters to reduce the difference, but because the negative stiffness is of secondary importance, this was not deemed necessary.

7.4 DESIGN OF A VARIABLE RANGE PRESSURE SWITCH

7.4.1 A DIAPHRAGM SPRING COMBINATION TO FORM A VARIABLE LOAD SENSOR

A snap-action diaphragm can be used to design a variable range pressure switch. As part of a switch, snap-through diaphragms are preferred over ordinary diaphragms, beacuse they are more positive action, have higher travel for the same overall dimensions, and have better reproduc bility.

Figure 7.11 shows a possible combination of a snap-action diaphragm and a spring to form a variable range switch for concentrated load.

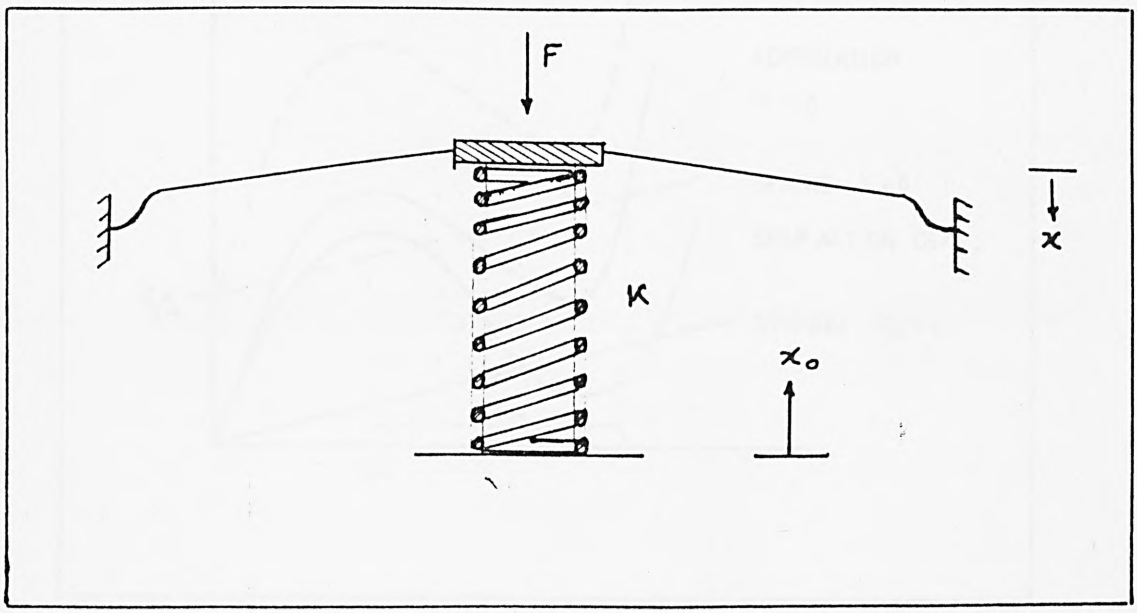

Figure 7.11

The overall behaviour of the system is given by the combination of the diaphragm and spring behaviours. The peak load at which the diaphragm will snap can be altered by varying x_o . Mathematically, this can be expressed:

$$F = K_d(x).\ x + K_s\ (x + x_o)$$

where
- F - Applied load
- $K_d(x)$ - Non-linear diaphragm stiffness
- K_s - Linear spring stiffness
- x, x_o - Displacements (figure 7.11)

Graphically, the applied load and centre displacement behaviour is shown in figure 7.12.

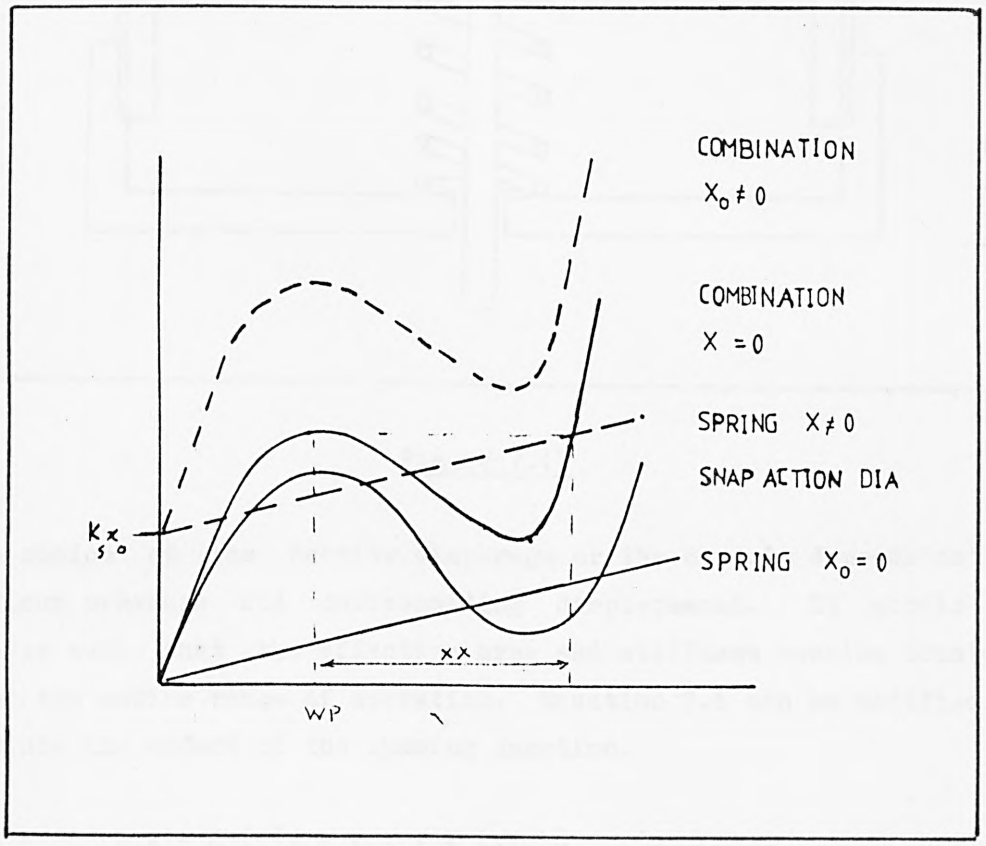

Figure 7.12

The spring stiffness 'K_s' should be less than the negative stiffness of the diaphragm so that the combined system will have suitable hysteresis. The choice of spring stiffness depends on the required sensitivity of the switch. In addition, the diaphragm needs to be restrained from moving up to a new equilibrium position when x_o is altered, otherwise, assumed origin of displacement will change.

The diaphragm spring system can be easily adapted to act as a variable range pressure switch. This can be achieved by including a 'summing junction' to transduce pressure into concentrated load (figure 7.13). A barrier diaphragm or a capsule can be used as a summing junction.

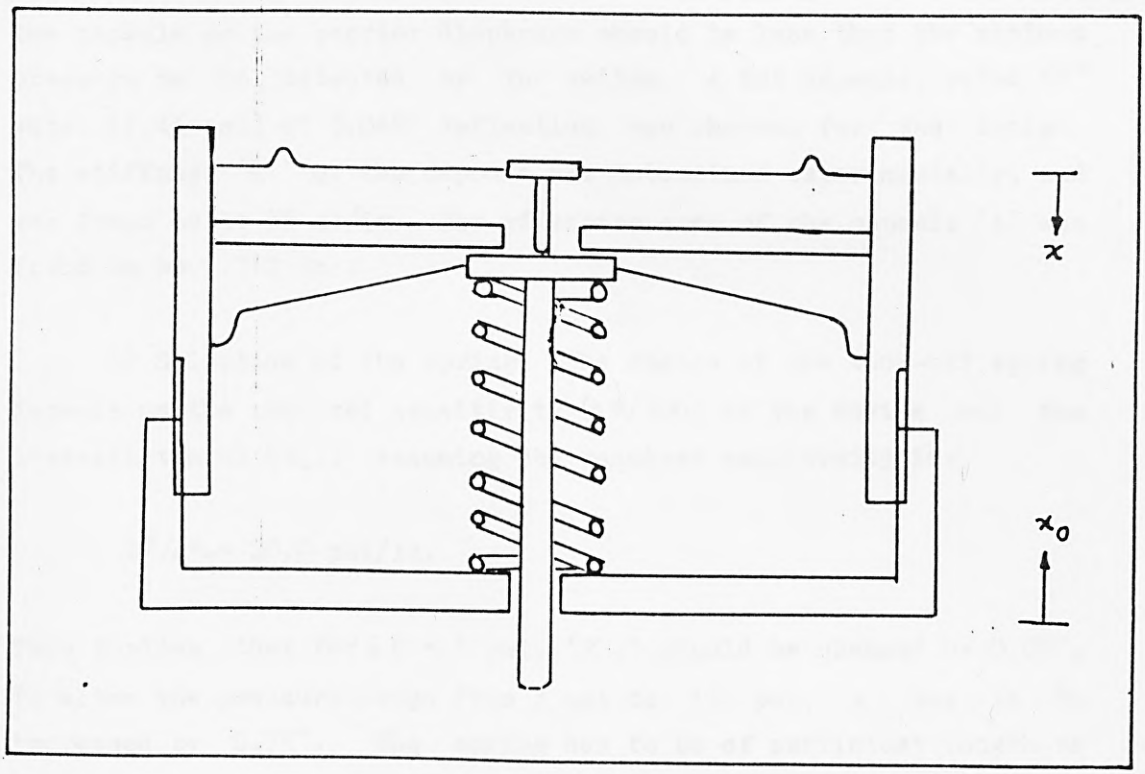

Figure 7.13

The choice of the barrier diaphragm or the capsule depends on the maximum pressure and corresponding displacement. It should be chosen such that the effective area and stiffness remains constant over the entire range of operation. Equation 7.6 can be modified to include the effect of the summing junction.

$$P.A = K_d(x)x + K_j x + K_s(x+x_o)$$

where P - Applied pressure

A - Effective area of the junction

K_j - Stiffness of the summing junction

The other terms on equation 7.7 have the same meaning as equation 7.6.

7.4.2 DESIGN OF 3 psi to 15 psi PRESSURE SWITCH

Design of a variable range pressure switch involves:

a) Selecting a suitable summing junction: It should be linear over the entire range of operation. The maximum pressure rate of the capsule or the barrier diaphragm should be less than the minimum pressure to be detected by the switch. A KGD capsule, rated 40" water (1.44 psi) at 0.048" deflection, was choosen for the design. The stiffness 'K ' of the capsule was determined experimentally, and was found to be 55 lb/in. The effective area of the capsule 'A' was found to be 1.712 in .

b) Selection of the spring: The choice of the back-off spring depends on the required sensitivity ($\partial P/\partial x_o$) of the device and the over-all travel (x_o). Assuming the required sensitivity is:

$$\partial P/\partial x_o = 20.0 \text{ psi/in.}$$

This implies that for $\delta P = 1$ psi, 'x_o' should be changed by 0.05". To alter the pressure range from 3 psi to 15 psi, x_o has to be increased by 0.75". The spring has to be of sufficient length to allow such compressions. The sensitivity ($\partial P/\partial x_o$) can be improved at the expense of increasing the spring length or reducing the pressure range of the switch. The stiffness of the spring can be determined using equation 7.7.

$$K = \frac{\partial P}{\partial x_o} A = 20.0 \times 1.712 = 34.24 \text{ lbs/in.}$$

c) Specifications for the diaphragm and design: The specification for the diaphragm design can be determined from the specifications of the capsule and the spring. The negative stiffness of the diaphragm must be greater than the combined stiffness of the capsule and the spring for the system to have hysteresis.

$$S > K_j + K_s$$
$$> 89.23 \text{ lbs/in.}$$

The maximum travel of the diaphragm (WP + xx, figure 7.12) should be less than or equal to the maximum displacement allowed for the capsule (0.048").

The diameter of the diaphragm should be less than or equal to that of the capsule so that step up adaptors do not have to be used for the assembly of the components.

The peak load carrying capacity 'FP' of the diaphragms and the corresponding displacements 'WP' can be determined using equation 7.7.

$$FP = P.A - (K_s + K_j)WP$$

But from figure 7.7,

$$WP = 2.0 \times T$$

where T - Diaphragm thickness
P - 3.0 psi
A - 1.712 in
K_j - 55 lbs/in
K_s - 34.24 lb/in

Standard blanks are used to form diaphragms, therefore, T can assume a limited number of values. This limits the number of iterations necessary in determinimg a suitable diaphragm profile.

The existing diaphragm design program was modified to take the forementioned considerations into account.

The critical parameters defining the diaphragm profile obtained from the design program, are shown in figure 7.14 The assumed values of other parameters are given below:

R1 = R2 = 0.07"

H2 = 0.14"

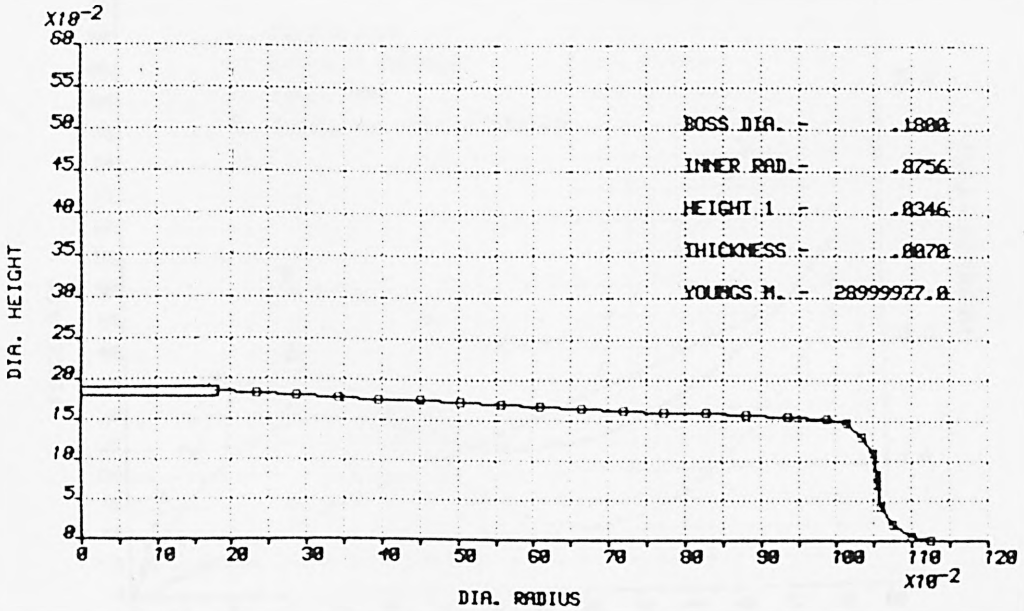

Figure 7.14

The diaphragm characteristic, obtained from the finite element program is shown in figure 7.14 (curve 1). Curve 2 indicates the combined characteristic of the diaphragm and the capsule. Curve 3 shows the combination of curves 1 and 2. The pressure deflection characteristic of the system (curve 4) is obtained by dividing the combined force-deflection characteristic of the system by the effective areas of the capsule (equation 7.7).

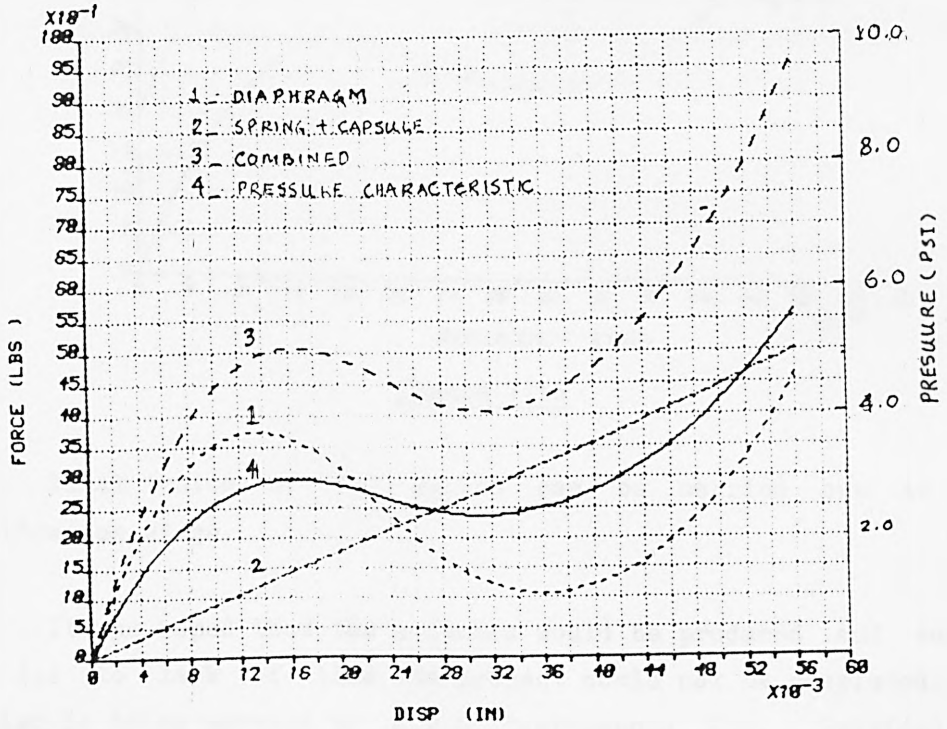

Figure 7.15

The effect of variation of x_o, is to change the threshold of the device, as shown in figure 7.16.

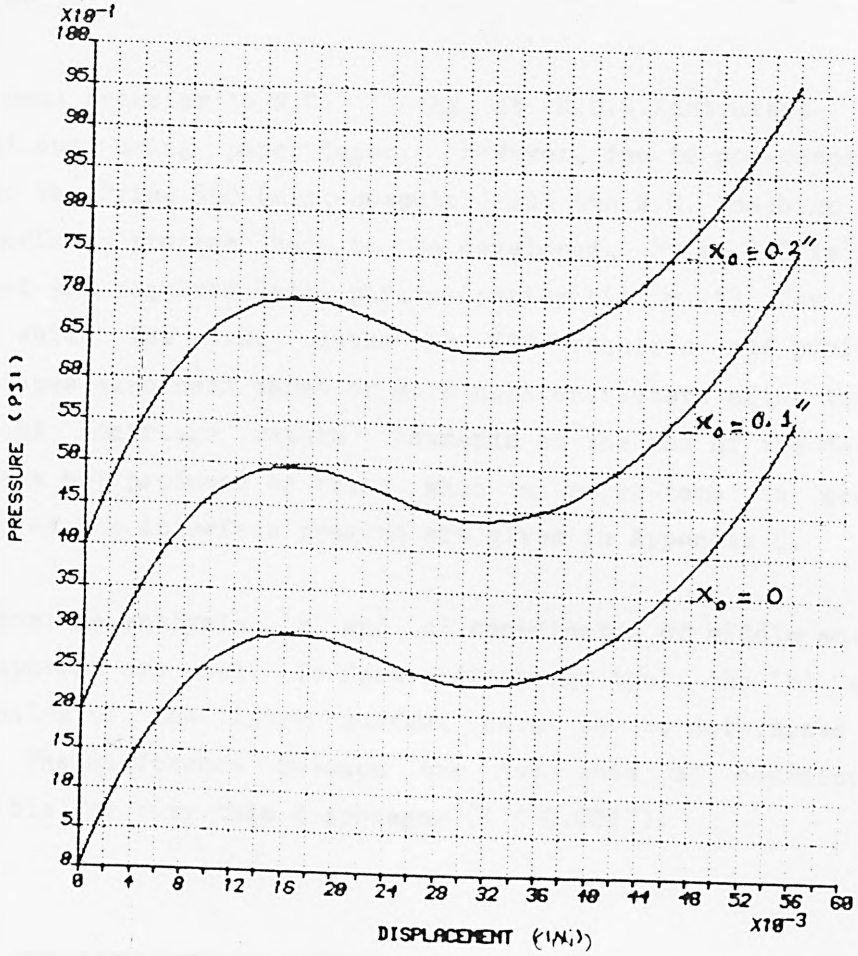

Figure 7.16

Final tuning of the switch can be carried out at the calibration stage.

It was hoped that the switches would be produced and tested, but due to lack of time the project could not be completed. The design is being pursued by K.D.G Instruments Ltd. Provided the diaphragm profile is formed according to the design, it is expected that the switch will perform satisfactorily.

7.4.3 DIAPHRAGM MANUFACTURE

In the past mechanically adjustable tools or lathe turned forming tools were used for diaphragm manufacture. With the increasing use of computer-aided techniques, numerically controlled lathes are used to produce forming tools; diaphragms are then press formed using these 'tools'.

Data transfer to N.C. lathe at K.D.G.Instruments Ltd was carried out using paper-tapes. However, due to non-compatibility between the Prime 550 (mini-computer) and the N.C. machine at KDG, an interface program had to be developed. Prime 550 is a 16 bit computer and requires 'set' parity (parity bit = 1) for all the data, while the N.C. lathe at KDG requires odd parity data. Paper-tapes also need three or more null characters after the 'line feed' and 'carriage return' commands at the end of the data line. These are not produced by Prime when a paper-tape is generated. Details of the interface program are given in Appendix C.

For the analysis, 'r' and 'z' coordinates of middle surface of the diaphragm are used. To form a diaphragm tool, the 'r' and 'z' coordinates of the inner surface have to be determined (figure 7.17). The difference between the two sets of coordinates is negligible for very thin diaphragms (T < 0.004").

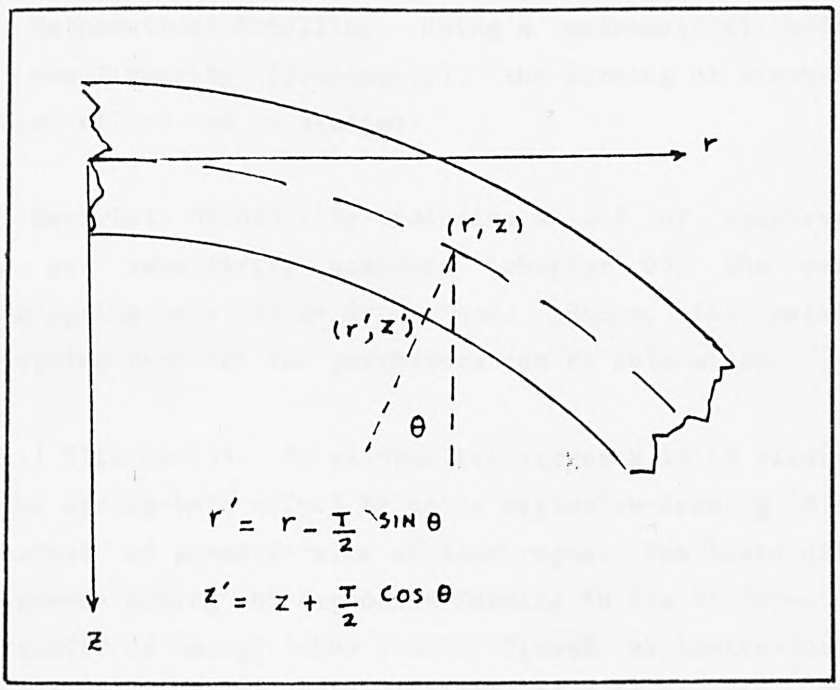

Figure 7.17

When a diaphragm is formed from a tool, the profile of the diaphragm is different from the tool. The difference in the profiles is due to the spring-back effect of the diaphragm after it has been pressed. The amount of spring-back depends on the material

properties of the blank (Young's modulus and thickness) as well as the profile of the tool. The required diaphragm profile is obtained by trial and error method. This is achieved by using a tool with exaggerated convexitivity (H1 > desired H1) so that after spring-back, the diaphragm, hopefully, will have the desired profile. Further study needs to be carried out to quantify the spring-back effect. There are two methods available to tackle the problem:

(i) Compensation.

(ii) Elimination.

(i) Compensation: In the present method of manufacturing, diaphragms are based on compensation techniques. The spring-back effect needs to be quantified so as to avoid the hueristic method of achieving the desired diaphragm profile. This can be achieved by:

a) Mathematical Modelling - Using a mathematical model with material non-linearity (plasticity), the forming of diaphragms and spring-back effect can be studied.

b) Empirical Method - By producing a set of diaphragms and carrying out sensitivity analysis (chapter 6), the parameters effecting spring-back can be determined. Hence, the relationship between spring-back and the parameters can be determined.

(ii) Elimination: An alternative approach is to eliminate or reduce the spring-back effect by using explosive-forming (Blazynski, 1983) instead of press-forming of diaphragms. The basic difference between press-forming and explosive-forming is the different rate at which transfer of energy takes place. Closed explosive-forming is carried out by placing a blank on top of a female die. Explosive material is placed on top of the blank and the system is submerged into an energy transferring media, usually water (figure 7.18).

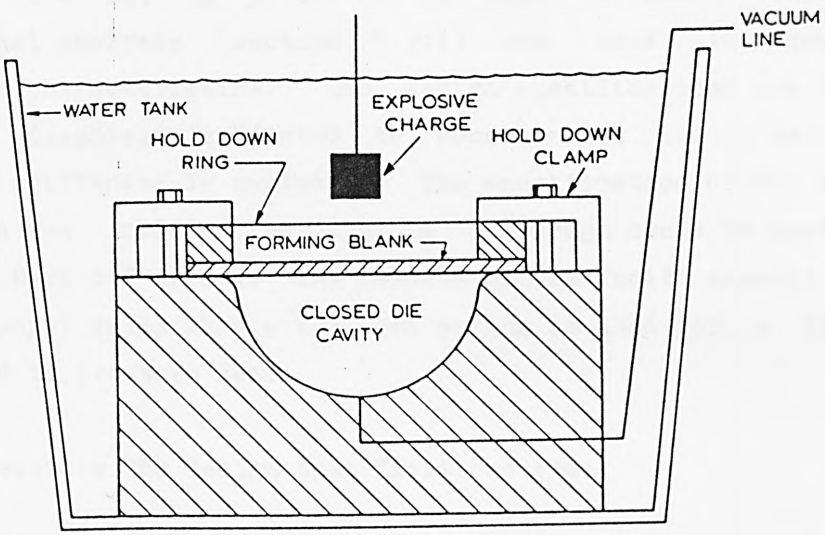

Explosive forming in a closed die.

Figure 7.18

There is more control over the shape of the diaphragm when explosively formed. This is achieved by varying:

a - Type of explosion.
b - Distance of explosive from the blank.
c - Distribution of the explosive.
d - The type of energy transformer medium and its temperature

A considerable amount of work has been carried out on explosive forming and extremely accurate symmetrical parts have been formed using the method.

7.5 DIAPHRAGM DESIGN FOR PRESSURE LOAD

A systematc procedure for diaphragm design, subjected to pressure loading, is presented in this section. Concepts of dimensional analysis (section 7.3.1) are used to generalize diaphragm characteristics. The design specifications are the same as for a diaphragm subjected to concentrated load, except the negative stiffeness is neglected. The specification of the negative stiffness was included so that a diaphragm could be used with a suitable back-off spring. The results of the finite element program are no longer valid when a back-off spring is used for a diaphragm subjected to pressure load.

Therefore the design specifications are:

a) Peak load 'FP' and corresponding displacement 'WP'.

b) Minimum load 'FT' and corresponding displacement 'WT'.

Again the constraints are those of thin-shell theory, and on the maximum radius of the diaphragm (geometric constraint). The objectives are to determine the critical parameters ie. 'RO', 'H1', 'T', and 'E' (chapter 6). The effect of the centre-boss is not included. The parameters necessary to describe the diaphragm profile are as suggested in sections 7.3.2 and 7.3.3. The choice of dimensional groups is based on the theory presented by Andreeva for snap-action diaphragms. Andreeva's analytic model cannot be used for design because it is inadequate (chapter 4, section 2.1).

The non-dimensional groups suggested by Andreeva are:

$$\frac{P}{E}\left(\frac{RO}{T}\right)^4 \quad \text{and} \quad \frac{W}{T}$$

where P - Applied pressure
E - Young's modlus for the material
RO - Inner radius for the diaphragm (chapter 5)
T - Diaphragm thickness
W - Centre-displacement

The results obtained from the finite element program are presented in figure 7.19 (in non-dimensional form). Under pressure load, conical diaphragms are found not to show any hysteresis for $H1/T < 3$. For $H1/T > 9$, sudden stiffening of the diaphragm is detected in the unstable region. This is because when 'H1' is large ($H1/T > 10$), sudden change in the profile takes place in the unstable region. This was detected for several diaphragm profile. The diaphragm parameters used in obtaining the results, are given below:

RO = 0.4567"
R1 = R2 = 0.07"
H2 = 0.14"
T = 0.007"
E = 29.0 x 10 lbs/in.
γ = 0.3
$3T < H1 < 10T$

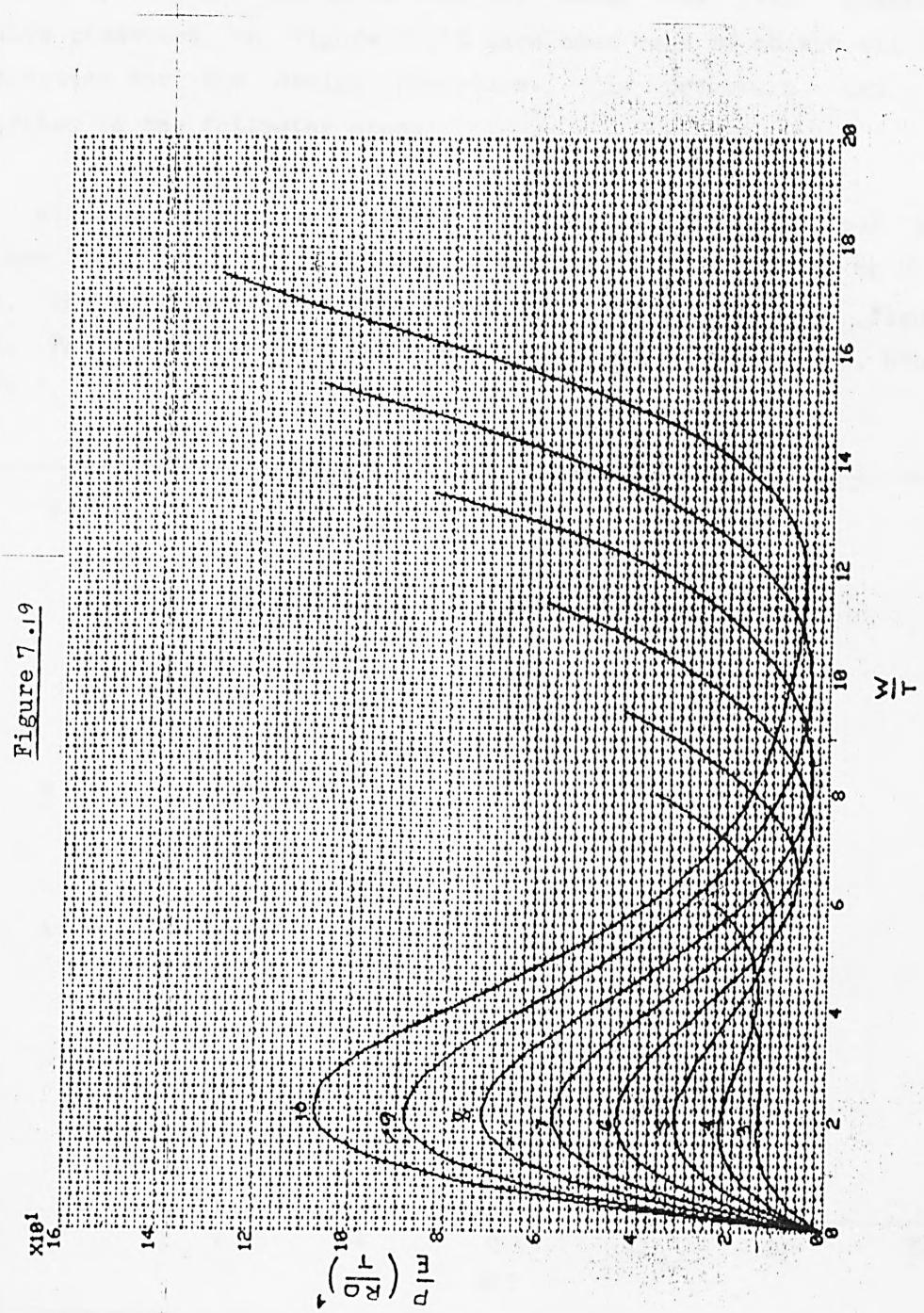
x10¹
16
14
12
10
8
6
4
2
0
fl'D (R/D)
0
2
4
6
8
10
12
14
16
18
20
W/T
10
12
8
7
6
5
4
3

Figure 7.19

The design procedure presented here is approximate. The errors being of the same order as for diaphragm design subjected to point load (section 7.3). To obtain accurate results, tuning in the diaphragm parameters can be carried out using the F.E. program. Results presented in figure 7.19 have been used to obtain all the information for the design procedure. The procedure can be described in the following steps.

a) Determination of 'H1/T': The ratio of peak load and minimum load (RPT = FP/FT) can be assumed to be dependent on H1/T only. The relationship between 'PRT' and 'H1/T' is shown in figure 7.20. For specified 'FP' and 'FT', 'RPT ' can be determined, hence 'H1/T '.

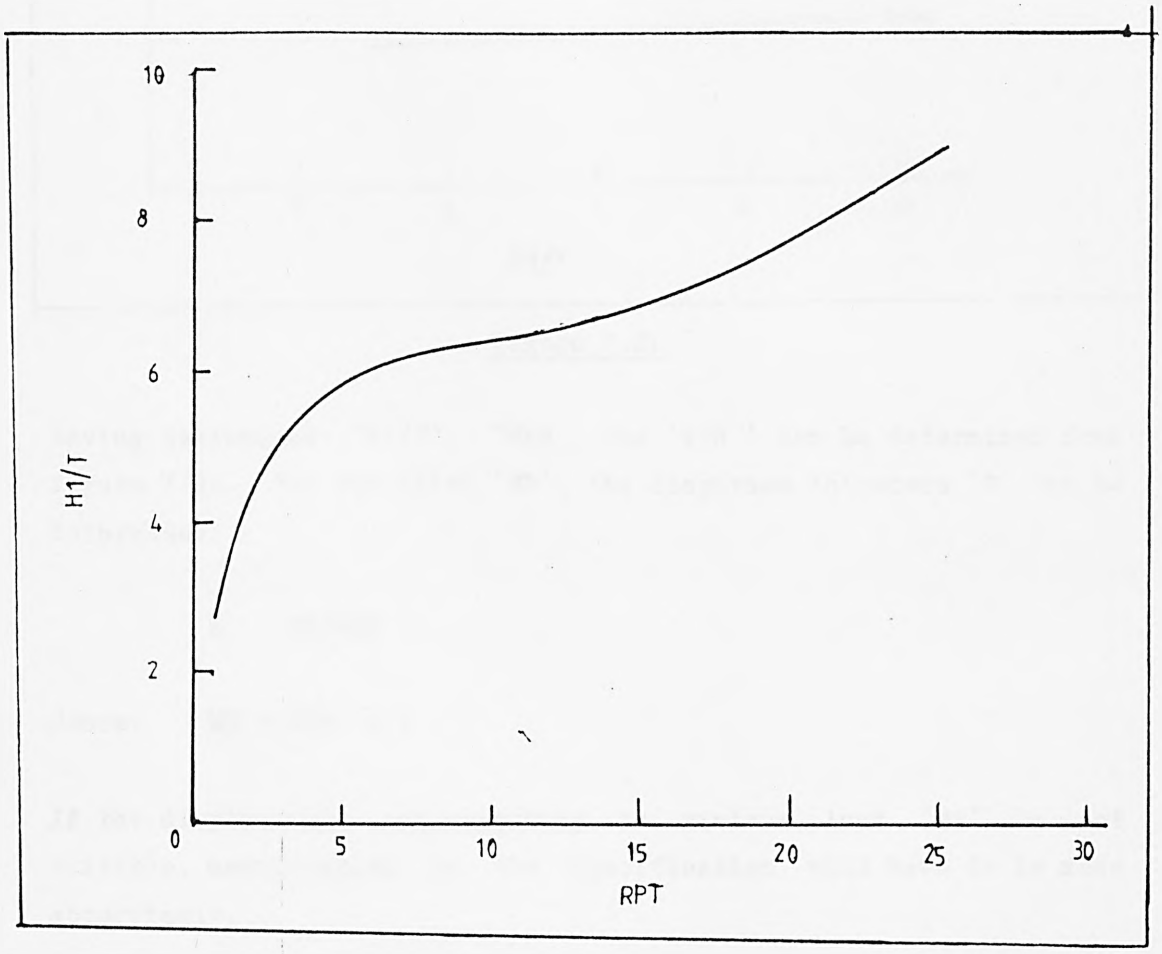

Figure 7.20

b) Determination of 'WP', 'WT', 'H1', and 'T': Figure 7.21 shows the non-dimensional displacements 'WPN' and 'WTN' corresponding to peak load 'FP' and minimum load 'FT' respectively.

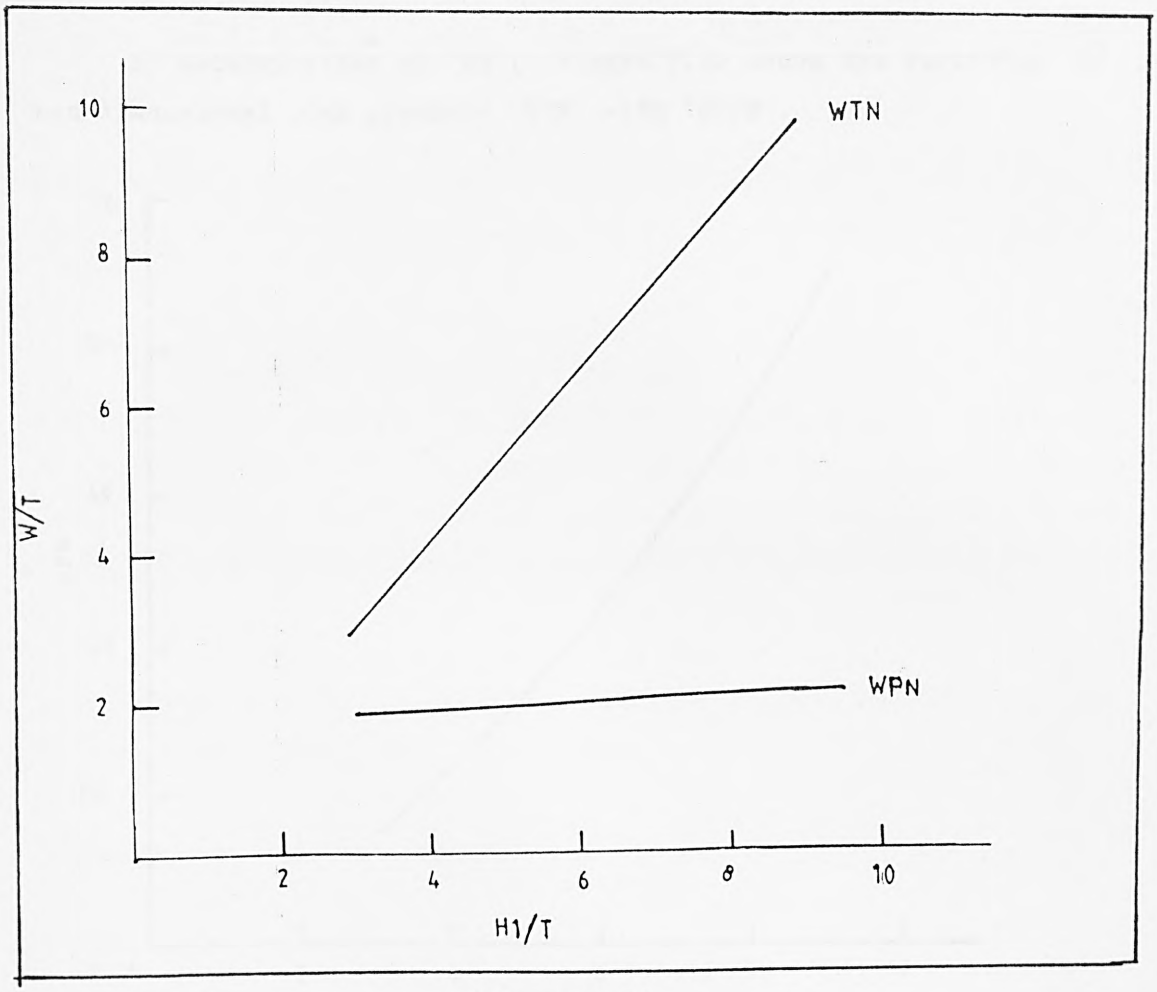

Figure 7.21

Having determined 'H1/T', 'WPN ' and 'WTN ' can be determined from figure 7.21. For specified 'WP', the diaphragm thickness 'T' can be determined:

$$T = WP/WPN$$

Hence, $WT = WTN \times T$

If the displacement corresponding to minimum load 'WT' is not suitable, modification in the specification will have to be made accordingly.

Alternatively 'T' can be determined from 'WTN ', depending which displacement ('WP' or 'WT') has priority. 'H1' can also be determined at this stage.

c) Determination of 'RO': Figure 7.22 shows the variation of non-dimensional peak pressure 'FPN' with 'H1/T'.

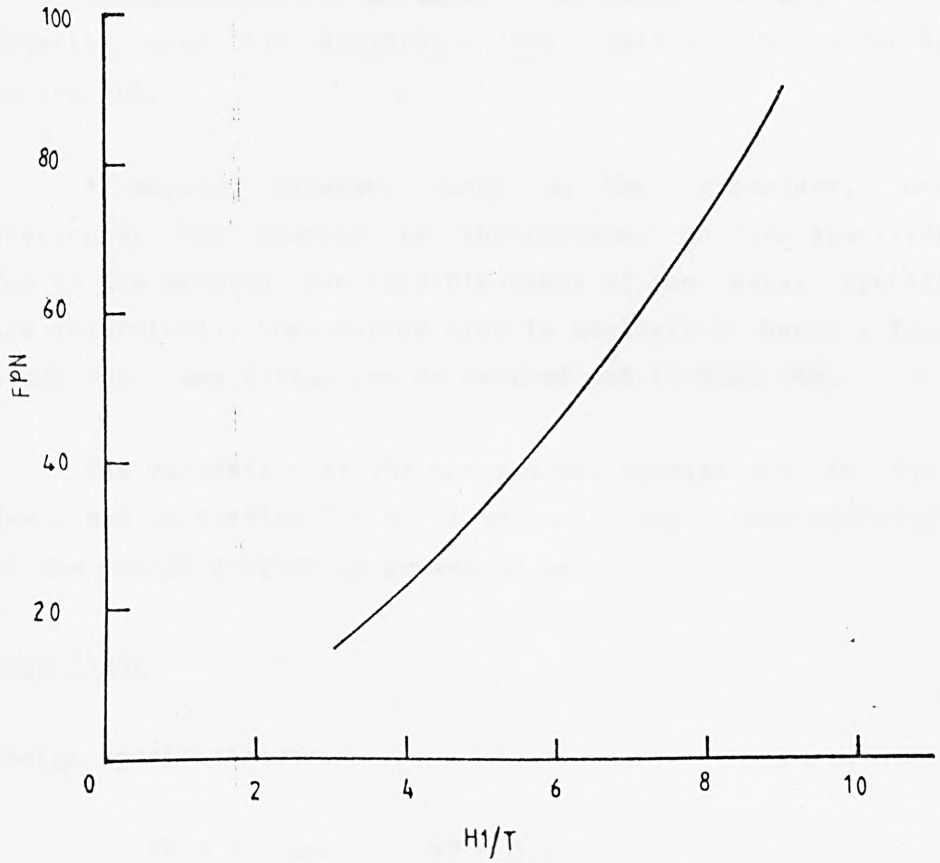

Figure 7.22

For given 'H1/T', 'FPN ' can be determined, and hence the 'RO'.

$$RO = (FPN .E.T)$$

If 'RO' is not desirable, suitable modifications in the specification will have to be made.

The other parameters necessary to describe the diaphragm can be assumed as:

$$R1 = R2 = 10 \times T \qquad \text{(thin shell constraint)}$$

$$H2 > (R1 + R2) \qquad \text{(physical constraint)}$$

However, 'H2' should be as small as possible to minimize the variation of thickness.

Youngs modlus 'E' is taken as an input variable because the materials used for diaphragms are limited; hence can be chosen beforehand.

A computer program, based on the procedure, has been developed. The program is interactive. As each specification is fed to the program, the feasible range of the other specifications are determined. Computation time is negligible, hence a feasibility study for a new design can be carried out in minu tes.

The validation of the program was carried out in the manner described in section 7.3.3. A typical example demonstrating the use of the design program is presented here.

Case Study

Design specifications:

FP = 3.0 psi WP = 0.01"
FT = 1.0 psi WP = 0.029"
Maximum Radius = 1.0"
E = 29 x 10 lbs/in

Critical parameter determined by the program:

T = 0.05"
RO = 0.67"
H1 = 0.0253"

The other parameters assumed to fully describe a conical diaphragm a re:

R1 = R2 = 0.05"
H2 = 0.1"

The results from the finite element program, for such a diaphragm are shown in figure 7.23. There is good agreement between

design specification and the finite element results. There is +12% error between the minimum load specified and that determined by the finite element program. Also, the corresponding displacement (WT) is out by -7%. Tuning of the design can be carried out using the results of sensitivity analysis (chapter 6).

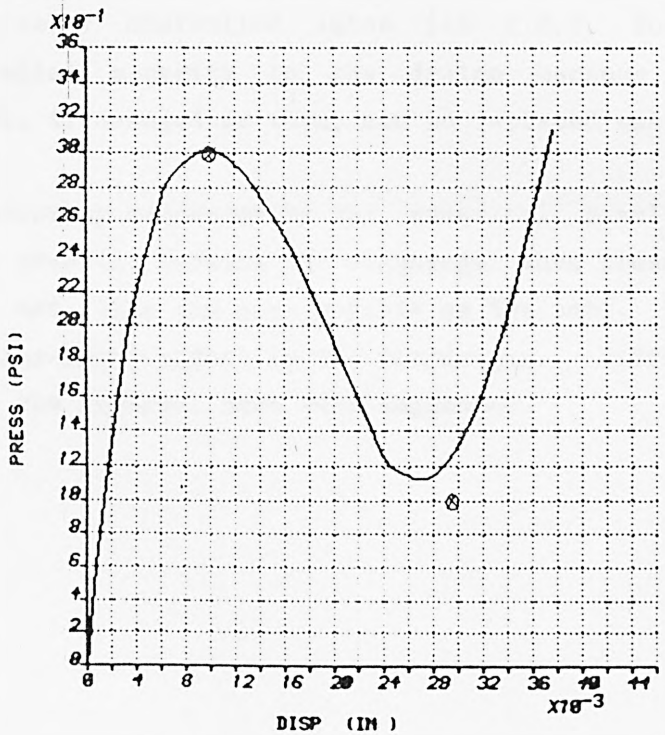

Figure 7.23

7.6 CONCLUSION

Procedures for designing snap-action diaphragms, subjected to pressure and point loading, are presented in this chapter. From the design specifications, the procedures enable the designer to determine the diaphragm shape and size. The design methodologies are based on the results from the finite element model for a set of diaphragms. The results from the finite element model are general ized using the Dimensional Analysis techniques so that they can be applied to any similar diaphragm. The computer programs, based on the design procedures, are interactive and guide the designer in choosing feasible specifications. Using these programs, a feasibility study for a new design can be carried out in a matter

of a few minutes. The design curves are approximate (due to generalization), therefore, the diaphragm parameters may not produce the required load-deflection characteristic exactly. Modification in the parameters can be made using the guidelines in the chapters. It was found that, at the most, three iterations are needed for the design to comply with the specification. The entire diaphragm design procedure has been upgraded, including the transfer of data to a numerically controlled lathe (at K.D.G. Instruments Ltd). This gives added security to the design because the diaphragm forming tool, if damaged or worn, can be replaced easily.

The accuracy suggested by the numerical results, cannot be achieved in practice because the diaphragm, when press-formed with a tool, does not take the same profile as the tool. This is because of the 'spring-back' effect in the diaphragms. Different methods, to overcome the problem, have been suggested.

CHAPTER 8

CONCLUSIONS

The objectives of the presented study were:

a) to develop an accurate and efficient mathematical model for the analysis of axi-symmetric snap-action diaphragms.

b) To establish a methodology for the design of such diaphragms.

A finite element model, based on thin shell theory and employing two noded line elements with six degrees of freedom has been developed and validated. Validation of numerical models, generally involves three stages:-

(i) Comparison with analytically solvable exact solutions.

(ii) Comparison with previously published analytic or numerical results.

(iii) Comparison with detailed experimental results.

Because of the complex load-deflection characteristics that arise in snap-action diaphragms no exact analytic theory was available for comparison at stage 1. However, the model was tested for the large deflections of a circular flat plate and a spherical cap, both under pressure loadings for which analytic results are available. At stage 2 comparison with published analytic results for snap-action diaphragms (Andreeva, 1966) showed a large variance when compared with the Finite Element (F.E.) results. It turned out that Andreeva's analytic model is totally inadequate. Also at stage 2 tests were conducted on a spherical cap with a ring load and good agreement was obtained between the F.E. model and other previously published numerical results. At stage 3 detailed comparisons were made with a number of diaphragms which were both mathematically modelled and tested experimentally by the author.

The results indicate that the load deflection characteristics can be predicted accurately except at large displacements where errors of about 15% occured. A plausible explanation for this error is given.

Having established that the F.E. model was accurate and efficient, a systematic study of two types of snapping diaphragms - conical and spherical - were carried out with a view to establishing a design methodology.

The approach was to provide a parametric representation to characterise the geometry of the diaphragms, to identify important design variables and then use dimensional analysis type methods to produce a non-dimensioned design curves. These curves can be used to develop a methodology for design. Given that a parametric representation of a snap-action diaphragm has approximately six geometric and two material variables to describe it this was considered the way to use the computer in a cost effective manner and develop a viable design methodology.

Having established the normalised design curves a methodology of design using these curves was presented. This methodology is simple and can be done in an iterative method either manually or using a simple programmable calculator. To be sure of any design it is advisable to make a final check on the performance using the F.E. model.

The design methodology has been illustrated by way of examples including that of an adjustable pressure operated switch in the 1 bar (3-15psi) range. This device is still to be constructed and tested. Provided that the diaphragm can be formed to the design specified there is no reason to expect that the system will not perform as predicted.

Further work should be concerned with applying the methods outlined in the thesis to the design of snap-action diaphragms for the variety of applications indicated in chapter 2. Only in this way will further confidence be built up in the methods presented here.

The design methods produce a diaphragm geometry for a given

material. This information is used to produce a tool (using a numerically controlled lathe) from which the diaphragm is press formed. No account is taken of spring-back. There is therefore a need to study spring-back. This can be achieved theoretically by developing finite element models for the formation process (ie. an elasto plastic model) or by empirical means to study what form spring-back takes. In the latter approach a profile plotter being developed as another project for measuring the profiles of corrugated diaphragms would assist. In this plotter the r-z (radial-axial) coordinates of the diaphragm surface are measured to about 10 microns (0.0004") using a stepper motor driven carriage which moves the diaphragm under a displacement sensing head. The whole profile can be measured and stored on a micro computer within a minu te or so. If such a plotter is used to study both the tool profile as well as the formed diaphragm using a graphics VDU, then it would be possible to identify factors contributing to spring-back so leading to an experimental study of the problem. Once the principal factors contributing to spring-back are identified it should be possible to compensate for it at the design stage. Explosive forming of diaphragms is a method which may get around the problem of spring-back. This also needs to be explored further, although it may not be economically feasible for production purposes.

In the present work two types of loading have been considered:- pressure and point loadings. An area mentioned but not explored is temprature operated snap-action devices. A finite element model could be developed for such devices. Since the operation of these devices are based on composite shells having different thermal expansion coefficients, some effort would be needed in developing a finite element model. However, much of the basic approach in the development of the present finite element model will remain.

REFERENCES

Abdullah,F., Finkelstein,L. (1982) Review of Mathematical Modelling of Instrument Transducers. Acta IMEKO Scparatum, Budapest, Hungary.

Abdullah,F., Li,C.W. (1983) 'Finite Element Modelling of Load Cell Billets'. Presented at Weighteck '83 Conference and published in 'Weighing and Force Measurement in Trade and Industry'. (Institute M.C. publication)

Andreeva,L.E. (1966) 'Elastic Elements of Instruments' Israel Program for Scientific Translations, Jerusalem.

Batoz,J.L., Chattopadhyay,A., Dhatt,G. (1976) 'Finite Element Large Deflection Analysis of Shallow Shells' International Journal of Numerical Methods in Engineering, Vol. 10, pp 39-58.

Bergan,P.G., Clough,R.W. (1973) 'Large Deflection Analysis of Plates and Shallow Shells using the Finite Element Method' International Journal for Numerical Methods in Engineering, Vol. 5, pp 543-556.

Bergan,P.G., Horrigoe,G., Frakeland,B., Soreides,T.H. (1978) 'Solution Techniques for Non-linear Finite Element Problems' Internation Journal for Numerical Methods in Engineering, Vol. 12, pp 1677-1696.

Bathe,K.J, Ramm,E., Wilson,E.L. (1975) 'Finite Element Formulation for Large Deformation and Dynamic Analysis' Internation Journal for Numerical Methods in Enginnering, Vol. 9, pp 353-386.

Blazynski,T.S. (1983) 'Explosive Welding, Forming and Compaction' Applied Science Publishers Ltd., London and New York.

Crisfield,M.A. (1980) 'Incremental/Iterative Solution Procedures for Non-linear Structural Analysis' Numerical Methods for Non-linear problems, edited by C. Taylor et.al. Vol. 1, pp 261-290, Pieridge, Swansea, 1980.

Donnell,L.H. (1934) Stability of Thin-Walled Tubes under torsion, N.A.C.A. TR 479.

Dhatt,G.S. (1970) 'Instability of Thin Shells by the Finite Element Method' Proc. Symp. Int. Assoc, Shell Structures, Vienna.

Doherty,W.P., Wilson,E.L., Taylor,R.L. (1969) 'Stress Analysis of Axi-symmetric Solids using Higher Order Quadrilateral Finite Elements' Structural Engineering Lab. Report No. SESM 69-3. University of California, Berkeley.

Fenner,R.T. (1978) 'Computing for Engineers' MacMillan Press Ltd., London.

Fenner,R.T. (1979) 'Finite Element Method for Engineers' MacMillan Press Ltd., London.

Fox,L. (1964) 'An Introduction to Numerical Linear Algebra' Clarendon Press, Oxford.

Flugge,W. (1962) 'Stresses in Shells' Berlin: Springer - Verlag.

Gallagher,R.H. (1972) 'The Finite Element method in Shell Stability Analysis' Nat. Sympo. Computerised Structure Analysis and Design. George Washington University.

Gallagher,R.H. (1975) 'Shell Elements' World Conference on Finite Element Method in Structural Mechanics. E1 - E35, Dorset, U.K.

Hafiz,M. (1981) 'Computer Aided Mathematical Modelling of Turbulent Flow for Orifice Metering' Ph.D. Thesis, The City University, London.

Huebner,K.H. (1975) 'The Finite Element Method for Engineers' John Wiley and Sons Ltd., U.K.

Hayes,J. (1970) 'Numerical Approximation to Functions and Data' The Othlone Press, U.K.

Hinton,E., Salonen,e.M., Bicanic,N. (1978) 'A Study of Locking

Phenomena in Isoparametric Elements' MAFELAP III, Academic Press Inc., London.

Haisler,W.E., Stricklin,J.A., Stebbins,F.J. (1972) 'Development and Evaluation of Solution for Geometrically Non-linear Procedure' AIAA J. 10, pp 246-272

Korishin,H.S., Isanbaeva,F.S. (1968) 'Flexible Plates and Panels' Nanka, Moscow.

Kraus,H. (1967) 'Thin Elastic Shells' John Wiley and Sons, Inc.

Leong,H.K. (1981) 'Mathematical Modelling of Bourdon Gauges using Finite Element Techniques' M.Phil. Thesis, The City University, London.

Marguerre,K. (1938) 'Zur Theorie der Gekrummten Platt Groser Formanderung' Proc. of Fifth International Congress of Appl. Mech., Wiley and Sons, pp 93-101

Murray,D.W., Wilson,E.L. (1969) 'Finite Element Large Deflection Analysis of Plates' J. Engng. Mech. Div. ASCE 95 (EM1), pp 143-165.

Mescall,J.F. (1965) 'Large Deflections of Spherical Shells Under Concentrated Loads' Transactions of then ASME. Journal of Applied Mechanics, pp 936-938.

Massey,B.S. (1971) 'Units, Dimensional Analysis and Physical Similarity' Von-Nostrand, Reinhold, Tricetown, N.J.

Nath,B. (1974) 'Fundamentals of Finite Elements for Engineers' Athlone Press, London.

NAG (Numerical Algorithm Group) (1978)

Novozhilov,V.V. (1953) 'Foundation of the Non-Linear Theory of Elasticity' Grahlock Press, Rochester, N.Y.

Nayak,G.C. (1971) 'Plasticity and Large Deformation Problems by the

Finite Element Method' Ph.D. Thesis, The University of Wales, Swansea.

Pawsey,S.F., Clough,R.W. (1971) 'Improved Numerical Integration of Thick Shell Finite Elements' International Journal for Numerical Methods in Engineering, Vol. 3, pp 575-586

Reissner,E. (1950) 'On Axi-Symmetric Deformation of Thin Shells of Revolution' Proc. Soc. Symp. in Appliedd Mathematics, Vol. 3.

Rahman,M.M. (1979) 'Mathematical Modelling and Computer Aided Design of Field Coupled Electromechanical Transducers' Ph.D. Thesis, The City University, London.

Suraner,K.S. (1982) 'Geometrically Non-Linear Formulation for the Axi-Symmetric Shell Elements' International Journal for Numerical Methods in Engineering, Vol. 18, pp 477-502

SERC (1980) 'Library Documentation for Finite Element Programming' The Science and Engineering Research Council, Rutherford and Appleton Laboratories, Chilton, Didcot, U.K.

Sabir,A.B., Lock,A.C. (1972) 'The Application of Finite Elements to the Large Deflection Geometrically Non-Linear Behavior of Cylindrical Shells' Variational Methods in Engineering, Southampton University Press, pp 7166-7175

Sanders,J.L. (1963) 'Non-Linear Theories for Thin Shells' Quart. Appl. Math. 21, pp 21-36

Stricklin,J.A., Haisler,W.E., MacDougall, Stebbin,F.J. (1968) 'Non-Linear Analysis of SHells of Revolution by the Matrix Displacement Method' AIAA Journal, Vol. 6, No. 12, pp 2306-2312

Timoshenko,S. Goodier,J.N. (1951) 'Theory of Elasticity' McGraw-Hill Book Company, Inc, U.S.A.

Timoshenko,S. Woinowsky-Krieger,S. (1959) 'Theory of Plates and Shells' McGraw-Hill Book Company, Inc, U.S.A.

Turley,A.J. (1977) 'Mathematical Modelling and CAD of Diaphragms and Capsules for Instrument Transducers' Ph.D. Thesis, The City University, London.

Taylor,E.S. (1974) 'Dimensional Analysis for Engineers' Clarendon Press, Oxford.

Wood,R.D., Zienkiewics,O.C. (1977) 'Geometrically Non-Linear Finite Element Analysis of Beams, Frames, Arches and Axi-Symmetric Shells' Computers and Structures, Vol. 7, pp 7255-735. Pergamon Press, U.K.

Yang,T.Y. (1972) 'Elastic Snap-Through Analysis of Curved Plated using Discrete Elements' AIAA Journal, Vol. 10, No. 4, pp 371-372.

Zienkiewicz,O.C. (1977) 'The Finite Element Method', 3rd Edition. McGraw-Hill, London (1971)

Zienkiewick,O.C. (1978) 'New Parts for the Finite Element Method' MAFELAP, edited by J.R.Whiteman, Academic Press, U.K.

Ziekiewicz,O.C., Nayak,G.C. (1973) 'A General Approach to Problems of Plasticity and Large Deformation using Isoparametric elements' Proc. Conf. Matrix Math. Struct. Mech. Wright-Paterson AFB, Ohio, (1971), (pub 1973).

Zienkiewicz,O.C., Bauer,J., Morgan,K., Onate,E. (1977) 'A Simple and Efficient Element for Axi-Symmetric Shells' International Journal for Numerical Methods in Engineering, Vol.11, pp 1545-1558.

APPENDIX A

DERIVATION OF THE RESIDUAL VECTOR AND THE TANGENTIAL STIFFNESS MATRIX

From equations 3.11 and 3.13, the residual vector 'R' is given by the following equation. Subscripts and superscripts have been neglected for the sake of clarity.

$$R = \int_V \bar{B}^T D B \, dv \, \underline{a} - \lambda F \tag{A.1}$$

BUT $\sigma = D B a$

$$R = \int_V \bar{B}^T \sigma \, dv - dv - \lambda F \tag{A.2}$$

The above expression is used to determine the residual vector.

Tangential stiffness matrix, by definition,

$$\frac{\partial R}{\partial a} = \int_V \left(\frac{\partial \bar{B}^T}{\partial a} . \sigma + \bar{B}^T \frac{\partial \sigma}{\partial a} \right) dv \tag{A.3}$$

FROM EQUATION 3.11

$$\frac{\partial \bar{B}}{\partial a} = \frac{\partial B_L}{\partial a}$$

IF $\underline{A}^T = \begin{bmatrix} \beta & 0 & 0 & -\frac{\cos\phi}{R} & 0 \end{bmatrix}$

AND $\underline{G} = \begin{bmatrix} 0 & 0 & 1 \end{bmatrix}$

THEN $\underline{B}_L = \underline{A} \, \underline{G}$

ALSO $\beta = \underline{G} \, \underline{a}$

WHERE $\underline{a}^T = \begin{bmatrix} u & w & \beta \end{bmatrix}$

$$\frac{\partial \bar{B}^T}{\partial a}\,\sigma = G^T \cdot \frac{\partial A^T}{\partial a} \cdot \sigma$$

$$= G^T \cdot \frac{\partial A^T}{\partial \beta} \cdot \frac{\partial \beta}{\partial a} \cdot \sigma$$

$$= G^T \cdot \frac{\partial A^T}{\partial \beta} \cdot \sigma \cdot \frac{\partial \beta}{\partial a}$$

$$= G^T \frac{\partial A^T}{\partial \beta}\, \sigma \cdot G$$

$$= G^T \left[N_s - M_\theta \frac{\cos\phi}{r} \right] G \qquad (A.4)$$

Similarly, it can be shown that,

$$\bar{B}^T \frac{\partial \sigma}{\partial a} = \bar{B}^T D \bar{B} \qquad (A.5)$$

From equations A.3, A.4 and A.5,

$$K_T = \frac{\partial R}{\partial a}$$

$$= \int_V \left[G^T \left(N_s - M_\theta \frac{\cos\phi}{r} \right) G + \bar{B}^T D B \right] dV$$

Because 'D' is a symmetric matrix, 'K ' will also be a symmetric matrix. The overall tangential stiffness matrix will be symmetric and banded. The bandwidth of 'K ' will depend on the degree of freedom of the element.

APPENDIX B

SOURCE LIST OF TOTAL LAGRANGIAN FINITE ELEMENT PROGRAM

The source list of the Total Lagrangian Finite Element program is given in this appendix. The program has been developed using Finite Element library routines (SERC, 1980), wherever possible. Because the library doesnot contain any 'shell elements', all the routines relevent to thin shell elements had to be developed by the author. However, the structure of the program is similar to the ones presented in the library. In most cases the same variable names have been used as in the library programs. Additional variables have been assigned meaningful names. Familiarity with the theory (see text) and access to the library documentations is essential to understand the program.

The computer program
(p.135-156)
has been removed for copyright reasons

APPENDIX C

INTERFACE PROGRAM FOR N.C. LATHE TAPE GENERATION

The source list of the macro 'MATE' and the Fortran program 'PAPE' are given in this appendix.

The macro edits the ASCII data file and inserts '@@@' at the end of each data line. '@@@' are used by the Fortran program to detect the end of the data line. In addition, the macro compiles, loads and runs the Fortran program.

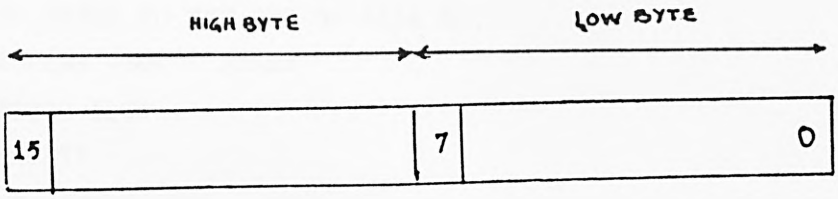

Figure A1

A Prime 550 is a 16 bit word computer (figure A1). ASCII characters require 7 bits for the data, and an additional bit for the parity. Hence a Prime word stores two ASCII characters, one in each byte. On a Prime, the parity bits are set to 1, regardless of the characters in the computer word. Even parity ASCII code is required for the data to be compatible to the N.C. machine. This was achieved by masking the entire computer word apart from bit 0 and checking its contents. If bit 0=1, then a counter was increased by 1. The process is repeated after shifting the word to right by one bit. Depending on the contents of the counter the parity bits (7 and 15) are modified accordingly. The paper-tape also needs to have at least 3 null characters after 'line-feed' and 'carriage-return' commands. These are also generated by the Fortran program.

To run the program 'MACRO MATE' needs to be typed on the terminal.

The computer programs (p. 158-161) have been removed for copyright reasons